STUDIES ON HIGH CURRENT ELECTRON RINGS IN A TOROIDAL DEVICE

by

D. CHENNA REDDY

A THESIS
SUBMITTED FOR THE DEGREE
OF

DOCTOR OF PHILOSOPHY

OF THE
GUJARAT UNIVERSITY

SEPTEMBER 1988

PHYSICAL RESEARCH LABORATORY
AHMEDABAD 380 009
INDIA

TO

MY PARENTS

CERTIFICATE

I hereby declare that the work presented in this thesis is original and has not formed the basis for the research of any degree or diploma by any University or Institution.

D. Chenna Reddy.

D. Chenna Reddy

Certified by :

P.I.John

Professor-in-charge

Place : Ahmedabad

Date : September 1988

ACKNOWLEDGEMENTS

First and foremost, I would like to thank my thesis advisor Prof. P.I.John for his able guidance and constant support throughout my thesis work. It had been a great experience to learn from him. From the beginning of this work, his constant vigilance and supervision with a right amount of academic freedom had helped me in gaining confidence to do the quite complex experiments.

I thank Prof. P.K.Kaw for his keen interest in my work and progress. I am grateful to his enthusiastic support which had been a source of inspiration throughout the course of my thesis work. I am thankful to Prof. Y.C.Saxena, for his encouragement and constructive criticism. I express my gratitude to him for allowing me to work on the computer after office hours and on holidays. I also thank Prof. A.Sen and Prof. A.K.Sundaram for their interest and encouragement.

I thank Dr. K.K.Jain for helping me learn many useful techniques related to my doctoral work, particularly during the initial stages of the work. I also thank Dr. Dhiraj and Dr. Venkat for their encouragement and support throughout the work. I am thankful to Dr. Chitra for her interest in my work. I thank the other academic staff of IPR for their co-operation.

During the data analysis, Dr. Sethia had helped me in overcoming many problems in using the data analysis and plotting software (DAPS). I thank him for being available

whenever I was in need. Digitization work was done in SAC computer centre. I thank Dr. Prakash and Dr. Sharma of SAC for allowing me to use their digitizer and computer and my friend Gopala Krishna who helped me in digitizing the oscillograms.

I sincerely thank the staff of workshop, library, drafting section, electronics lab, office and purchase who provided necessary help with least possible delay. I am also thankful to Pathak, Bhatt, Lali, Pujara, Sivanarayana, Korde and Shaikh for their assistance during the first assembly of BETA.

I am thankful to Suthar and others of PRL who assisted me during the fabrication of Tesla transformer. My sincere thanks are due to Kurup and Shivasankaran of PRL glassblowing section for the help rendered by them. I thank the staff of PRL library for their co-operation.

My special thanks are due to Satyanarayana, Madanlal, Mohandas and Sarada Sree for being ready to help me during the experiments and after, whenever I needed it.

During the course work in the first year, Amarendra, Subramanyan, Ashok and Meenakshi had provided a nice and friendly atmosphere. I am grateful to them.

I am fortunate in having friends like Viju, Deshpande, Sharadini, Puravi, Ajay, Jitesh, Bevli and Ganesh Prasad who were ever ready to provide any kind of assistance that I needed. I am thankful to all of them. I thank Dey and Dwivedi for their help in proof reading.

I gratefully acknowledge the financial assistance

received from PRL and IPR.

Finally, I am grateful to my wife who had shown remarkable patience and understanding. I thank her for her encouragement and support throughout the course of this thesis, which contributed in no less way in completion of the work. I am indebted to my sons Sekhar and Harsha whose playfulness provided necessary relief which helped me relax from the day's strenuous work.

The Thesis was prepared on IBM PC and was typed by Mr.Sourabhan. I am thankful to him for his quick and neat typing of the thesis.

ABSTRACT

In this thesis, we report, studies on high current electron rings formed by injecting a Relativistic Electron Beam (REB) into a toroidal device filled with plasma. These studies are motivated to understand the dynamics of beam injection and trapping. Another important objective is to study the plasma heating by REB in a toroidal device, where only limited experimental data is available.

An REB generator based on Tesla transformer high voltage source was fabricated for these studies. Plasma was injected into the torus with the help of a gas injected, washer stack plasma gun. Beam was injected into a pre-formed plasma. Beam injection was studied in two different plasma densities, characterized by operating the plasma gun with two different pulse forming net works.

When beam was injected into low density ($\approx 5 \times 10^{12}$ cm^{-3}) plasma, it was found that the beam was lost by hitting the injector from the back after one toroidal transit. No net toroidal current was observed in this case. However in the case of injection into a high density ($\approx 10^{13}$ cm^{-3}) plasma, the beam drifted inward and cleared the injector and was trapped. A net toroidal current ($\approx$ 5 kA) was generated in this case.

Temporally and spatially resolved measurements with miniature Faraday cups and small Rogowski coils showed that

beam trapping was due to a fast return current decay. The return current decay times calculated from ion-acoustic turbulence were found to be consistent with the observed net current rise time. At low plasma densities, where no trapping was observed, the condition for exciting the ion-acoustic turbulence was not satisfied.

Localized measurements of the poloidal field were done which indicated a net current channel moving radially inward with no observable vertical motion. This was found to be consistent with the drift injection-energy loss mechanism proposed for beam trapping. Wall fields were found to significantly influence the current profile calculations from the poloidal field profiles.

To understand the plasma heating process, localized measurements of δB_t (change in toroidal field) were done. It was found that in a toroidal experiment, use of a diamagnetic loop to measure plasma temperature would be inadequate. Localized measurements not only eliminated the uncertainties involved in using a diamagnetic loop but also gave the time evolution of the beam-plasma system. From these measurements it was found that about 50% of the beam energy appears as plasma perpendicular energy and the heating was mainly due to return current dissipation.

The q profiles obtained from the magnetic field measurements indicated that the system goes into a low q state as time progresses.

The beam goes into an equilibrium position from the launch position without applying any vertical field. The

equilibrium therefore is maintained by wall fields, indicating a force free equilibrium of the current ring. The beam energies calculated from the observed net currents and shift of the current channel were found to be consistent with the beam energy transfer observed from diamagnetic measurements.

LIST OF FIGURES

CONTENTS

CHAPTER-I

INTRODUCTION

The rapid development of the high-voltage pulsed power technology since early 1960s and its application to generation of Intense Relativistic Electron Beams (IREBs) has made high energy (≈100 keV to 10 MeV) and high current (≥ 10 kA) beams available for various applications. Although these beams were originally developed for use in material studies and as sources of bright x-ray flashes, they soon found applications in a number of other areas of physics and technology such as controlled thermonuclear fusion, microwave generation (Nation, 1970), collective ion acceleration (Graybill and Uglum, 1970) etc. At present these beams also hold great promise in areas such as free electron lasers, food processing and environmental treatment (Kapetanakos and Sprangle, 1985).

In the applications related to controlled thermonuclear fusion, IREBs have become attractive because of their high energy content, which if transferred to plasma can heat it to fusion temperatures. In both the approaches to controlled fusion, namely: (1) Inertial confinement fusion (ICF) and (2) Magnetic confinement fusion (MCF), IREBs were considered for plasma heating (Rudakov and Samarsky, 1973; Yonas et al., 1974; Budker, 1973; Hammer and Papadopoulos, 1975).

In ICF, these beams are used to heat a sub-millimetre size pellet of D-T mixture. The solid pellet is enclosed in a shell of heavy material. When the pellet is irradiated by powerful IREBs, the outer shall explodes, leaving an

imploding pellet behind. This implosion makes the density and temperature sufficient for fusion reactions, before the hot plasma disperses due to its thermal motion.

In MCF, the beam heats a high density plasma to fusion temperature. Since, the classical collisions of the beam electrons with plasma particles are rare because of the high beam energies, significant energy transfer can be effected only through collective interactions. Two such important interaction mechanisms identified and studied are: (1) return current heating (Cox and Bennet, 1970; Lee and Sudan, 1971; Lovelace and Sudan, 1971) and (2) two stream instability (Fainberg et al., 1970; Toepfer and Poukey, 1973; Ferch and Sudan, 1975; Papadopoulos, 1975; Thode and Sudan, 1975; Thode, 1976). These interactions were reviewed in a great detail by Breizman and Ryutov, (1974) and more recently by Miller, (1982).

Qualitatively, these interaction mechanisms can be understood as follows. In return current heating, the pulsed nature of the IREB induces a current in the plasma. This plasma current is mainly carried by the plasma electrons. These drifting plasma electrons excite the ion-acoustic instability (Sagdeev, 1967) under appropriate conditions. This instability results in an enhanced resistivity of the plasma, because of which plasma current is dissipated, thereby heating the plasma. In the two stream instability, the instability occurs due to a relative drift between the beam and the plasma electrons. Linear, quasilinear and wave-wave scattering models have been proposed for beam energy transfer.

A number of experimental studies on beam plasma interaction to date (Altyntsev et al., 1971; Kapetanakos and Hammer, 1973; Korn et al., 1973; Miller and Kuswa, 1973;

Ekdahl et al., 1974; Goldenbaum et al., 1974; Prono et al., 1975; Greenspan et al., 1980; Jansen et al., 1984) have established that a good fraction of the beam energy (10 to 20%) is transferred to the plasma. These results have been found to be explainable with either of the above two interaction models or both.

Another important application utilizes the strong self magnetic field of these beams to form plasma confining geometries. Some of these confining geometries are the Astron configuration (Christofilos, 1951), field reversed configurations and compact tori (Sethian et al., 1978; Jain and John, 1984 and 1986).

1.1 Beam generation and propagation

IREB generation is achieved by imposing a high negative voltage (hundreds of kV) on the cathode of a field emission diode. The anode is a thin metallic foil. The cathode surface has a large number of microscopic protrusions (called whiskers): The electric current flowing through these whiskers causes them to melt and vaporize forming a high density metal vapor layer at the cathode. This layer gets ionized in the electric field present in the anode-cathode gap. This is called cathode plasma. Electrons from this plasma are accelerated in the anode-cathode gap and come out of the anode foil as a beam (the range of these electrons is much higher than the foil thickness). A review of the beam generators has been given by Nation, (1979). The physical processes that happen during the diode operation have been discussed by Miller, (1982)

The electron current that flows in the diode is given by the Child-Langmuir law for space charge limited flow. For a non-relativistic, plane parallel geometry this current

density, J_e can be expressed as

$$J_e = 1.86 \left(\frac{4\epsilon_o}{9}\right) \left(\frac{2e}{m}\right)^{1/2} \frac{V^{3/2}}{x^2} \qquad (1.1)$$

where e and m are the electronic charge and mass respectively, ϵ_o is the permittivity of free space and V and x are the instantaneous values of the voltage on the cathode and the diode gap respectively.

The beam propagation is affected by self electric and magnetic fields. In the case of charge and current unneutralised beam and no external fields, beam experiences diverging force due to beam space charge electric fields and a pinching force due to self magnetic fields. Since, the force due to space charge electric fields is always more than the pinching force, stable propagation of a charge unneutralised beam is impossible. Thus for stable propagation of the beam use of external fields and/or space charge neutralization is essential. Even with a strong magnetic field, the beam current is limited because of the space charge electric fields. The critical current beyond which stable propagation is impossible for a beam propagating in a cylindrical cavity of radius, R is given (in cgs units) by (Bogdankevich and Rukhadze, 1971)

$$I_{cr} = \frac{mc^3}{e} \frac{(\Gamma^{2/3} - 1)^{2/3}}{[1 + 2 \ln(R/r_b)]} \qquad (1.2)$$

where r_b is the beam radius, c is the velocity of light and Γ is the relativistic factor. Since this current is obtained from the space charge considerations, it is known as space charge limiting current. This limiting current can be enhanced by a factor, $(1-f_e)^{-1}$ if the space charge is neutralized. Here f_e is the charge neutralization factor. Charge neutralization is achieved by injecting the beam into

a plasma.

Another limitation on the beam current still exists. This is due to the self magnetic field. If the Larmor radius of the beam electrons in the self magnetic field is comparable to the beam radius, then the beam electrons turn around and hit the anode from which they are starting and stable propagation is not possible. The limiting current at which this happens is given by (Alfven, 1939)

$$I_A = 17000\ \beta\Gamma \qquad (1.3)$$

and is known as Alfven-Lawson limiting current. Here $\beta = v_b/c$, where v_b is the velocity of the beam particles. For stable propagation of beam currents in excess of this limiting current partial or complete current neutralization or a strong external magnetic field is necessary.

1.2 Relativistic Electron Beam (REB) in a toroidal device

REBs trapped and confined in a toroidal device have a number of interesting applications. Plasma heating in a toroidal device should be more efficient than in a linear system, since the beam residence times are much longer in a toroidal device. Because of long residence times in the device, even classical collisions can be effective in addition to the collective interactions in transferring the beam energy. In a straight device the energy transfer due to classical collisions is negligible owing to small transit time (and hence small residence time) of the beam in the device.

Another important application is current drive in toroidal devices. Among various non inductive current drive and current sustainment schemes, the use of repetitively injected REB to produce the required poloidal field can in

principle make such devices continuously operational (Ikuta, 1972a; Ehst, 1982). If the plasma is produced and confined by other than the ohmic transformer as in present tokamak devices, the extremely congested central portion of the device will be more accessible; besides making the device smaller and compact. Since a large part of the central portion is available, adiabatic compression of the plasma in the major radial direction will be more effective and the plasma temperature can be raised.

In the Astron-Spherator configuration first proposed by Yoshikawa and Christofilos, (1971) an REB carrying current is injected and confined in a toroidal device. The favourable features of a spherator: viz. a deep magnetic well, a high magnetic shear and a short connection length between the bad and good curvature regions are possible with this configuration and at the same time eliminates the presence of solid conductors buried in a hot plasma. Since the energy of the beam can be moderate, the synchrotron radiation problem which plagued the Astron is less severe.

Successful beam trapping will produce interesting magnetic configurations which may not be accessible through the ordinary ohmic discharge in a tokamak. These configurations will be attractive from the controlled fusion point of view, since a large area is available for plasma confinement and adiabatic compression (Yoshikawa and Christofilos, 1971; Ikuta, 1972a and 1972b). Since the ring formation times are typically less than 1 μs, the system can go into a stable equilibrium state passing through dangerous unstable states, even if they are present on its way to the final state (Mohri et al., 1985).

Another important application that has attracted much recent attention is the modified betatron (Rostoker, 1973;

Sprangle and Kapetanakos, 1978; Rostoker, 1980). The important feature that makes it different from the conventional betatron is the presence of a strong toroidal magnetic field in addition to the betatron field. In a conventional betatron the maximum current is of the order of an Ampere and is limited due to the strong electrostatic fields present at the time of injection (i.e. when the beam Γ is low). Addition of a strong toroidal field was found to stabilize the beam even at very high currents (Sprangle and Kapetanakos, 1978; Rostoker, 1980). A number of other schemes involving more complicated fields like stellarator fields (Roberson et al., 1983)and bumpy torus fields (Chernin et al., 1984) were considered for high current beams since then.

In all the above mentioned applications of a toroidal beam, a strong toroidal field is present. This makes the beam injection and trapping more complicated.

1.3 Injection and trapping of an REB in a toroidal device

Realization of a high current REB in a toroidal system critically depends on the method of injection and trapping. Unlike in an open ended system, where the beam enters from one end and leaves from the other, injection into a toroidal system with a pre-existing toroidal field is more complicated.

Since the purpose of injection of an REB into a toroidal system is to trap the beam, one major concern is how to guide the beam such that it misses the injector as it propagates around the torus through 360° and subsequently gets trapped in an equilibrium orbit. This requirement eliminates the possibility of placing the field emission diode at the centre and demands that the space occupied by a field emission diode in the poloidal plane should be minimum. The different

injection schemes that have been used to inject and trap an REB in toroidal devices along with some injection schemes proposed in connection with modified betatron are briefly discussed in the following sub-sections.

1.3.1 Drift injection

From a single particle picture, the beam electrons moving along the toroidal field lines experience a drift in the $\mathbf{R}\times\mathbf{B}_t$ direction (R is the major radius and B_t is the toroidal field). It was proposed by Benford et al., (1973) to use this drift for trapping the beam. In the experiments (Benford et al., 1974b), a part of the toroidal field was extended to the diode and the beam was launched on the toroidal field lines. As the beam goes around, it drifted downward and by suitably adjusting the toroidal field, could be made to clear the injector. To control the drift a dipole field was used. The direction and the magnitude of this dipole field could be chosen to enhance, reduce or reverse the drift there by achieving a good control over the beam motion. With proper choice of the magnitude of this field this method of injection was found to be efficient (Benford et al., 1974b).

Even though the above method provided a good control over the beam motion in the $\mathbf{R}\times\mathbf{B}_t$ (i.e. vertical direction), it was found that the simple dipole field caused radial loss of the beam. To confine the beam for longer duration, the proposed scheme (Benford et al., 1974b) uses a betatron field along with a partial beam energy loss by self magnetic field generation and/or by heating the plasma. The radial and vertical components of the betatron type field are given by

$$B_R(R,z) = -\left(\frac{n}{R}\right) z\, B_o \left(\frac{R_o}{R}\right)^n \qquad (1.4)$$

and

$$B_z(R,z) = z\, B_o \left(\frac{R_o}{R}\right)^n \qquad (1.5)$$

respectively. Here R is measured from the major axis, z is measured from the mid plane, R_o is the major radius of the torus, B_o and n are the magnitude and index of the betatron field respectively.

A single particle trajectory calculation (Linhart, 1960) showed that for $B_z \ll B_t$, the projection of an electron trajectory on a poloidal (RZ) plane is an ellipse (with Larmor gyration superimposed) if $0 < n < 1$. The guiding centre analysis of the beam trajectory, where the beam self fields were included (Benford et al., 1974b; Bailey et al., 1982), showed the beam centre to be at R_e, given by

$$R_e = \frac{m\Gamma v_b}{eB_o(1-n)}\left[1 + \frac{I_n}{I_A}\left\{\ln\left(\frac{4\pi R_o}{r_b}\right) - 1.45\right\}\right] - \frac{nR_o}{1-n} \qquad (1.6)$$

where I_n is the net current increase following the beam injection and r_b is the minor radius of the beam.

If Γ and I_n vary with time suitably, the consequent time variation of R_e can be used to trap the beam. Differentiation of eq. (1.6) (taking the coupled time dependence of I_n, β, Γ and I_A into account) gives

$$\frac{dR_e}{dt} = -\frac{\mu_o\, dI_n/dt}{4\pi\, B_o(1-n)}\left[\ln\left(\frac{4\pi R_o}{r_b}\right) - 3.45\right] \qquad (1.7)$$

where μ_o is the permeability of free space.

From the above equation, we can see that as long as I_n increases R_e decreases and hence the beam can be moved away from the injector.

In forming a non-neutral relativistic electron ring Mohri et al., (1975) have used the following scheme. The

diode is located inside the torus (hence no guide field was necessary). The beam is launched on the field lines. As the beam propagates around the torus, it sets up self electromagnetic fields, the energy of which comes from the beam kinetic energy. In the presence of a vertical field, this reduction of energy leads to beam drift towards the major axis. Masuzaki et al., (1975) have also pointed out the importance of the partial beam energy loss and building up of a net current for beam trapping. In the presence of a metallic wall the net current rise in the torus induces a current in the vessel wall. The magnetic field due to the wall currents also rises as the net current rises. The trajectory of the beam, which is helical under the presence of a vertical field shrinks radially due to this increase of the wall field.

Landing of REB ring on equilibrium orbit was analyzed by Mohri et al., (1977a and 1982). In their analysis also, which takes into account the presence of a conducting wall, a fast rising net current was shown to be important for the beam to launch on an equilibrium.

In the experiments at IPP, Nagoya, Mohri et al., (1975 and 1977b) have used this method for injection and trapping the beam. Later on, the plasma anode method (similar to the plasma filled diode of Miller et al., 1975) was used for injecting the beam into a torus (Mohri et al., 1979 and 1981; Bailey et al., 1982). The important feature of this method is the absence of a foil anode. Plasma serves as the anode and the sheath which develops when a high negative voltage is applied to the cathode serves as the anode cathode gap. Except for this difference the injection and trapping of a beam is same as discussed earlier. The plasma anode method has two distinct advantages particularly in the case of

injection into a torus: (1) It obviates the use of a foil and hence no need of foil changer, making it possible to fire many shots without interruption. (2) Since the foil and foil changer are absent considerable amount of poloidal space can be saved for beam trapping.

1.3.2 Divertor injection

In this method, instead of guiding the beam towards the equilibrium orbit, the toroidal field is diverted during the beam injection such that the beam is launched on the field lines. In this method, due to Brower et al., (1974), a short segment of the cathode stalk was shaped in such a way that the current flowing through this stalk produces a field opposing the externally applied toroidal field. Because of this changed field configuration beam could be launched on the diverted field lines. To prevent the beam electrons coming back and hitting the injector after traveling around the torus, the diverted field lines should return to their original place before beam completes one transit. Thus this method is good for a single turn injection only. The advantage of this method is that the diode can be outside the torus and does not depend on any other mechanism such as fast net current rise and partial beam energy loss for beam trapping. The divertor injection was used in the experiments at Cornell (Gilad et al., 1974; Proulx, 1981).

1.3.3 Injection into modified betatron

Several other schemes were proposed for beam injection in connection with the modified betatron. In one of the injection schemes (Mako et al., 1984), beam is generated outside and transported into the torus along an axial pinch of high plasma density, where the current in the pinch is tapered at each end of the pinch. The transported beam is launched on the toroidal field lines.

In another injection scheme (Hui and Lau, 1984), a narrow channel of high density plasma is produced by a uv laser at the location of the beam entrance, which guides the beam to the minor axis (or equilibrium orbit). In the injection scheme for NRL modified betatron (Golden et al., 1983) the injected electron energy must be matched with the betatron field, so that the beam electrons will have required orbit radius.

Kapetanakos et al., (1982) considered the beam in toroidal and betatron fields. The self field of a straight beam at the centre of the beam is zero. But in a toroidal beam the self fields at the beam centre are non-zero, because of which the beam centre experiences a radially outward force. Since the self fields of the beam appear at the expense of beam energy, the final energy of the beam is less than that at the time of injection, due to which the beam experiences a major radially inward force (inductive effect). It was shown (Kapetanakos et al., 1982) that for $\Gamma^2 \gg 1$ and $r_b/R_b \ll 1$, these two forces balance each other even when the beam is injected off axis, due to which the injection becomes simpler.

Besides the injection schemes and their analysis mentioned earlier, simulation studies on the beam injection into a current carrying plasma have also been reported recently by Akopov et al., (1987). This is based on the reflection of the beam from the plasma boundaries when injected with a large angle of incidence. In the numerical simulation study of Tanaka et al., (1987), it was shown that the beam injected into a current carrying toroidal plasma with a toroidal magnetic field, penetrates into the plasma from the injection point as it goes around the torus many times.

1.4 Review of the existing work

Since the proposal by Yoshikawa and Christofilos, (1971) of an Astron-Spherator configuration using REB, many experimenters have produced REB rings in toroidal devices. Particularly the experiments at (1) Physics International Company and UCLA, (2) Cornell University and (3) IPP, Nagoya have resulted in the generation of high current REB rings.

1.4.1 Physics International (PI) and UCLA experiments

The early experiments at PI were done in a curved section and in a high pressure neutral gas (Benford et al., 1973). Significant result of these experiments was the observation of the beam drift in the vertical direction. The charge and current neutralization were almost complete and so the drift was attributed to the curvature and gradients in the applied toroidal field. The use of conducting walls caused an additional drift in the **FxB** direction (Benford et al., 1974a), where **F** is the force on the beam electrons due to the image currents in the wall. Using a rectangular beam and analyzing the distortion of the damage pattern, it was shown that the beam electrons followed the field lines.

Following the above experiments in curved sections, beams were injected into a full toroidal system with the help of a guide field (Benford et al., 1974b). Efficient injection (>80%) was achieved using curvature and gradient drifts. A dipole field was used to stabilize the vertical drift but the beam was lost rapidly due to the defocusing effect of this dipole field. In all the above experiments (i.e. partial or complete toroidal system) the charge neutralization as well as the current neutralization were almost complete. Hence the beam particles moved in the external fields and the results were well explained.

In the more recent experiments on macrotor tokamak

(Bailey et al., 1982) current drive capability of REB in a pre-existing plasma with a pre-existing plasma current was studied. Keeping the diode inside the torus, beam was directly launched on the toroidal field lines. In the experiments with neutral gas, it was found that a part of the beam was reincident on the injector. Curvature and gradient drifts carried the beam in the vertical direction before it hit the walls and lost. In the experiments with tokamak plasma the beam was found to follow the rotational transform of the tokamak while moving across the flux surfaces in accordance with the curvature and gradient drifts. Beam was found to make many toroidal transits before it was intercepted by the injector. Microwave signals indicated a beam life time of about 1 μs. The net current increase was found to be about 5 kAmps after the beam injection. The typical life time of this current (not necessarily of the beam) was found to be 800 μs. Co and counter injection (with respect to the pre-existing plasma current) indicated that this current was due to beam net currents initially and was sustained by additional OH-current later in time. A large fraction (75%) of the injected beam energy appeared in the region of the plasma near the minor axis.

1.4.2 Cornell experiments

In the initial experiments beam was injected into an aluminium torus section filled with neutral gas. The experimental data was interpreted in terms of a guiding centre solution and the solutions obtained (numerically) from the exact equations of motion (Kusse and Lockner, 1974). The experimental results were found to be in reasonably good agreement with the theoretical calculations in terms of closest approach of the beam to the wall. The analysis and the experiments indicated that the beam injected off the

equilibrium position developed drift motion around the equilibrium position (Kusse and Lockner, 1974). In the later experiments (Gilad et al., 1975), beam injection efficiencies using divertor injection and the beam propagation characteristics were studied as a function of toroidal field and the neutral pressure. These experiments were performed in a race track geometry and the beam was stopped by keeping an end plate before it completed one toroidal rotation. In the full racetrack experiment (Gilad et al., 1974), beams were trapped for about 300 ns. The beam injection duration was less than the beam transit time. Existence of a clear beam head was observed with x-ray detectors indicating no head tail interaction.

In the more recent experiments (Proulx, 1981), beam was injected into a plasma carrying current. The beam position was obtained from the damage patterns on nylon mesh targets. Beams were launched well into the plasma at lower toroidal field and was interpreted as the result of enhanced plasma resistance due to turbulence. An important observation of these experiments is an additional OH-driven current following the beam injection. This was found using co and counter injection of the beam. Another aspect of this work was the study of the interaction mechanism that was responsible for beam energy transfer. It was found that electron-electron two stream instability was mainly responsible for the observed beam energy transfer (≈5%).

1.4.3 IPP, Nagoya experiments

Study of formation of a stable high current REB ring was aimed in the experiments on a series of devices called SPAC devices. A non-neutral electron ring was formed in SPAC-II (Mohri et al., 1975). The ring was found to be in equilibrium and the life time was found to be dependent on the onset of

ion resonance instability. In the experiments on SPAC-II and SPAC-III with neutral gas and on SPAC-IV with a pre-existing plasma (Mohri et al., 1977b), high current REB rings were realized. In SPAC-III, a low q configuration was realized and the peak beam current was 30 kA with a life time of about 30 μs. In SPAC-IV, externally controlling the time rate of change of the toroidal field, the oscillations in the poloidal field signals and the fast fading of the beam current could be controlled.

In SPAC-V, (Mohri et al., 1979) a long lasting (≈1 ms) high current REB ring (40 kAmps) was formed. In these experiments the plasma ion temperature was obtained spectroscopically and was found to be 50 to 100 eV. The REB ring was compressed subsequently after formation by increasing the vertical field. This resulted in plasma heating and marginal increase in the ring current. In these experiments an interesting observation was step like dumps in the ring current. By injecting the beam into a high density plasma ($\approx 10^{14}$ cm^{-3}) a very high current REB ring (≈150 kA) was formed with a life time of 20 μs.

High current rings lasting even for longer times were observed in SPAC-VI (Mohri et al., 1981 and Narihara et al., 1983). This long life times were attributed to the long lasting external fields. Measurements on the confined plasma (Mohri et al., 1981) indicated that the cold gun injected plasma was heated to about 0.8 keV and confined by the poloidal field of the REB current. In these experiments also the current ring decayed slowly with intermittent step like dumps.

Spherator like configurations were formed with REBs in SPAC-VI (Narihara et al., 1983) and in SPAC-VII (Mohri et al., 1985 and Narihara et al., 1987). In the SPAC-VI

experiments the beam current lasted for almost 40 ms. The x-ray photograph and its luminosity densitometric curves indicated that the beam was held rigidly (confined to a very small area in the poloidal plane) and was probably in a force-free configuration. From the measurements it was shown that the plasma was confined in a configuration similar to that of a spherator.

In SPAC-VII (Mohri et al., 1985), a long pulse beam was injected and the beam current stacking was observed during the injection phase. In this experiment also a low q state (q at the periphery was 0.6) was observed. With an improved plasma anode method beams were injected into SPAC-VII (Narihara et al., 1987). In this method, outer conductor of the MITL (magnetically insulated transmission line) was removed inside the torus. Plasma around the cathode stalk worked as the outer conductor. This improved method has resulted in considerable saving of the poloidal space which was occupied by the material conductor and helped in preventing the loss of injected REB. This also helped in reducing the metallic impurities which were released when the REB came into contact with this outer conductor. Stability of the REB ring was studied and the step-wise current drops (observed in the earlier SPAC-experiments as well) were attributed to the strength of the toroidal field. The measurements on the plasma confinement showed that the confinement was better at the center than at the edge.

1.4.4 Theoretical studies on beam equilibrium

Most of the theoretical studies on toroidal beam equilibria (both analytical and numerical) are in connection with the modified betatron. In most of these calculations, the presence of a strong electrostatic force due to beam space charge has been considered. However in an earlier study

by Ott and Sudan, (1971), beam equilibria were calculated for the case of a space charge neutralized beam confined by (1) a vertical field and (2) by a toroidal conducting container. In this study the beam energy was assumed to be represented by a δ function. In a later study (Ott, 1971) electrically unneutralized REB was considered. In this study the strong self fields (both electric and magnetic) of the beam were included. Toroidal beam equilibria were calculated and stability of the equilibrium was analyzed for the case of a low beam energy spread using kinetic approach (Davidson and Uhm, 1982; Uhm H. et al., 1985). Numerical simulations of the beam equilibrium have also been reported (Kapetanakos et al., 1982 and 1983). Self consistent equilibria and adiabatic development of a high current electron ring in a modified betatron were reported by Finn and Manheimer, (1983), where no assumption regarding the charge and current profiles was made. The important point of all the above studies is the demonstration of an equilibrium for the toroidal beam. In the study by Barak and Rostoker, (1982) the orbital stability of a high current betatron was investigated. Some of the other studies are regarding the limitations on the beam current and stability of the beam equilibrium due to various instabilities.

1.5 Scope of the thesis

Efficient injection and trapping is essential for realizing high current REB in toroidal devices. Since the injection into a toroidal device and trapping the beam in an equilibrium involves many physical processes such as drifts, beam energy loss and net current build-up following a fast return current decay, the understanding of the initial phase is crucial for efficient beam injection and trapping. The

understanding of this phase is also important, since some of the injection schemes that were used in the earlier experiments and proposed in connection with modified betatron rely on the above mentioned physical processes.

Measurements during this initial phase were limited in the earlier experiments. Understandably, much attention was paid to find an efficient injection scheme (Brower et al., 1974; Benford et al., 1974b). In the early experiments, beams were injected into high pressure neutral gas (Benford et al., 1973; Kusse and Lockner, 1974). These experiments were not in complete toroidal systems, but only in curved sections. In these experiments and in later experiments (Benford et al., 1974a; Gilad et al., 1975) the current neutralization was almost complete and the beam dynamics were explainable as single particle behaviour in the applied fields (Benford et al., 1973) and the wall fields (Benford et al., 1974a; Kusse and Lockner, 1974).Since the current neutralization was almost complete, the collective effects were not appreciable and also since the experiments were in curved sections, the applicability of the results to complete toroidal systems is limited. Also the beam motion was inferred in these experiments and in the more recent experiments on macrotor tokamak (Bailey et al., 1982) and in the experiments at Cornell (Proulx, 1981) from the measurements with large diameter Faraday cups, calorimeters and damage patterns on nylon mesh targets. Considering the global nature of these measurements, the spatial and temporal evolution of the beam plasma system could not be inferred.

In the experiments at IPP, Nagoya, sustained efforts have resulted in producing long lasting Astron-Spherator configuration (Narihara et al., 1983 and 1987; Mohri et al., 1985). In these experiments also little attention was paid to

the localized measurements.

In our experiments we have aimed at making localized measurements of beam and net currents and self magnetic fields so that better understanding of the injection and trapping process is possible. The localized measurements of the self magnetic fields are also helpful in the study of equilibrium and its stability besides giving the beam energy transferred to the self magnetic fields.

Beam injection was studied in two different plasma densities,which established that fast return current decay was important for beam trapping.

Unlike in the linear devices, where a large number of experimental studies were made on plasma heating by REB, the experimental data available on the beam-plasma interaction and on the beam energy transfer in toroidal devices is limited.

In our experiments we have attempted to study the beam energy transfer to the plasma. To avoid the uncertainties that are present in the interpretation of diamagnetic loop measurements, localized δB_t measurements were done to study the beam energy transfer. These measurements are also important to understand the evolution of the beam plasma system.

In Chapter II, the experimental system is described. Various diagnostics used and grounding and shielding scheme and the triggering sequence are described briefly.

In Chapter III, the main results of the experiments are presented and discussed. These include space and time resolved measurements of beam and net currents, beam self fields and plasma diamagnetism. Evolution of beam-plasma system (q profiles) is obtained from poloidal field and δB_t measurements. Various physical processes which are important

in different phases of the experiment are also discussed in this chapter at appropriate places.

The main conclusions of the experimental study are briefly summarized in Chapter IV along with suggestions for further studies.

CHAPTER-II

EXPERIMENTAL DEVICE AND DIAGNOSTICS

The experimental study of REB injection and trapping was carried out in a toroidal device called BETA (Basic Experiments in a Toroidal Assembly). The experimental arrangement is schematically shown in fig. 2.1. As can be seen from this figure, the main subsystems are (1) the toroidal device - BETA, (2) REB generator, (3) plasma gun and (4) diagnostics. A brief description of these subsystems is given in the following sections.

2.1 BETA

BETA, as mentioned above, is a toroidal device. It consists of a toroidal vacuum vessel, vacuum pumps, magnetic field coils and supporting structure. Top view of vacuum vessel and the toroidal field coils is shown in fig. 2.2. A detailed description of all the subsystems is given in references 1 and 2. Hence only a brief description is given here for the sake of completeness.

2.1.1 Vacuum system

The vacuum vessel is a torus of circular cross-section and made of four quadrants made of s.s. 304. The major and minor radii of the vessel are 45.7 cm and 15.7 cm respectively. The vessel wall thickness is 5.5 mm. Each quadrant has 3 radial ports of 15.0 cm diameter, 3 bottom ports and 2 top ports of 10.0 cm diameter and 2 top ports of 5.0 cm diameter. The total number of ports is 40 and are used

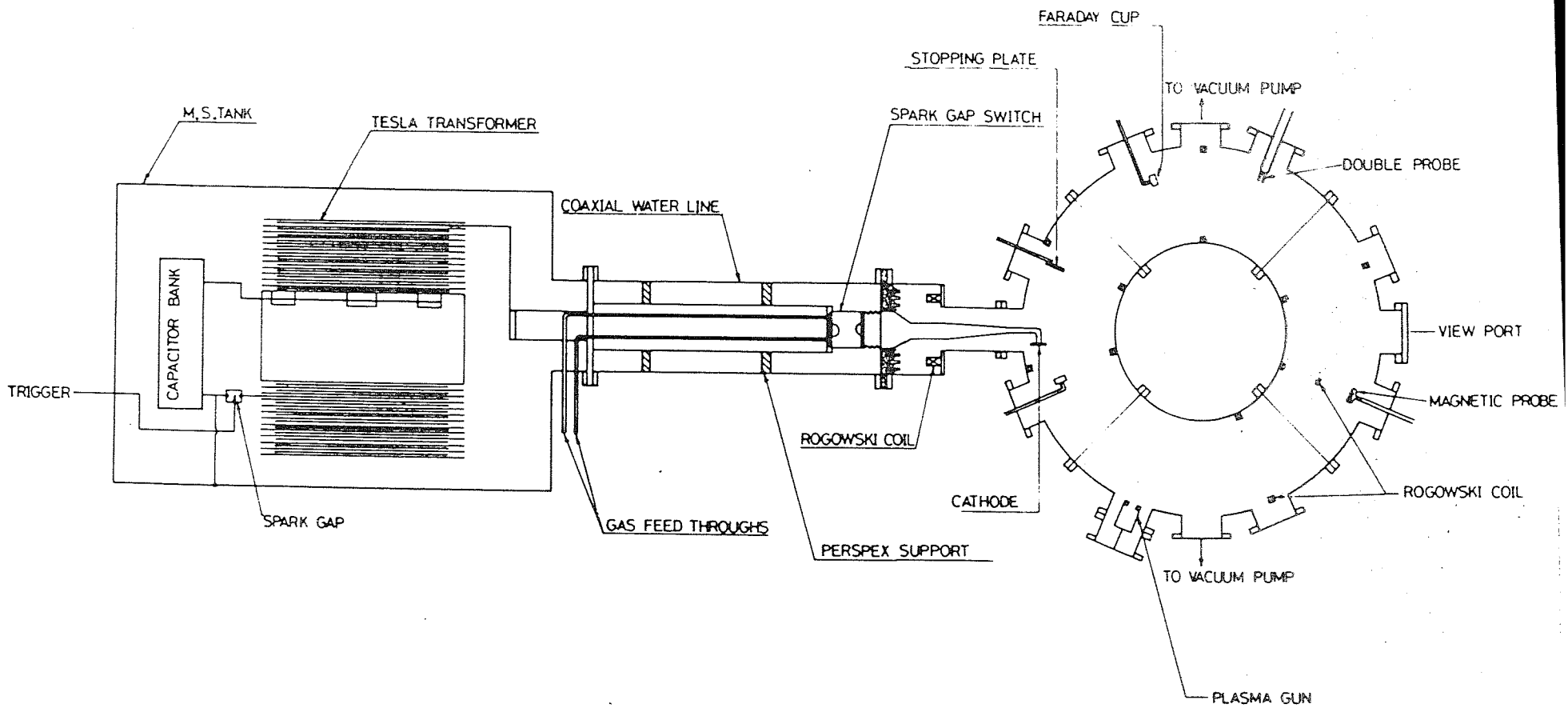

Fig. 2.1: Schematic illustration of the experimental arrangement

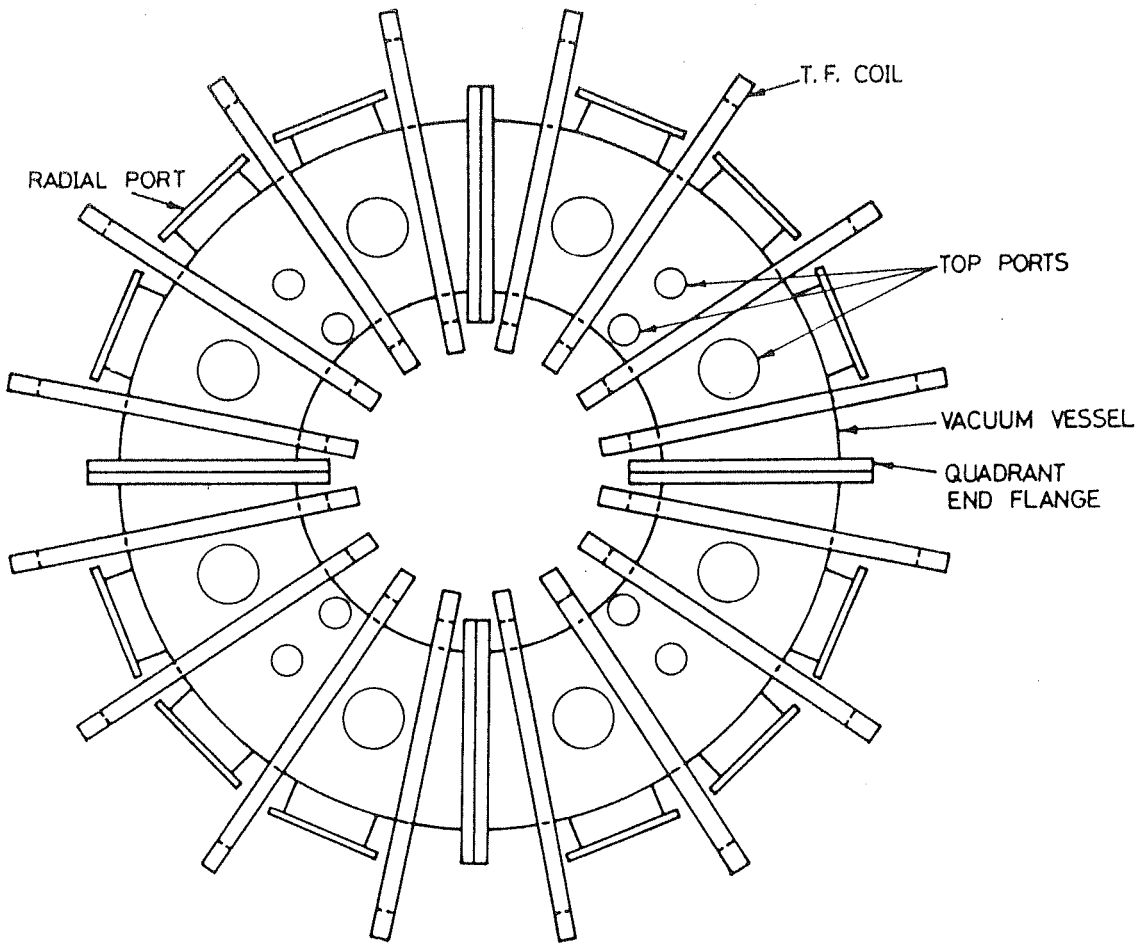

Fig. 2.2: Top view of the vacuum vessel with T.F. coils

for pumping the vessel and for deploying various diagnostics. The large number of these observation ports makes the plasma easily accessible for diagnostic purposes. Since the vessel is made into four quadrants and the seals are viton 'O' rings, the assembly of the system is fairly easy. There is a provision to break the electrical continuity of the vessel in the toroidal direction at two locations. However, in the experiments reported in this thesis the vessel is toroidally continuous. The measured magnetic diffusion times of the vessel for toroidal and vertical magnetic fields are 700 μs and 650 μs respectively.

The pumping system consists of two "diffstack" pumps, with a pumping speed of 2000 lit/s each, backed by two rotary pumps. The two diffstack pumps are connected to two radial ports of the vacuum vessel at 180° apart via two pumping lines, one metre long and 15.0 cm diameter each. The ultimate vacuum attainable is 2×10^{-7} Torr.

However, for the experiments of this thesis, only one diffstack pump was used. The pressure was monitored with an ionization gauge kept on the pumping line nearer to the diffstack pump. This location of the gauge gives a pressure reading lower by a factor two compared to the actual pressure in the vessel, but avoids the use of the gauge in the region of high magnetic fields. The base pressure in the system during these experiments was about 1×10^{-5} Torr (the working pressure was higher).

2.1.2 Magnetic field system

BETA is equipped with two sets of magnetic field coils: (1) toroidal field (T.F.) coils and (2) vertical field coils, which produce toroidal and vertical magnetic fields respectively.

The toroidal magnetic field is produced by a set of

sixteen picture frame type coils placed around the torus at equal angles. These coils are made of 1 cm x 5 cm copper busbar. Each coil has three turns insulated by 1 mm fibre glass sheet. These turns have three brazed joints at three corners of the square and current transfer from one turn to the other and from one coil to the other takes place at the fourth corner. Finally all the three turns of a coil are held together by insulated nut-bolt arrangement at the four corners. Cooling tubes soldered on the inner side of each turn provide a path for chilled water to cool the coils, when operated at high currents. These coils have an aperture of 50 cm x 50 cm and are placed at a major radius of 50 cm (i.e., the centre of the coils is 50 cm from the major axis). This is about 5.0 cm more than the major radius of the vacuum vessel. This was chosen, as it gives minimum ripple inside the torus. All the coils are connected in series. Coil interconnections are made of two 1 cm x 5 cm copper busbars. To reduce the error magnetic field due to the current flowing through the coil interconnections, the return current bus is placed just below these interconnections. These coils can give a maximum of 5 kgauss at the minor axis when the coil current is 26 kAmps.

The T.F. coils are energized by a capacitor bank. The capacitor bank consists of 30 capacitors of 700 μF each and can be charged to a maximum voltage of 5 kV. These capacitors are rack mounted in groups of 10 each and discharged into the load (i.e. T.F. coils) simultaneously using three ignitrons. Crowbarring of the current through the coils is achieved by using two more ignitrons which short circuit the capacitor bank when the current through the coils is at its peak. Charging and discharging circuit is schematically shown in fig. 2.3. A current transformer measures the current through

the coils. The waveform of this current is shown in fig. 2.4 for the uncrowbarred case. Table 2.1 contains the main parameters of the toroidal field system.

The vertical magnetic field is produced by a pair of coils placed symmetrically about the equatorial plane. These coils are circular and have 10 turns each. These coils are made of 1/8" x 1" copper strip. The coil inner radius is 115 cm and the coil separation is 120 cm. This configuration gives nearly uniform field inside the torus cross-section.

The vertical field coils are also energized by a capacitor bank. The capacitor bank is discharged into the coils using an ignitron switch. Another ignitron is used for crowbarring the current in these coils. Current in the coils is monitored by a current transformer. A maximum field of about 200 gauss (0.07 gauss/Amp inside the torus) can be obtained with these coils.

2.1.3 Supporting structure

Another important subsystem of BETA is its supporting structure. The structure, like the vacuum vessel, is also made into four quadrants: one fixed and the rest movable for easy assembly. The structural components were designed to withstand the forces due to the weight of the coils and vessel and the forces arising due to the interaction of the magnetic fields with the currents in the coils during the experiment. The vessel is supported by adjustable s.s. fixtures at four radial ports and at all the vessel quadrant end flanges. The T.F. coils are supported on both sides at top and bottom by s.s. 'L' channels fixed with the structure. A buckling cylinder kept at the centre on a fixed table prevents the T.F. coils from moving towards the centre during the shot. The out of plane forces (tilting forces) acting on the T.F. coils (when vertical magnetic field is applied) are

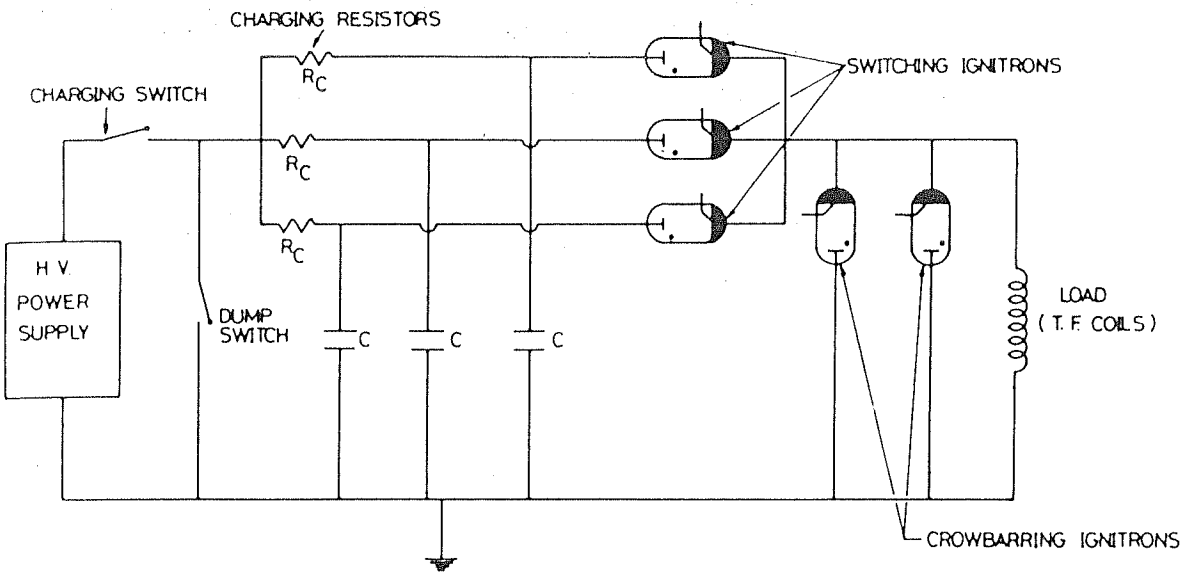

Fig. 2.3: Charging and discharging circuit for T.F. Coils

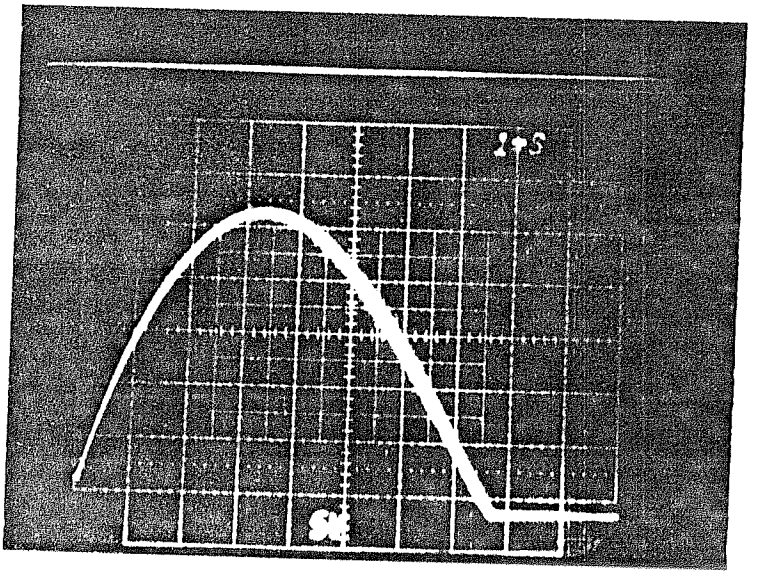

Fig. 2.4: Waveform of the T.F. coil current

TABLE 2.1

Toroidal Field System

Coil type	Square
Material	Copper
No. of coils	16
No. of turns in each coil	3
Conductor size	5.0 cm x 1.0 cm
Coil major radius	50.0 cm
Coil aperture	50.0 cm x 50.0 cm
Maximum field at R = 45.0 cm	5.0 kgauss
Maximum coil current	26.0 kAmps
Total Inductance	0.38 mH
Total Resistance (calculated)	4.6 mΩ
Total Resistance (including the coil interconnections and return current bus; measured)	10.0 mΩ
Power Source	Capacitor bank
No. of capacitors	30
Capacitance (total)	2.1 mF
Charging voltage (maximum)	5.0 kV
Coil current rise time	3.5 ms

taken care of by four cross-bars fixed on the structure. Wedge blocks made of s.s. are placed in between the inner legs and at the top and bottom of the outer legs.

To assemble the system, four T.F. coils are mounted on each of the four quadrants of the supporting structure and the vessel quadrants are slid into the coils. Then the movable structure quadrants are brought together and integrated. The structural quadrants are connected to each other with nut-bolt arrangements.

2.2 Plasma gun

The plasma source is a washer stack plasma gun, similar to the one used by Jain et al., 1980. Unlike the conventional washer gun, where gas desorbed from the titanium washers is ionized, in this gun, gas injected externally is ionized.

The plasma gun along with a pulse forming network, which energizes the gun, is schematically shown in fig. 2.5. The gun consists of a number of brass and nylon washers of 25 mm i.d. stacked together alternately. The assembly is held together by four bolts. The first brass washer acts as the cathode and the last brass washer (anode) is connected to the ground via the bolts.

In the early experiments on plasma injection into the torus (Jain et al., 1985), an electromagnetic gas valve was used for gas injection. The plasma gun operated in an over pressurized, self break down mode. Since this left very little control over the amount of gas puffed into the gun and hence into the torus, for beam injection experiments this was replaced by a piezo-electric gas valve. The necessary control over the gas puffing was achieved by adjusting the parameters (duration and height) of the voltage pulse which opens the

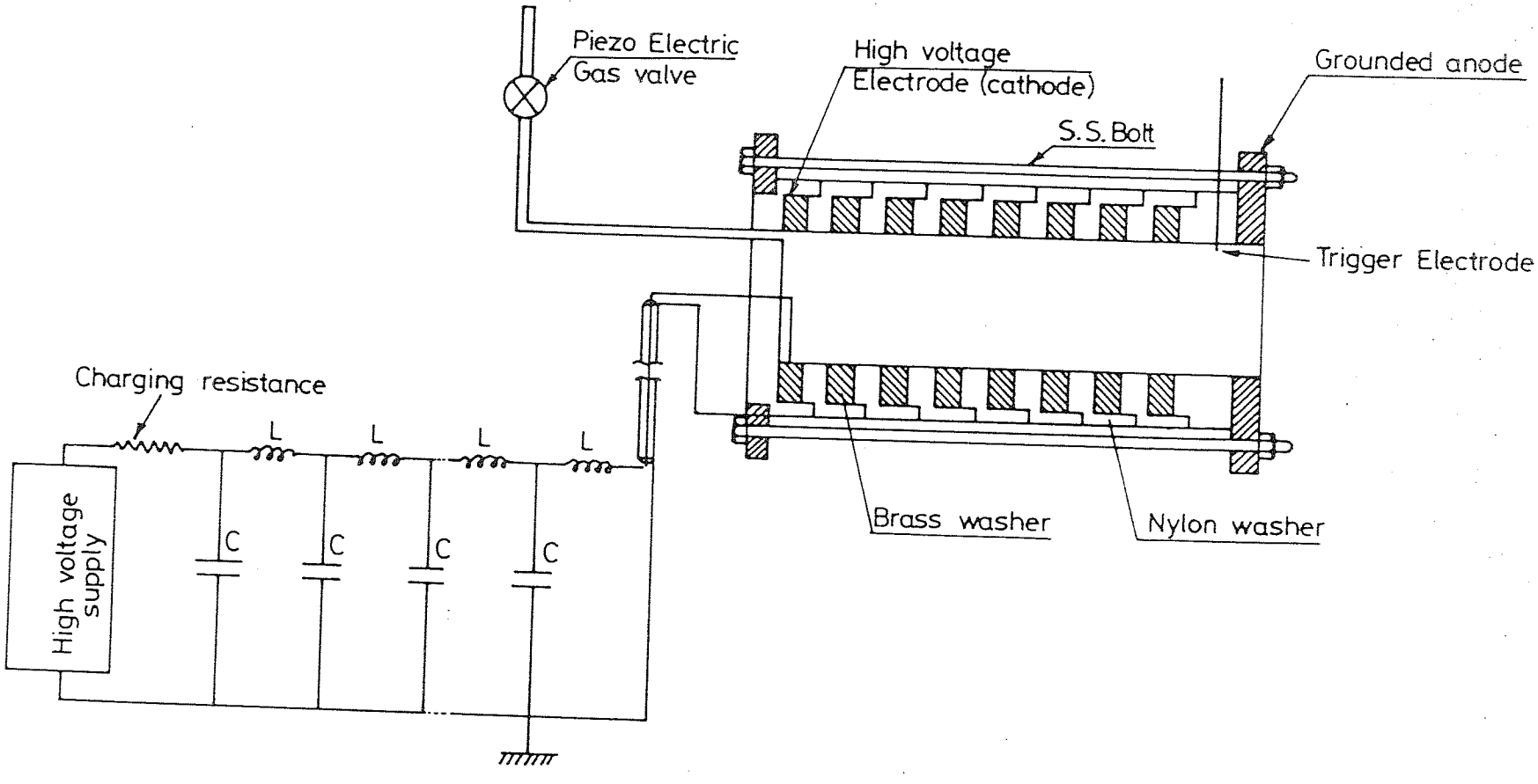

Fig. 2.5: Plasma gun.

gas valve. To avoid the jitter problem that followed the controlled gas puffing, a third electrode was used in this case for triggering the plasma gun.

2.3 REB generator

A typical REB generator consists of a pulsed high voltage source, a pulse forming line (PFL) and a field emission diode. The high voltage source, whose pulse width is of the order of a microsecond, pulse charges the PFL. During this phase PFL acts as a lumped capacitance, since the charging time is longer than the electromagnetic transit time of the PFL. When the PFL is charged to a predetermined voltage (which is of the order of hundreds of kV), a spark gap switch in the PFL closes and connects the PFL to an impedance matched field emission diode. During this phase PFL acts as a distributed line and delivers a high voltage pulse, whose pulse width is twice the electromagnetic transit time of the PFL and amplitude is half the line voltage, to the field emission diode. The field emission diode converts the energy in this short duration (≈100 ns) electrical pulse into the kinetic energy of a beam of electrons known as Relativistic Electron Beam (REB).

The pulsed high voltage source can be either a Marx generator or a Tesla transformer. In the case of Marx generator a number of capacitors are charged in parallel and discharged in series. This, therefore requires a number of elements such as charging resistors and spark gaps besides the energy storage capacitors. A Tesla transformer has more advantages such as,

a) Simpler circuit design and construction;

b) Possibility of operation at high repetition rates;

c) Only one spark gap switch is needed;

d) Overall cost is low since the number of energy storage capacitors is less;

A Tesla transformer type high voltage generator was designed and fabricated for the REB experiments on BETA (Jain et al., 1986). In the following subsections various subsystems of the beam generator including the Tesla transformer are described.

2.3.1 Tesla transformer

Over the years a number of Tesla transformer type high voltage generators were built at various laboratories through out the world (Finkelstein et al., 1966; Abramyan, 1971; Hoffmann, 1975; Boscolo et al., 1975; Suzuki et al., 1980; Matsuzawa and Suganomata, 1982; Nagesh, 1982; Fiorentino et al., 1982). The theory of the transformer was discussed by many authors (Finkelstein et al., 1966; Abramyan, 1971; Hoffmann, 1975). Matsuzawa and Suganomata, (1982) pointed out the importance of the tuning ratio over that of the coupling coefficient with the help of design charts for high energy transfer from the primary capacitance to the secondary capacitance. Jain et al., (1986) considered the effect of the leakage resistance of the secondary capacitance. The analysis and the experiments showed that even though the time at which the second peak occurs is not very much affected, the attainable secondary voltage was found to be greatly affected by this resistance. This has a direct bearing on the design of the secondary capacitance, which here is a water line.

Theory and principle of operation

An equivalent circuit of Tesla transformer is shown in fig. 2.6. This consists of two resonant 'LC' circuits coupled through their mutual inductance M. The primary resonant circuit has an inductance of L_p and capacitance of C_p and the

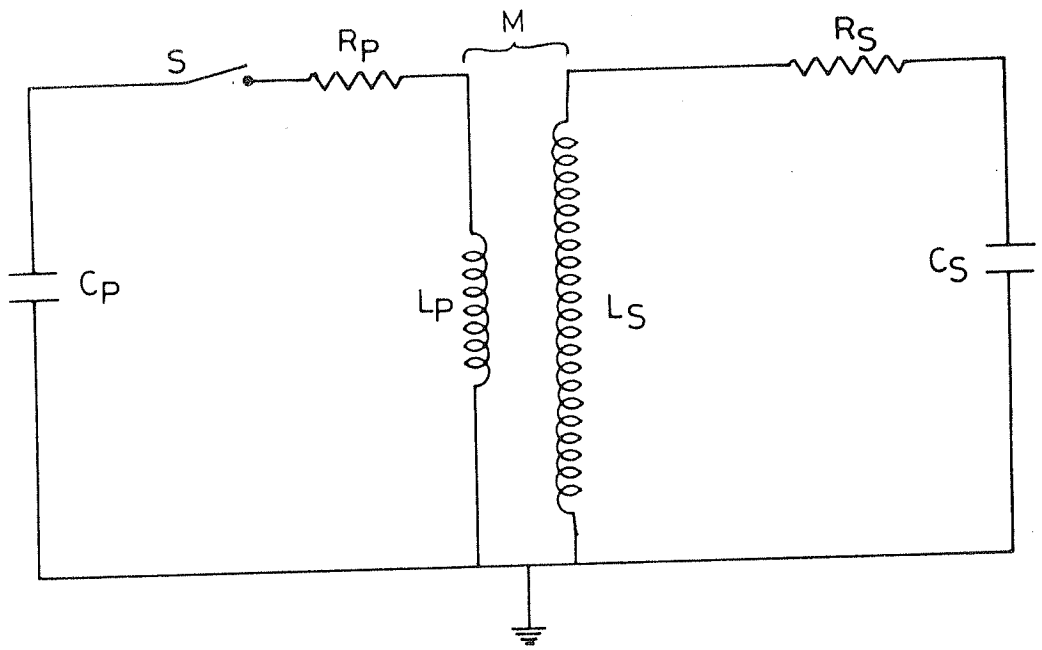

Fig. 2.6: Equivalent circuit of Tesla transformer.

secondary resonant circuit has an inductance L_s and capacitance C_s respectively. R_p and R_s are the loss resistances in the primary and secondary resonant circuits respectively. Initially the primary capacitor, C_p is charged to a voltage V_o, corresponding to a charge of q_o. When the switch S is closed, operation can be described by the following two coupled equations.

$$\frac{M}{L_p}\frac{d^2q_s}{dt^2} + \frac{d^2q_p}{dt^2} + \frac{R_p}{L_p}\frac{dq_p}{dt} + w_p^2 q_p = 0 \qquad (2.1)$$

and

$$\frac{d^2q_s}{dt^2} + \frac{R_s}{L_s}\frac{dq_s}{dt} + w_s^2 q_s + \frac{M}{L_s}\frac{d^2q_p}{dt^2} = 0 \qquad (2.2)$$

where q_p and q_s are instantaneous charges on C_p and C_s respectively and $w_{p(s)} = \{L_{p(s)}C_{p(s)}\}^{-1/2}$ is the angular resonant frequency of the primary (secondary) when the secondary (primary) is open. Eqs. (2.1) and (2.2) can be combined to yield an equation for the charge on the secondary capacitance.

$$(1-k^2)\frac{d^4q_s}{dt^4} + \left(\frac{R_p}{L_p} + \frac{R_s}{L_s}\right)\frac{d^3q_s}{dt^3} + \left(w_p^2 + w_s^2 + \frac{R_pR_s}{L_pL_s}\right)\frac{d^2q_s}{dt^2}$$

$$+ \left[\left(\frac{R_p}{L_p}\right)w_s^2 + \left(\frac{R_s}{L_s}\right)w_p^2\right]\frac{dq_s}{dt} + w_p^2w_s^2q_s = 0 \qquad (2.3)$$

where k is the coupling coefficient defined by $k = M/(L_pL_s)^{1/2}$. As can be seen, this is a fourth order equation and has four roots, which are in general complex. Analytical solution for the above equation can be obtained in a straight forward manner for the case of no damping, i.e. $R_p = R_s = 0$, (Craggs and Meek, 1954). In this case the roots have only imaginary parts. The secondary voltage consists of a high frequency (w_+) sine wave modulated by a low frequency (w_-)

sine wave and has some maximum value U. If the higher frequency is an odd harmonic of the lower frequency then U takes a maximum possible value, U_m. It was shown by Finkelstein et al., (1966), for 100% energy transfer from the primary capacitor to the secondary capacitor, the tuning ratio, defined as $T = w_p/w_s$, should be equal to one. This gives a condition on the coupling coefficient, k which can be expressed as (Hoffmann, 1975)

$$k = k_0 = \frac{2n - 1}{2n^2 - 2n + 1} \; ; \; n = 2, 3, 4, \ldots\text{etc.} \qquad (2.4)$$

$$= 3/5, \; 5/13, \; 7/25, \; \ldots\ldots\text{etc.}$$

Under these two conditions, namely: (i)tuning ratio, T=1 and (ii)coupling coefficient $k = k_0$, energy stored in the primary capacitor C_p at time t = 0, will be completely transferred to the secondary capacitor C_s at a later time $t = t_p$. At this instant of time (i.e. $t = t_p$) the currents in the primary and secondary circuits and the voltage on C_p are zero. For the particular value of $k_0 = 0.6$, the coupled primary and secondary circuits have frequencies (w_+ and w_-) in the ratio 2:1. Hence it is also known as double resonance (Finkelstein et al., 1966) condition.

Design and construction of the Tesla transformer

The transformer was designed to deliver maximum energy to the secondary capacitor, which is a water dielectric PFL. Since the dielectric breakdown voltage is inversely proportional to the third root of time (Nation, 1979), the maximum voltage on the secondary capacitor should appear in minimum time. This restriction fixes the value of k_0 as 0.6. The other values of k_0 will make this time more.

Two types of windings are commonly used (Nagesh, 1982), viz. (i) helical winding and (ii) radial or spiral winding.

In the case of helical winding, the secondary winding is on an insulated former in the axial direction. The primary, which covers the secondary windings, is usually tapered with maximum separation on the high voltage terminal side of the secondary. Even though easy to construct, this winding gives a poor coupling coefficient and hence poor efficiency. The spiral type of winding was chosen for our transformer in view of the following advantages.

a) high coefficient of coupling and hence high efficiency;

b) the secondary windings are capacitively graded and so there is no necessity of guard rings to protect the secondary;

c) the system is compact;

The primary of the transformer is a two turn coil made of 0.3 mm thick 60 cm wide copper sheet wound on a hollow high density polythene (HDPE) cylinder of 40 cm diameter. The secondary is made of 57 turns of 0.1 mm thick and 60 cm wide aluminium foil. The turn to turn insulation is provided by 9 layers of PVC sheets of 0.3 mm thickness each. The design values of the inductances of the primary and secondary windings are 1.0 μH and 0.85 mH respectively. The transformer can be considered as a 59 turn coil, where the innermost two turns are made of copper and the remaining 57 made of aluminium. The joining point of the second and third turns being the common point of the transformer. The transformer was placed in a mild steel tank which was then filled with transformer oil.

The primary capacitance, C_p is made of three Maxwell low inductance capacitors connected in parallel. The total capacitance of this bank is 7.2 μF. The maximum voltage to which these capacitors can be charged is 30 kV. The primary spark gap, which when switched discharges these capacitors

into the primary of the transformer, is made of brass electrodes housed in a perspex housing and is triggerable. The trigger pulse is generated by discharging a small capacitor through a resistance using a thyratron.

2.3.2 Pulse forming line (PFL)

A coaxial line with water as the dielectric acts as the secondary capacitor. Since the dielectric constant of water is high (ϵ_r = 80), the energy is stored at high density and the PFL becomes compact. The parameters of PFL were determined from the secondary capacitance requirements, allowable electrical stresses at which the dielectric can operate without failure and the output pulse duration (John, 1982). These considerations led to a PFL, with inner and outer conductors of 15 cm and 30 cm diameter respectively and length of 100 cm. The inner conductor was supported by two perspex supports.

Due to the comparatively longer duration of charging (of the order of few microseconds), the problems of dielectric breakdown and losses due to finite leakage resistance of water are of greater concern here, than in a Marx generator. The breakdown problem was taken care of during design, while the high water resistance required is maintained by circulating the water continuously through a commercially available deionizer.

2.3.3 High voltage switch, vacuum transmission line and field emission diode

Conventionally the pulse line is switched on to the diode using a high voltage switch which usually operates in a self breakdown or triggered mode. In our experiments for injecting the beam into the torus, we decided to use the plasma anode method in its extended version (Narihara et al., 1987), where the diode can be located inside the torus.

This necessitated an intermediate line of small cross-section between the PFL and the diode. The high voltage switch is a spark gap and is pressurized with dry nitrogen. The electrodes are made of brass and housed in a perspex chamber. The high pressure tubing is kept inside the hollow inner conductor of the PFL and come out through the oil-water interface (i.e., input end of the PFL). By adjusting the pressure in the spark gap it is possible to fire the switch at a pre-determined voltage level. The wave form shown in fig. 2.7(a) is the PFL voltage waveform (measured at its input end) when the high voltage switch did not fire. Fig. 2.7(b) shows the waveform when the switch fired at the second peak of the secondary voltage. To prevent any surface flashover along the vacuum-water interface flange, the flange is graded with metallic rings and the flange surface was machined to an angle of 45° between the gradings (Suzuki and Kato, 1984). The intermediate line (vacuum transmission line) connecting PFL and the diode was designed to match the PFL at one end and the radial port of BETA at the other end. The inner conductor consisted of two sections: (i) a tapered section and (ii) a straight section of small diameter (1 cm) which is connected to the cathode of the diode. The small dimension was chosen to prevent any electrical breakdown because of the smaller dimensions of the line. The current flowing in this smaller diameter inner conductor produces a large azimuthal magnetic field at the surface and hence will prevent the electrons from reaching the outer conductor (magnetic insulation). The cathode of the field emission diode is made of brass and 4.0 cm in diameter. The cathode is kept inside the torus and immersed in plasma where the latter acts as the anode (plasma anode method).

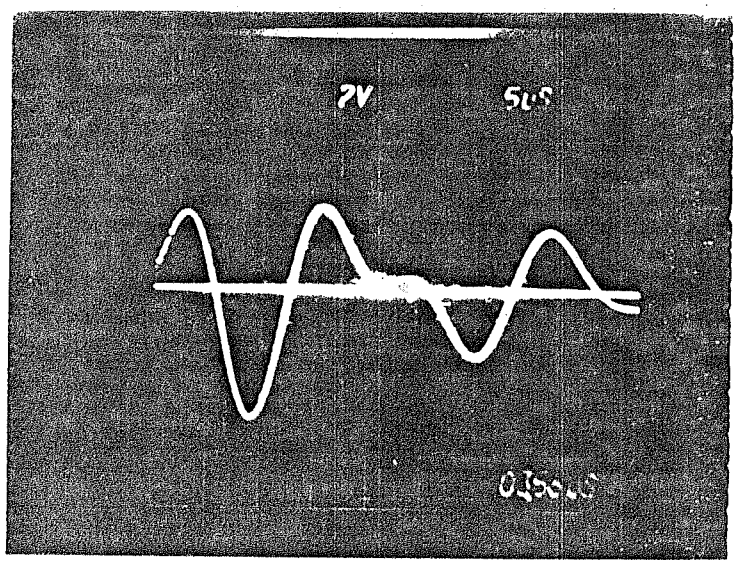

(a) When the secondary spark gap did not fire; 1V = 50 kV

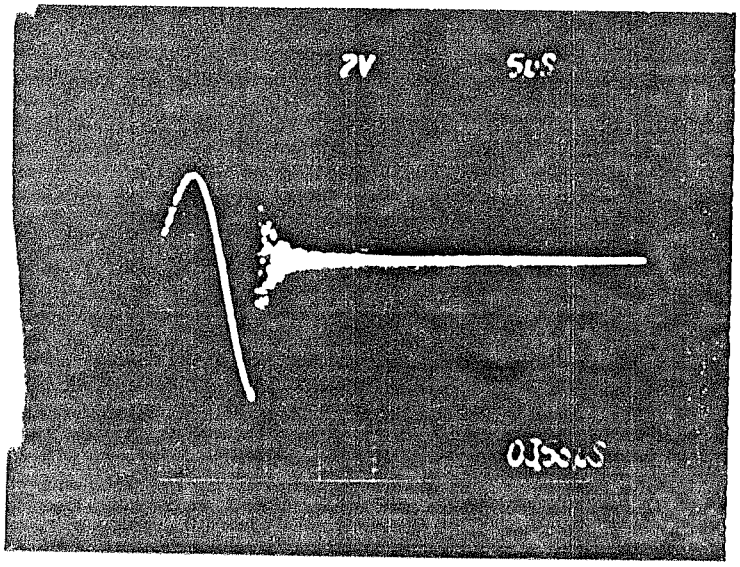

(b) When the secondary spark gap fired; 1V = 50 kV

Fig. 2.7: Tesla transformer secondary voltage wave forms.

2.4 Diagnostics

Like in any other pulsed experiment the diagnostics used should be reliable and should be able to respond to the fast changes in the experimental parameters which are intended to be measured. Another important aspect that needs attention is the noise which is present due to many fast switchings and the pulsed nature of the experiment. Special care was taken to eliminate the electrical noise. Some of these measures include making the signal to noise ratio better through proper design and use of the diagnostics, shielding of the diagnostic against the noise, shielding the cables which transfer the signals from the diagnostics to the data recording equipment (oscilloscopes), keeping the data recording equipment in a shielded room, proper grounding of the device and diagnostics etc.

In the case of magnetic measurements (i.e. magnetic probes and Rogowski coils), the signals were passively integrated with RC-integrators. Since the signal duration turned out to be longer than the RC time constant of the integrator, (large RC values deteriorate the signal to noise ratio), a correction was needed. This was done numerically after digitizing the oscillograms, in the following way.

Consider the following circuit diagram, where R and C are the elements of the integrator, L is the inductance of the probe, in which the voltage is induced. The induced voltage, which is proportional to the time differential of the magnetic flux threading L is represented as v_i.

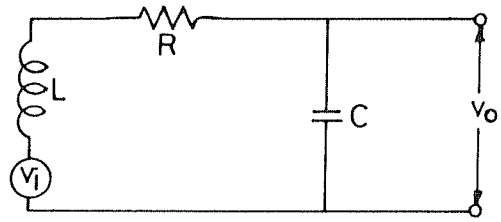

The circuit equation can be written as

$$L\frac{di}{dt} + iR + \frac{1}{C}\int idt = v_i \qquad (2.5)$$

When L/R is much smaller than the characteristic time of the signal, v_i the above equation can be written as

$$i + \frac{1}{RC}\int idt = \frac{v_i}{R} \qquad (2.6)$$

If we further choose the RC time constant to be much longer than the characteristic time of v_i, the second term on the L.H.S. can be neglected and we get

$$i = \frac{v_i}{R} \qquad (2.7)$$

i.e. the current flowing in the circuit is proportional to v_i which is nothing but the time rate of change of magnetic flux. To get the magnetic flux, v_i has to be integrated. Integrating eq. (2.7), we get

$$\int v_i dt = R\int idt$$

$$= RC\, v_o \qquad (2.8)$$

$$\left(\text{since } \frac{1}{C}\int idt = v_o\right)$$

In other words the voltage v_o on the capacitor C is proportional to the magnetic flux. This is the usual and familiar way of integrating the signals passively. But, when the condition that RC time constant is much larger than the characteristic time of the signal is not satisfied, eq. (2.8) has to be suitably modified. The correct expression for $\int v_i dt$ can be obtained from eq. (2.6), which can be witten as

$$i + v_o/R = v_i/R \qquad (2.9)$$

Integrating the above equation and substituting v_o for $\frac{1}{C}\int i dt$, we get

$$\frac{1}{RC}\int v_i dt = v_o + \frac{1}{RC}\int v_o dt \qquad (2.10)$$

The second term on the R.H.S. is the correction term which had to be added to v_o to get the properly integrated signal. This is achieved by digitizing the oscillograms and adding the numerically computed value of $\frac{1}{RC}\int v_o dt$ to v_o.

The calibration of the magnetic probes and Rogowski coils was done by a current pulse whose rise time was comparable to the actual signal rise times in the experiment. For calibrating the magnetic probes, the pulsed current was passed through a small Helmholtz coil. The probe to be calibrated was kept at the center of the Helmholtz coil where the field is nearly uniform.

Besides the magnetic measurements, the other diagnostics include single and double Langmuir probes for plasma density measurements, small Faraday cups for beam current profile measurements and high voltage copper sulphate resistance to monitor the Tesla transformer output voltage. The currents in the magnetic field coils and the plasma gun discharge current were monitored with the help of standard current transformers. A number of resistive voltage dividers used to monitor the charging voltages on the various capacitor banks constitute the pre-shot diagnostics.

2.4.1 Plasma density measurements

Plasma density was obtained from the ion saturation current collected by Langmuir probes. Two problems were observed while using a single Langmuir probe: (1) arcing from the probe (2) changing floating potential during the pulse.

To overcome this, double probes were used (Jain et al., 1985). The two cylindrical probe tips of the double probe were made of tungsten and were separated by less than 1 cm. The ion saturation current was obtained by biasing one probe with respect to the other. The current through the probe circuit was monitored with a current transformer.

2.4.2 Copper sulphate solution resistance

A copper sulphate solution resistance was used to measure the output voltage of the Tesla transformer (fig. 2.8). The resistance is made of a perspex tube of about 2.5 cm inner diameter and 30 cm length. The concentration of the solution was adjusted to get a resistance of about 5.0 kΩ. One end of this resistance is connected at the input end of the PFL, the other end being grounded. The current through this resistance, which is a measure of the voltage on the PFL, is measured with the help of a current transformer.

2.4.3 Miniature Faraday cup

A miniature cup (shown in fig. 2.9) with and without a foil cover was used to monitor the beam current profile. The current collected by the cup was measured either by a current transformer or by measuring the voltage dropped across a small, known resistance. The collector is a graphite piece of 8 mm diameter and was kept in a perspex housing. The Faraday cup was connected to the vacuum chamber, which is grounded, through a resistance or directly. In the case of a resistance, the voltage drop, which is a measure of the current flowing through the resistance, was measured. When connected directly ,the current was measured with the help of a current transformer.

2.4.4 Rogowski coils

A number of Rogowski coils were designed and constructed for the use in the experiment. All of them were used with a

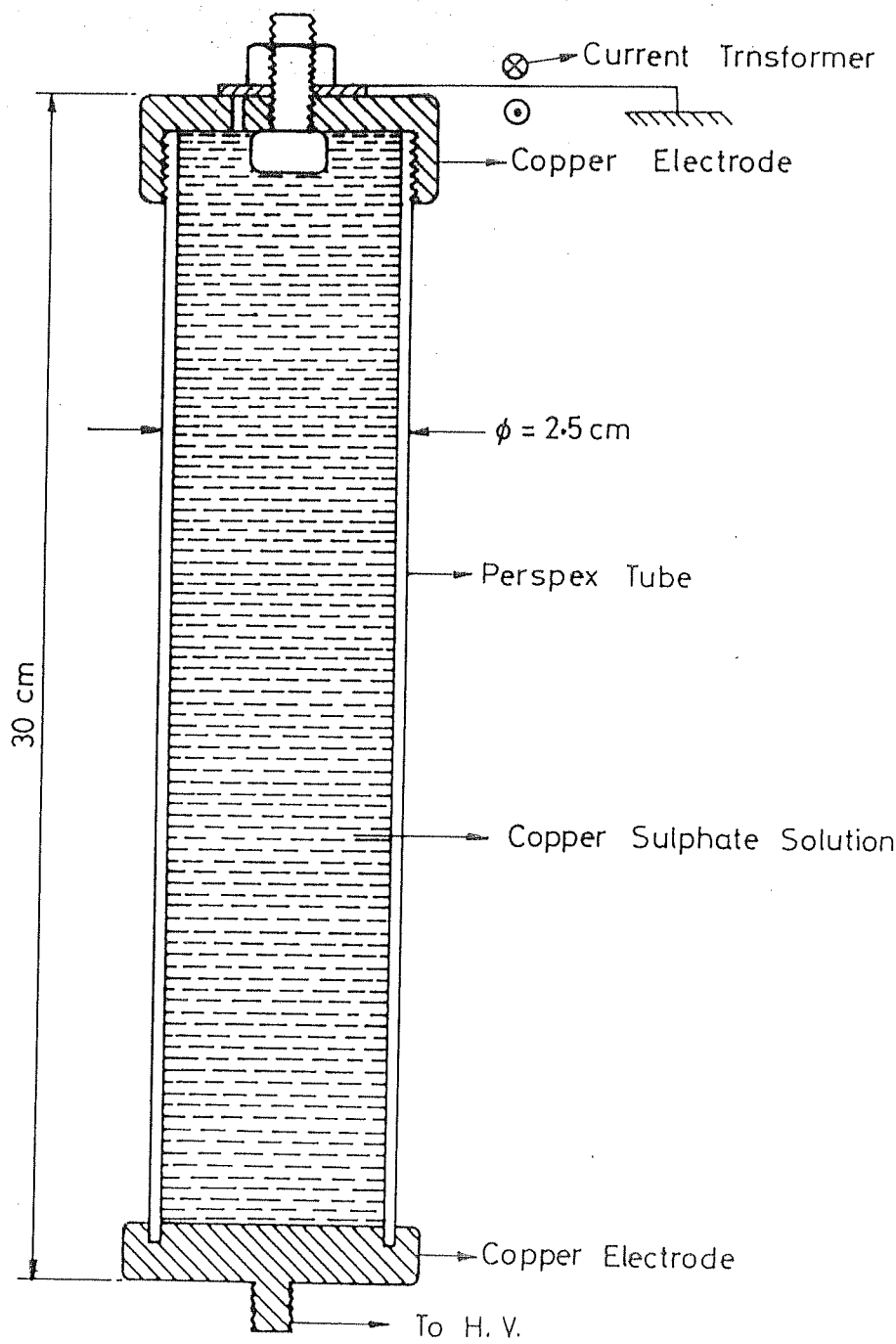

Fig. 2.8: Copper sulphate solution resistance.

passive integrator, and the output was corrected wherever the time constant of the passive integrator was inadequate. They were used to measure the diode current and net currents in the torus. Smaller Rogowski coil (15 cm diameter) which could be moved along the major radius was used to obtain the gross motion of the net current channel in the torus. These coils were fabricated with enameled copper wire or insulated copper wire. The coil is kept in a metallic housing with a toroidal cut for magnetic field penetration. One end of the coil is brought back through the turns of the coil (as shown in fig. 2.10) to cancel the one turn loop signal due to axial fields. The leads of the coil are brought out with a twisted pair, shielded in an s.s. tube, to the BNC connectors from where a coaxial cable carries the signal to the oscilloscope.

2.4.5 Magnetic probes

The poloidal magnetic field and changes in toroidal magnetic fields were measured with the help of small magnetic probes. The magnetic probes were wound on an insulator piece and potted with epoxy. The leads were taken out like in the case of Rogowski coils. To reduce the electrostatic noise pickup by the probe, a probe with a center tap was used. That is, the probe is essentially made of two coils, with sense of winding opposite to each other. The signal induced due to the changes in the magnetic field is opposite in both these coils. These two signals were brought to the scope, integrated and one signal was inverted and added to the other at the oscilloscope. This inversion eliminates the electrostatic pickup to a very large extent. Even though this arrangement worked well in measuring the poloidal field, during the diamagnetic measurements (i.e. changes in toroidal field) this was found to be inadequate. The two probes which were adjacent to each other picked up different

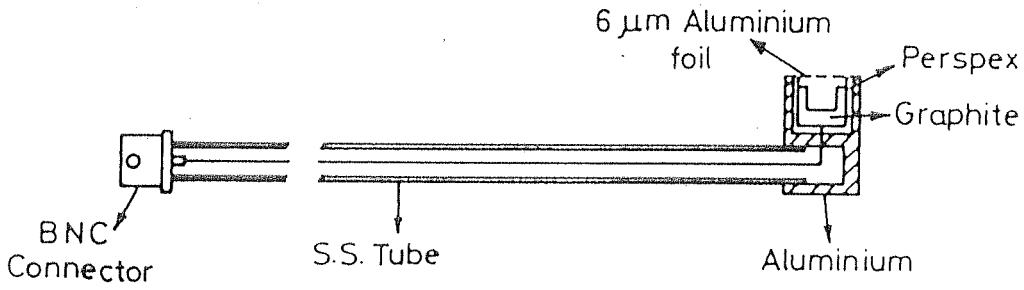

Fig. 2.9: Miniature Faraday cup.

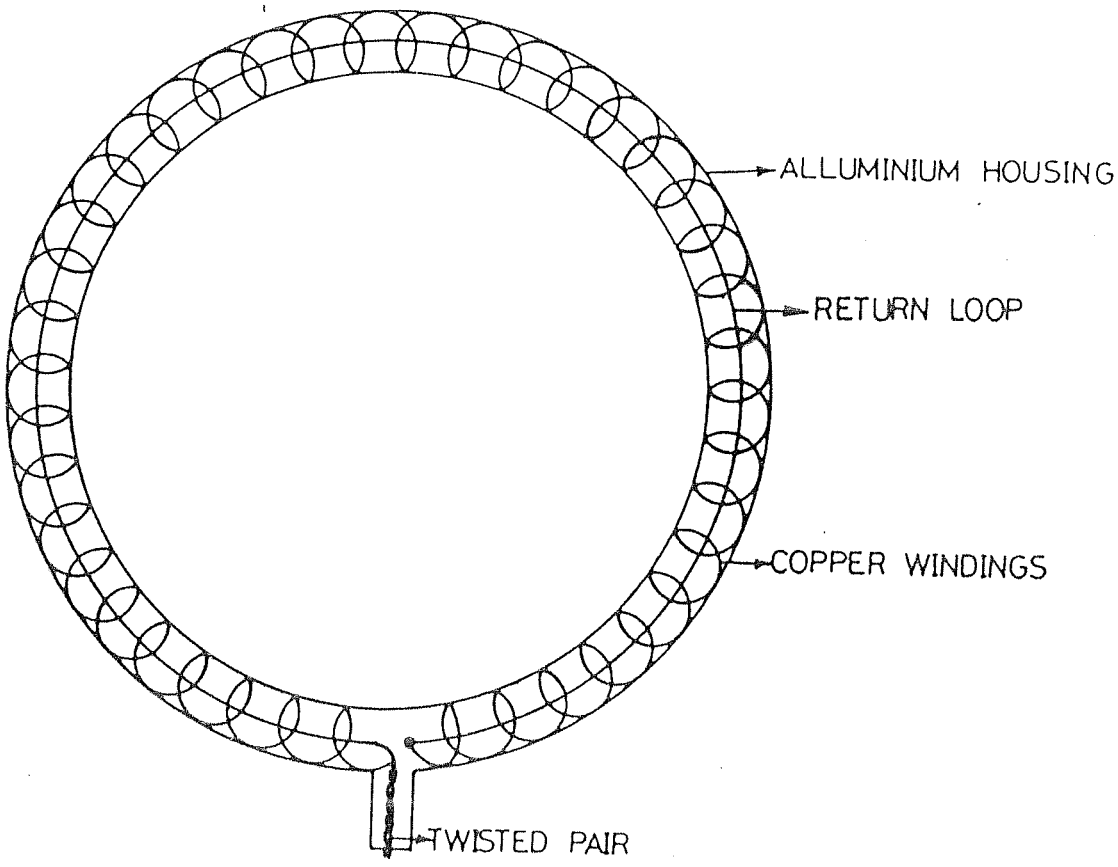

Fig. 2.10: Rogowski coil.

electrostatic noise and could not be eliminated. To overcome this problem the two coils of the probe were wound such a way that between every two turns of a coil there was one turn of the second coil (bifiller winding). This type of winding worked satisfactorily for the diamagnetic measurements. The magnetic probes were electrostatically shielded with an aluminium foil.

2.5 Grounding and shielding

Since the experiment is a pulsed one involving high voltages and currents, proper grounding of various systems is essential for safety of the personnel and equipment. Since the experiment also involves fast switchings, shielding from the electromagnetic and electrostatic noise is an important aspect in data collection. A grounding scheme was developed and implemented, where all the systems such as beam generator, data acquisition equipment were grounded on the vacuum vessel, which in turn was earthed at a single point. As far as possible, loop formation (including ground loops) was avoided. The oscilloscopes were delinked from the power ground using isolation transformers. Pulse transformers with proper isolation voltages were used in the triggering circuits to provide isolation from the high voltage and to delink them from the high voltage supply grounds. In addition, the coaxial cables which carry the signals to the data recording equipment (oscilloscopes) were enclosed in a copper pipe to shield from electrical noise. The oscilloscopes were kept in a shield room so as to reduce the noise pick-up. These measures improved the signal to noise ratio and almost completely eliminated misfiring due to false triggering.

2.6 Triggering sequence

The experiment is a pulsed one and involves triggering of various systems with pre-set time delays. In the experiment, various systems have different response and operating times. The gas valve had to be opened for about 15 ms, the toroidal and vertical magnetic field rise time is typically few ms, the plasma gun operates for less than a ms, the beam generator operates for few μs and the beam injection is for less than a μs. Proper time synchronizaion with minimum jitter of various triggerings is a pre-requisite of the experiment.

In the experiment the triggering sequence is as follows. Initially the gas valve is opened. After about 12 ms delay the toroidal field is switched on. The toroidal field reaches its peak value in about 3.5 ms. Plasma gun is fired after 3ms from the start of toroidal field. Beam is fired at the peak of the toroidal field. Since the beam life time is less than 100 μs, the beam generator should be reliably fired at a pre-determined delay with respect to the plasma gun firing. Any jitter in the plasma gun firing or the beam generator firing has to be avoided since this can lead to beam injection into an improper plasma filling. To avoid this the beam generator is triggered with a pulse derived from the plasma gun discharge current with a pre-set delay time. After the plasma gun discharge is over, the gas valve is closed. Time sequence of the various triggering events is shown in fig. 2.11(a). The oscillogram shown in fig 2.11(b) shows the actual time sequence in the experiment.

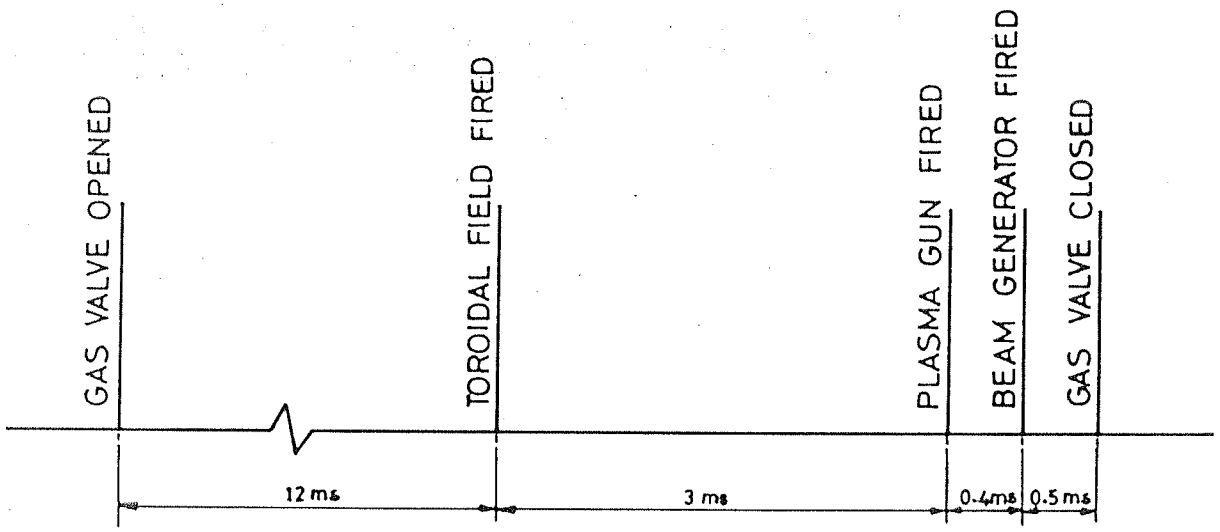

(a) Time delays between various triggerings

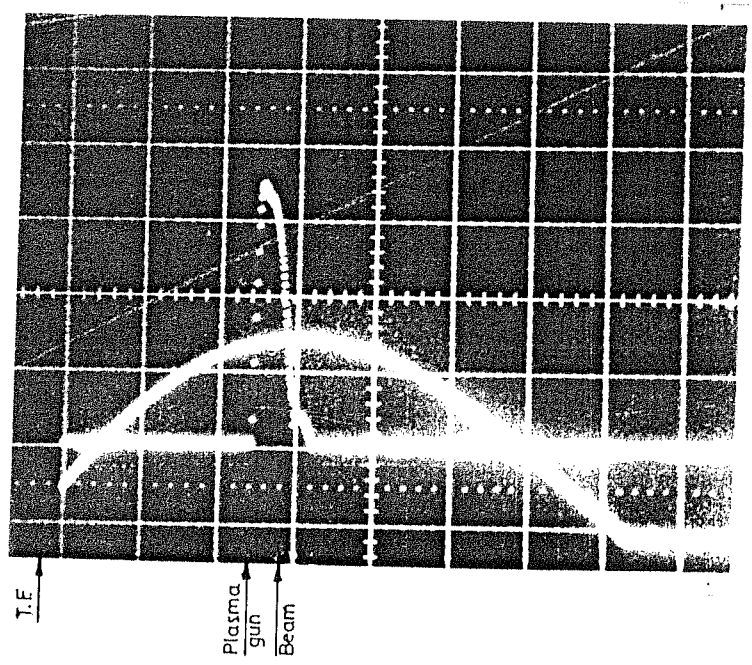

(b) T.F., Plasma gun and beam generator firing sequence in the experiment; sweep speed 1ms/div.

Fig. 2.11: Triggering sequence.

CHAPTER-III

RESULTS AND DISCUSSION

In this chapter the main results of the experiment are presented and discussed. For the sake of continuity relevant physical processes are also discussed at appropriate places.

The beam injection experiments were carried out in hydrogen plasma with two different plasma densities categorized as low and high densities. This was achieved by operating the plasma gun with two different pulse forming networks. In the case of injection into low density plasma the vertical magnetic field was varied from 0 to 200 gauss. No appreciable difference was found in the diode current, net current and the beam current profiles with varying the vertical field. The toroidal magnetic field and the delay between the plasma gun discharge and the beam injection were optimized with respect to the net current near the cathode. These values are 1.0 kgauss and 100 μs respectively. In the high density case no vertical field was used and the optimized values of toroidal field and the delay were about 500 gauss and 400 μs respectively.

3.1 Plasma Pre-fill

Plasma is injected into the torus from a radial port. For the experiment, the plasma gun was operated in three different modes characterized by three different pulse forming networks (PFNs) used for the gun operation. In the first case a seven stage PFN consisting of 5.0 μF capacitors and 1.0 μH inductors was used. To match the PFN

impedance with that of the gun (fraction of a Ohm), a series resistance was used in the transmission line. This reduced the available energy for gun operation to about 15% of that stored in the capacitors. Henceforth this case will be referred to as low power short pulse (LPSP) case. In the second case referred to as high power short pulse (HPSP), a low impedance four stage PFN (consisting of 60 μF capacitors and 1.0 μH inductors) was used. In the third case, called High power long pulse (HPLP), a four stage PFN with 700 μF capacitors and 5.0 μH inductors was used.

The plasma gun discharge current is shown in fig. 3.1(a), 3.1(b) and 3.1(c) for the three cases respectively. The discharge current in the LPSP case is unipolar (due to the series resistance) with a peak current of about 1.5 to 2.0 kAmps and with a main pulse duration of about 100 μs. In the HPSP case (fig. 3.1(b)), peak discharge current is about 14 kAmps with about 100 μs main pulse duration. This is a ringing pulse (no series resistance has been used in this case). In the HPLP case, the peak discharge current is about 12-13 kAmps, but lasts for much longer time, the total duration being about 800 μs. Here the gun impedance is higher than the PFN impedance. The main pulse lasts for more than 400 μs.

The gun was operated with a pulsed electromagnetic (em) valve in the LPSP case and with a piezo-electric valve in the HPLP case. In the HPSP case, the gun was operated with em valve for plasma injection experiments and with piezo-electric valve for beam injection experiments. In all the beam injection experiments the gas puffing was with a piezo-electric valve.

Typical ion saturation current in the LPSP case is shown in fig. 3.2(a). The ion saturation current is spiky in nature

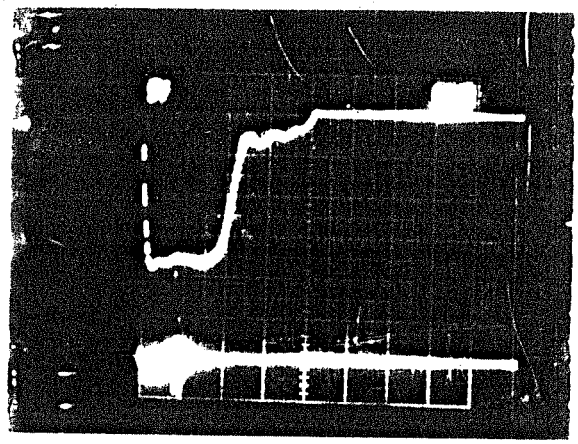

(a) Low power short pulse (LPSP); vertical scale 500 Amps/div., horizontal scale 50 us/div.

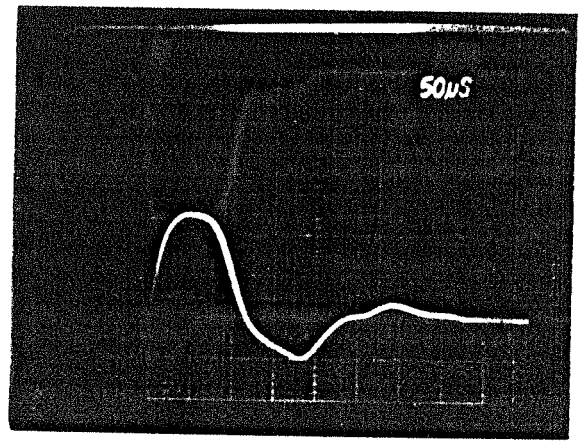

(b) High power short pulse (HPSP); vertical scale 5 kA/div.

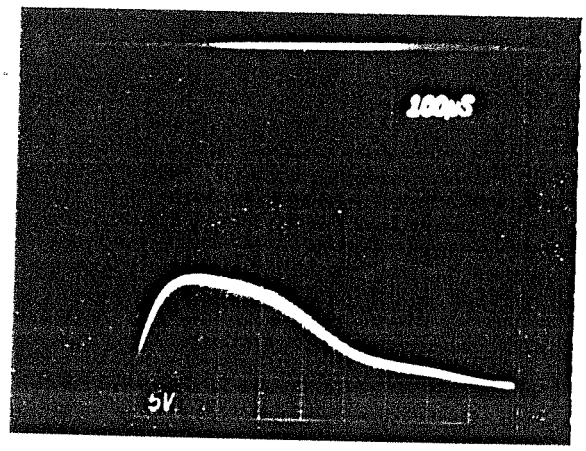

(c) High power long pulse (HPLP); vertical scale 5 kA/div.

Fig. 3.1: Plasma gun discharge current

and the average density corresponds to about 1 x 10^{11} cm^{-3}. In the plasma injection experiments it was also found that the plasma did not penetrate more than a few cm across the toroidal field. Both these observations (low plasma density and improper plasma filling of the torus) prompted us to use a lower impedance bank (HPSP case). A typical ion saturation current is shown in fig. 3.2(b). In this case even though the peak densities obtainable are high, these peak densities do not occur at the same time at different toroidal locations. The maximum density that could be used for beam injection was about 5 x 10^{12} cm^{-3}. A radial profile of the density is shown in fig. 3.3. In this case the pulse length of plasma gun discharge ($\approx$100 μs) is comparable to the propagation time of plasma around the torus. Fig. 3.2(c) shows the ion saturation current in the case of HPLP operation of the plasma gun. The peak densities obtained are 5 x 10^{13} cm^{-3}; the peak densities coming after 200 μs at θ = 180° (θ is the toroidal angle) from plasma gun. Plasma density profile at θ = 180° for this case is shown in fig. 3.4. The density is high (10^{13} cm^{-3}) from the outer wall to the minor axis but falls sharply to less than 10^{12} cm^{-3} beyond the minor axis.

To avoid large amount of neutral gas in the system, which may be detrimental for the diode operation, the gas puffing was done with a piezo-electric valve. The time evolution of gas pressure in this case is shown in fig. 3.5(a). The valve is kept open for about 10 to 15 ms before the plasma gun is fired, so that there is enough gas in the plasma gun for the gun operation. As can be seen from the oscillogram (fig 3.5(a)), there is almost no change in the pressure for the first 15 ms. Even after these 15 ms the pressure rise is marginal compared to that of em valve case. The maximum pressure is about 5 x 10^{-5} Torr when the piezo-

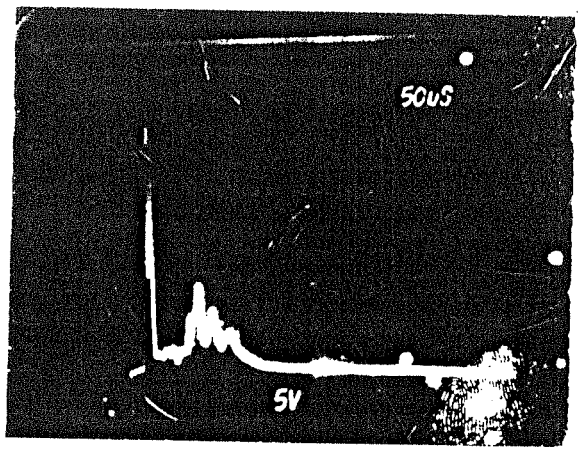

(a) LPSP

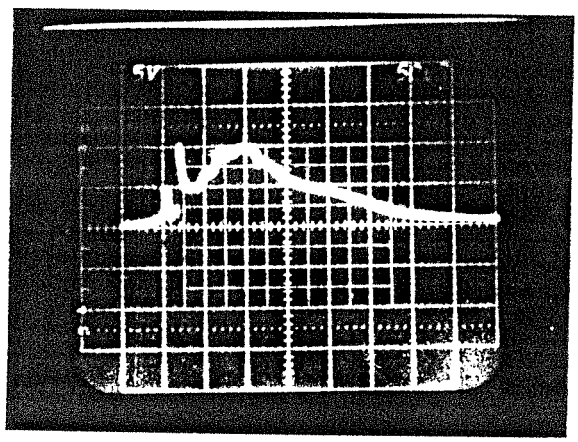

(b) HPSP

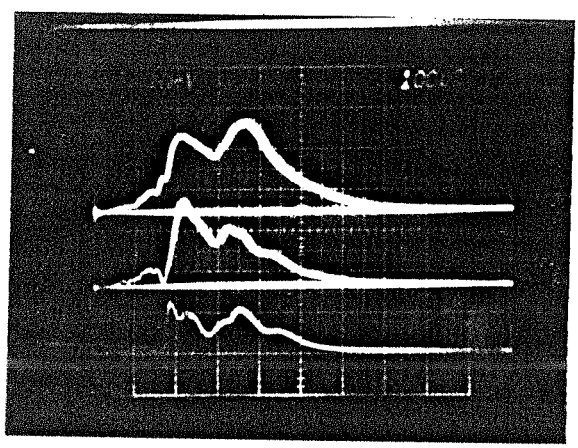

(c) HPLP

Fig. 3.2: Ion saturation current

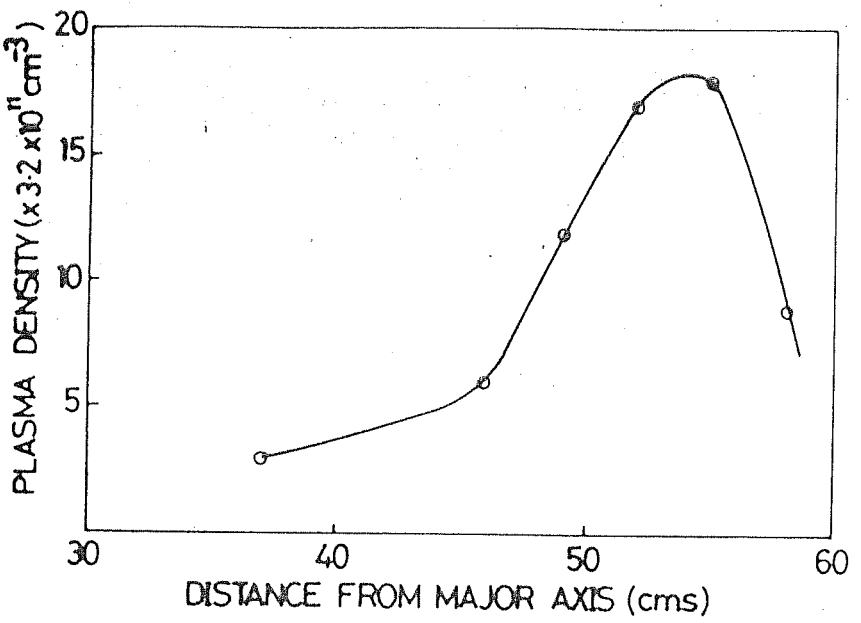

Fig. 3.3: Radial profile of plasma density (HPSP)

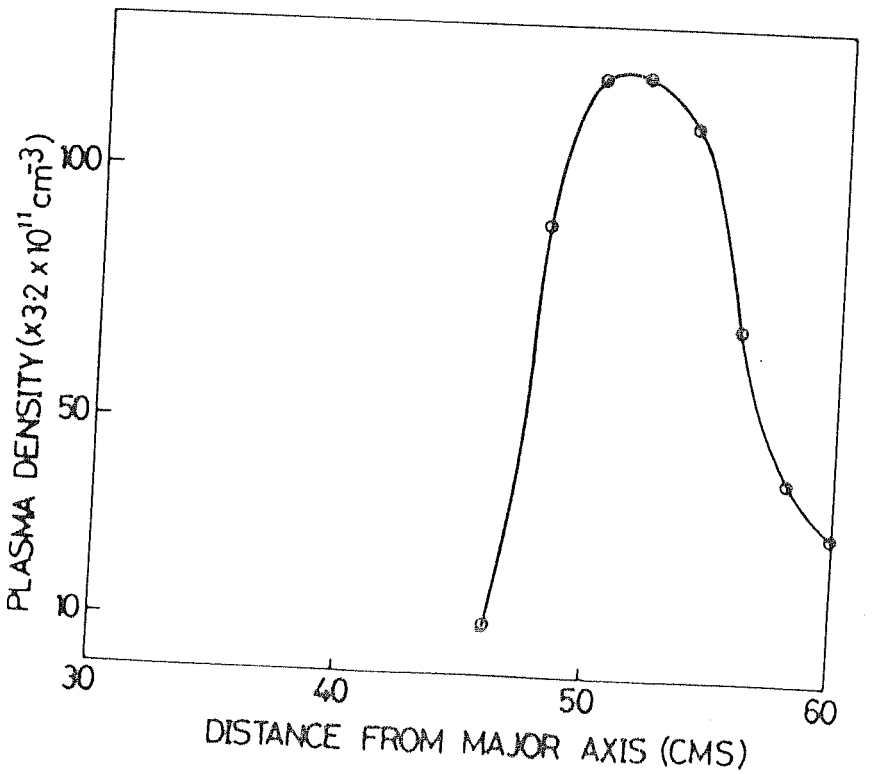

Fig. 3.4: Radial profile of plasma density (HPLP)

electric valve is used for puffing the gas.

The above measurements were made with pulsing the gas valve but without firing the gun. An attempt was made to see whether the plasma gun discharge brings an extra amount of gas into the system by eroding the washers (which has been actually seen when the plasma gun is operated in HPLP mode). The pressure is monitored with an ionization gauge mounted on the top port near the plasma gun location. Fig. 3.5(b) shows the typical response of the ionization gauge when the plasma gun is operated. Piezo valve is opened for about 15 ms prior to the plasma gun firing. As can be seen from this figure, the rise in the pressure is negligible during the plasma gun operation. For few milliseconds after the gun is fired, the pressure is less than 6×10^{-5} Torr. (But this slow rise could be due to the mounting of the ionization gauge head and the associated electronics as well, in which case this pressure is an underestimate of the actual pressure).

3.2 Plasma anode operation

In the plasma anode technique, a high density plasma is injected into the anode-cathode gap (plasma filled diode of Miller et al., 1975) or the cathode is immersed in the plasma (Mohri et al., 1979). In the latter case, where there is no material anode present, is commonly known as the plasma anode method. In both the above cases the behavior of the sheath, which is formed at the cathode surface, is same as long as the physical separation between the ground and the negatively biased cathode (Miller et al., 1975) is more than the sheath thickness. A brief description of the physical processes followed by our experimental observation and their comparison with the theoretical predictions is given here.

The formation of a transient sheath and its time

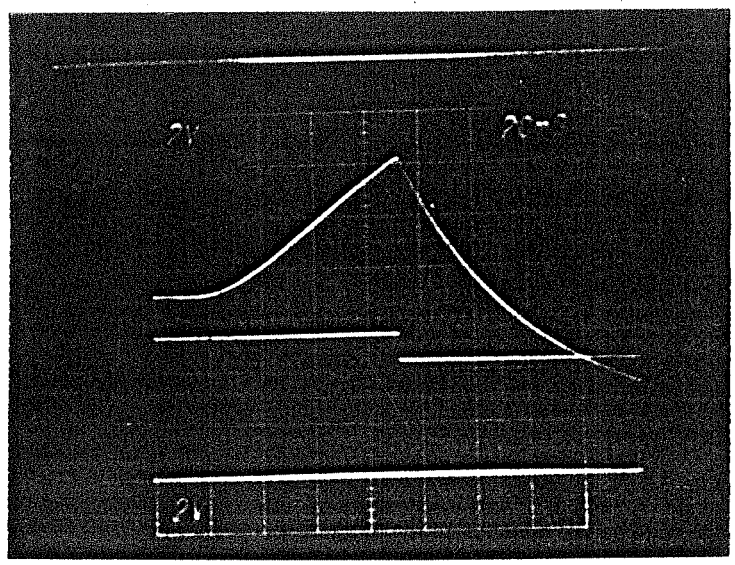

(a) Without firing the plasma gun;
sweep speed 20 ms/div.

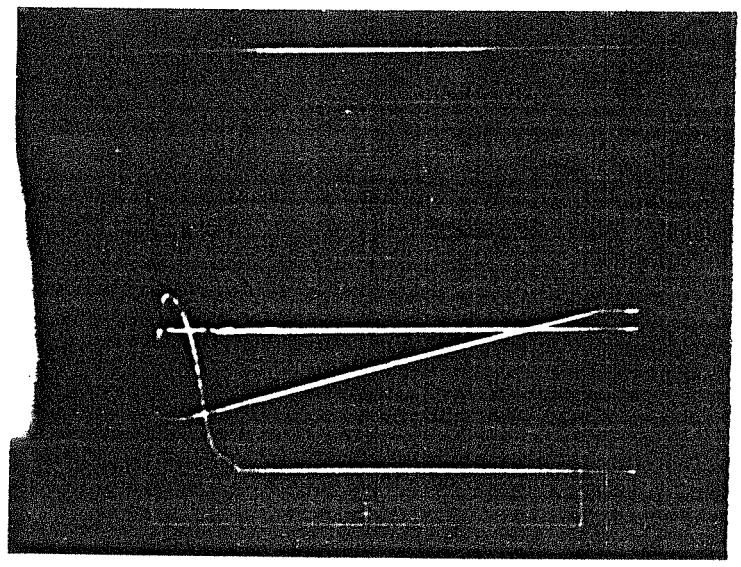

(b) With plasma gun firing sweep speed 500 us/div.

Fig. 3.5: Time evolution of neutral gas pressure

evolution at the surface of an electrode immersed in plasma on which a high negative voltage, V_o ($eV_o \ll KT_e$, where K is the Boltzmann's constant and T_e is the plasma temperature) is impressed has been investigated by Sander, (1969); Alexeff et al., (1969); Widner et al., (1970) and Widner and Poukey, (1976). The transient sheath thickness in case of a step voltage was found to be given by

$$x_t = \left(\frac{2eV_o}{KT_e}\right)^{1/2} \lambda_D \qquad (3.1)$$

where λ_D is the Debye length.

Now consider a cathode immersed in a plasma of uniform density, n and Temperature, T_e driven with a step negative voltage V_o, such that $eV_o \ll kT_e$ and let the sheath thickness at any instant of time be $x = x(t)$. Using Miller's model for plasma filled diode (Miller et al., 1975), which considers the sheath thickness as the anode-cathode gap of conventional diode, we can estimate the accelerated REB current. In a plane parallel geometry the electron and counter streaming ion current densities flowing across the sheath of thickness x are given by Langmuir's expressions (Langmuir, 1929) for the space charge limited, bipolar flow (relativistic effects neglected)

$$J_e = 1.86 \left(\frac{4\epsilon_o}{9}\right) \left(\frac{2e}{m}\right)^{1/2} \frac{V_o^{3/2}}{x^2} \qquad (3.2)$$

and

$$J_p = (m/M)^{1/2} J_e \qquad (3.3)$$

where J_e and J_p are the electron and ion current densities, e is electronic charge, m and M are the masses of electron and ion respectively, ϵ_o is the permittivity of free space.

The space charge limited current density J_p, given by

eq. (3.3) is the value required for the electric field to become zero at the plasma boundary of the sheath. If the maximum positive ion current density J_{ps} that can be supplied by the plasma is less than J_p, then there will be an electric field at the plasma-sheath boundary. This electric field drives away the plasma electrons from the boundary as a result of which positive ions are uncovered and the sheath thickness increases. If the increase in the sheath thickness is δx in a time δt, the positive charge uncovered per unit area is $ne\delta x$. This uncovering of positive ions constitutes a current, the density of which is given by

$$J_p = ne \frac{dx}{dt} \tag{3.4}$$

where n is the plasma density and dx/dt is the rate at which sheath thickness increases. Eq. (3.4) is valid as long as

$$ne \frac{dx}{dt} \geq ne \left(\frac{KT_e}{M}\right)^{1/2}$$

i.e.
$$\frac{dx}{dt} \geq v_{ia} \tag{3.5}$$

where v_{ia} is the ion acoustic velocity.

Beyond this time, i.e., when the sheath expansion velocity falls below the ion acoustic velocity, a rarefaction wave separates from the sheath and propagates into the plasma (Miller et al., 1975 and Widner and Poukey, 1976). Behind this rarefaction wave the space charge sheath approaches the equilibrium Langmuir sheath and the ion current required by eq. (3.3) is provided by the wave accelerated ions streaming into the sheath.

For a step voltage the sheath velocity is obtained by substituting eq. (3.4) for J_p in eq. (3.3)

$$\frac{dx}{dt} = \frac{1.86}{ne} \left(\frac{4\epsilon_o}{9}\right) \left(\frac{2e}{M}\right)^{1/2} \frac{V_o^{3/2}}{x^2} \qquad (3.6)$$

This is same as the equation obtained by Widner and Poukey, (1976) except for the factor 1.86, which appears through the definition of J_e in eq. (3.2). Following Widner and Poukey, (1976) we can write the sheath velocity as

$$\dot{x} = \frac{1}{ne} \left(\frac{4\epsilon_o}{9}\right) \left(\frac{2e}{M}\right)^{1/2} \frac{V_o^{3/2}}{x^2}$$

$$= k_1 \frac{V_o^{3/2}}{x^2} \qquad (3.7)$$

where $k_1 = \frac{1}{ne} \left(\frac{4\epsilon_o}{9}\right) \left(\frac{2e}{M}\right)^{1/2}$

By integrating eq. (3.7), we get the sheath thickness, x which is given by

$$x^3 = x_t^3 + 3k_1 V_o^{3/2} t \qquad (3.8)$$

where x_t is the transient sheath thickness at time, t = 0. In practice, however the voltage rises with a finite rise time and hence eq. (3.8) should be treated as an upper limit of the sheath thickness. The sheath thickness at $dx/dt = v_{ia}$ is given by

$$x_b = 0.793 \left(\frac{eV_o}{KT_e}\right)^{3/4} \lambda_D \qquad (3.9)$$

and occurs at time, $t = t_b$ given by

$$t_b = \frac{3}{2^{5/2}} \frac{1}{w_{pi}} \left[\frac{(x_b^3 - x_t^3)}{\lambda_D^3 \left(\frac{eV_o}{KT_e}\right)^{3/2}}\right] \qquad (3.10)$$

where w_{pi} is the ion plasma frequency.

The equilibrium Langmuir sheath thickness is given by (Widner and Poukey, 1976)

$$x_L = 1.31 \left(\frac{eV_o}{KT_e}\right)^{3/4} \lambda_D \qquad (3.11)$$

In applications to produce REBs, a high negative voltage (of the order of hundreds of kV) is applied for a time t_o (≈100 ns). If the plasma anode is to work, the sheath should be confined to a distance, d, comparable to the normal anode-cathode gaps (≈1 cm). Under these conditions we can find the minimum required plasma density, n_{min} (Widner and Poukey, 1976) and is given by

$$n_{min} = 10^{12}\, t_o\, \frac{V_o^{3/2}}{d^3} \qquad (3.12)$$

where n_{min} is expressed in cm^{-3}, t_o in seconds, V_o in volts and d in cm.

Using eq. (3.12), the minimum required plasma density for our experimental conditions of $V_o \approx 100$ kV, $d \approx 1.0$ cm and $t_o \approx 100$ ns is about 3×10^{12} cm^{-3}. Since our operation of the beam generator is typically in the density range of 5×10^{12} cm^{-3} to 10^{13} cm^{-3}, the requirement for plasma anode method to work is satisfied.

The actual diode voltage and current waveform calculation involves solving of the above equations for sheath evolution and space charge limited current flow together with the circuit equations of the beam generator, pulse forming line and the diode (Miller et al., 1975, Bailey et al., 1983). However, for an understanding of the general behavior of the diode operation, the experimentally observed diode currents can be compared with the expected diode currents in the appropriate limits.

Beam injection is studied in two different plasma fillings. The two plasma fillings correspond to the operation of the plasma gun in HPSP and HPLP modes, as described

earlier. They will be referred to as low density and high density respectively. The diode current in the low density case is shown in fig. 3.6. The peak current is about 15 kAmps with a duration (FWHM) of 100 ns. Beam injection into high density yielded a peak current of about 12 kAmps with a duration (FWHM) of 200 ns as shown in fig. 3.7.

The peak current in the low density case is higher than that in the high density case contrary to the expectations. This is likely due to emission from the inner conductor (cathode stalk) of the vacuum transmission line connecting the water line and the diode. In the high density case the current lasts for longer time than the voltage pulse, which is typically 100 ns (foil covered Faraday cup in front of the cathode show a pulse of about 100 ns). Currents lasting for times longer than the voltage pulse duration have also been observed by Bailey et al., (1983).

The maximum sheath thickness is given by eq. (3.8), where t is at the end of the voltage pulse duration, if the sheath expansion continues till the end of the voltage pulse. Otherwise the expression given in eq. (3.9) should be used for the sheath thickness to calculate the currents. That is, the lower value of the sheath thickness obtained from eq. (3.8) and (3.9) should be used. Since this is the maximum value of the sheath thickness, the current calculated will be the lower limit (I_L). The upper limit (I_U) can be obtained by using the transient sheath thickness at t = 0. The actual observed peak current (I_O) should be within these two limiting values. The table below (table 3.1) gives the values of these calculated limits and the observed currents for two different densities and for a step voltage of 100 kV and a plasma temperature of 10 eV.

The upper limit obtained from the calculation is

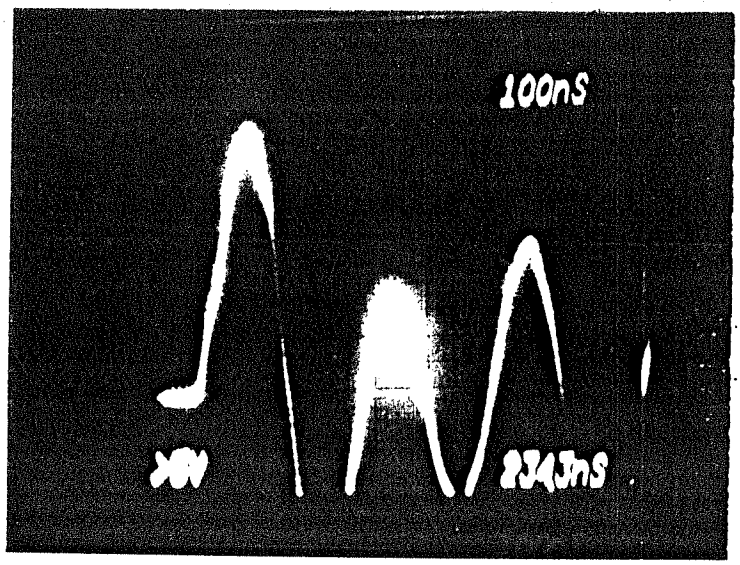

Fig. 3.6: Diode current (low density); 3 kA/div

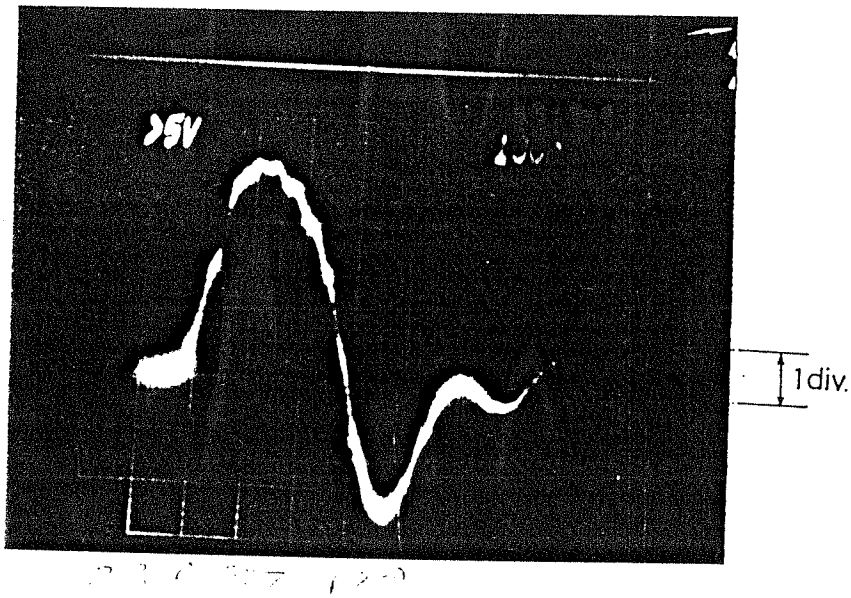

Fig. 3.7: Diode current (high density); 3 kA/div

considerably higher than the observed peak currents. This is only to be expected because of the step voltage used (Miller et al., 1975). In a more realistic case of a finite rise time, this would be lower. In conclusion the observed currents are with in the limits expected from plasma anode model calculations.

TABLE 3.1

n (cm_{-3})	λ_D (cm)	x_b (cm)	x_{100ns} (cm)	I_L (kAmp)	I_U (kAmp)	I_O (kAmp)
$5x10^{12}$	$1.0x10^{-3}$	0.15	0.83	1.4	41.3	15.0
10^{13}	$7.43x10^{-4}$	0.59	0.69	2.7	76.8	12.0

3.3 Characterization of the injected beam

To characterize the injected beam, measurements were done with a miniature Faraday cup in front of the cathode. The Faraday cup was used with and without a foil cover. These measurements for the two cases of beam injection viz. (1) into a low density plasma and (2) into a high density plasma are described here.

3.3.1 Beam injection into low density plasma

Plasma density near the cathode is about 5×10^{12} cm^{-3} in this case. A typical foil covered Faraday cup signal in front of the cathode at a toroidal location of $\theta = 22.5^{o}$ (θ is measured from the cathode) is shown in fig. 3.8(a). The ringing seen in the diode current (fig. 3.6) is due to mismatch of the impedances of the diode and the water line. (However, the beam injection is for about 100 ns as can be seen from the Faraday cup signal, fig. 3.8(a)). As shown in the oscillogram, fig. 3.8(a), the pulse duration is about 100

ns. The peak current density in the shadow of the cathode is about 10 Amps/sq.cm. A profile of the peak current densities is shown in fig. 3.9. This shows a relatively higher current density in the shadow of the cathode compared to the current density outside cathode shadow. The total current obtained from spatial integration of this profile is about 250 Amps.

Measurements with a foilless Faraday cup however showed much higher currents. A typical signal from the foilless cup is shown in fig. 3.8(b). The peak current densities in the shadow of the cathode are as high as 400 Amps./sq.cm. The total duration also is much longer (≈2.0 μs) than that observed from the foil covered cup and diode currents. A profile of the current density obtained from foilless Faraday cup is shown in fig. 3.10. This also show a higher current density in the shadow of the cathode than outside as was observed in the case of the foil covered cup. However the spatially integrated current in this case is about 10.0 kAmps.

The large difference in the Faraday cup measurements with and without foil is clearly evident. This is because of the stopping of the low energy part of the beam by the foil covered cup. The cut off energy of the aluminium foil that was used is about 25 keV. That is beam, electrons with energy 25 keV and less will not be able to penetrate through the foil. The percentage of transmission as a function of energy is shown in table 3.2 and the mean energy loss due to transmission through the foil for various beam energies is shown in table 3.3.

3.3.2. Beam Injection into high density plasma

Typical plasma densities in this case is about 10^{13} cm^{-3}. The signal from a foil covered Faraday cup in front of the cathode is shown in fig. 3.11(a). This shows a peak current

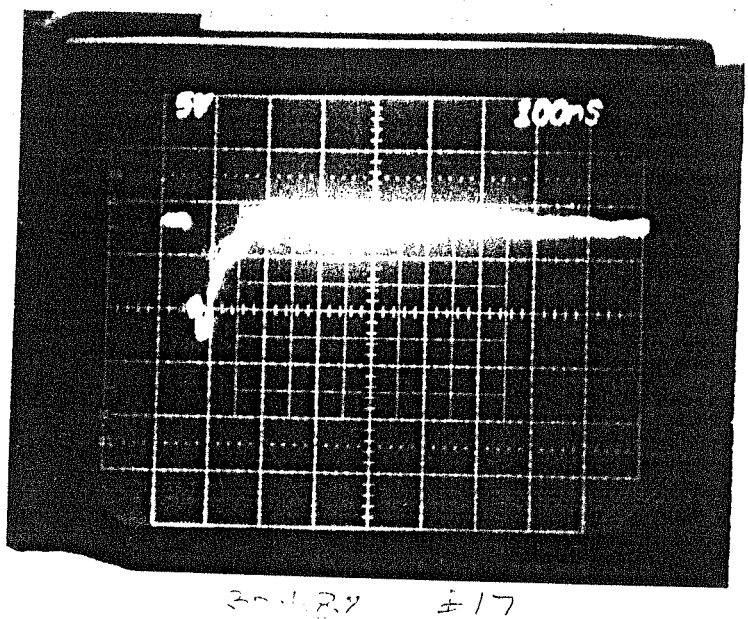

(a) With a foil cover; vertical scale: 5 Amps/div.

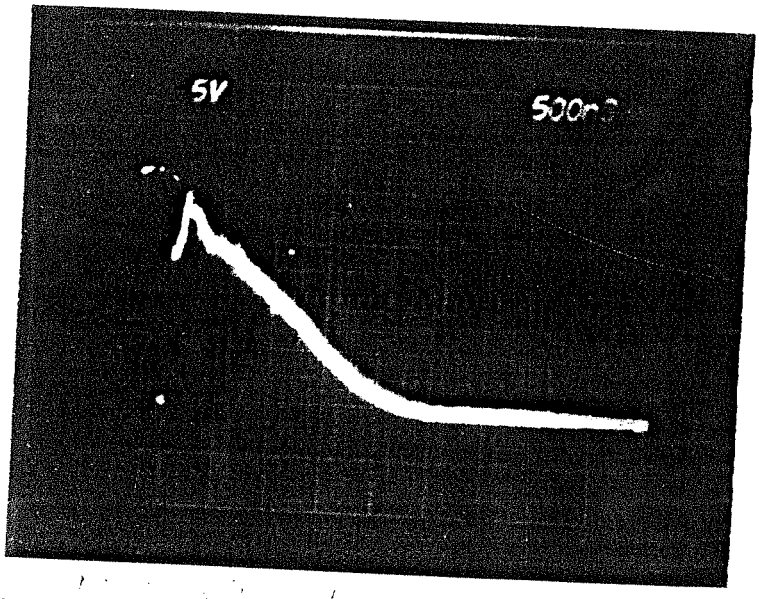

(b) Without a foil cover; vertical scale: 50 Amps/div.

Fig. 3.8: Current collected by the Faraday cup (low density)

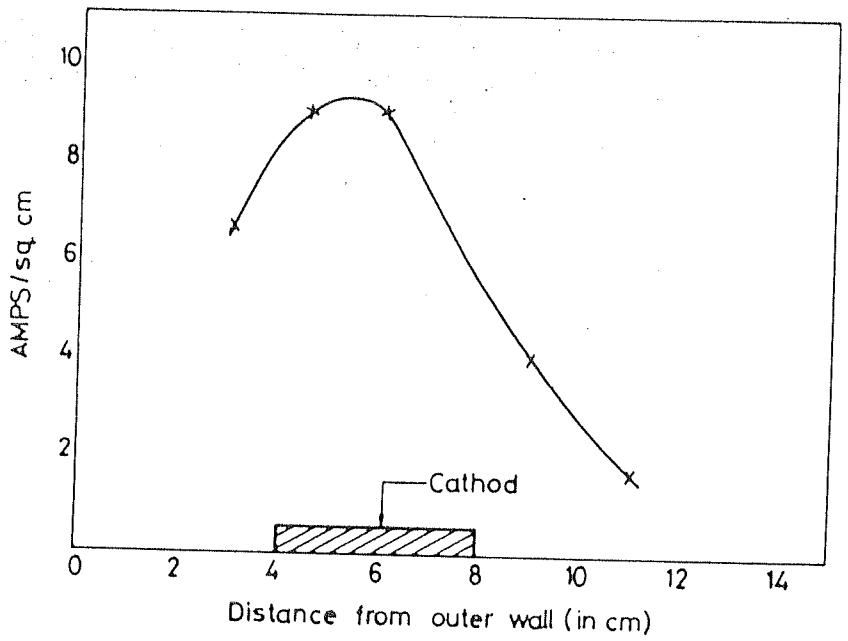

Fig. 3.9: Radial profile of the beam current (foil covered cup; low density)

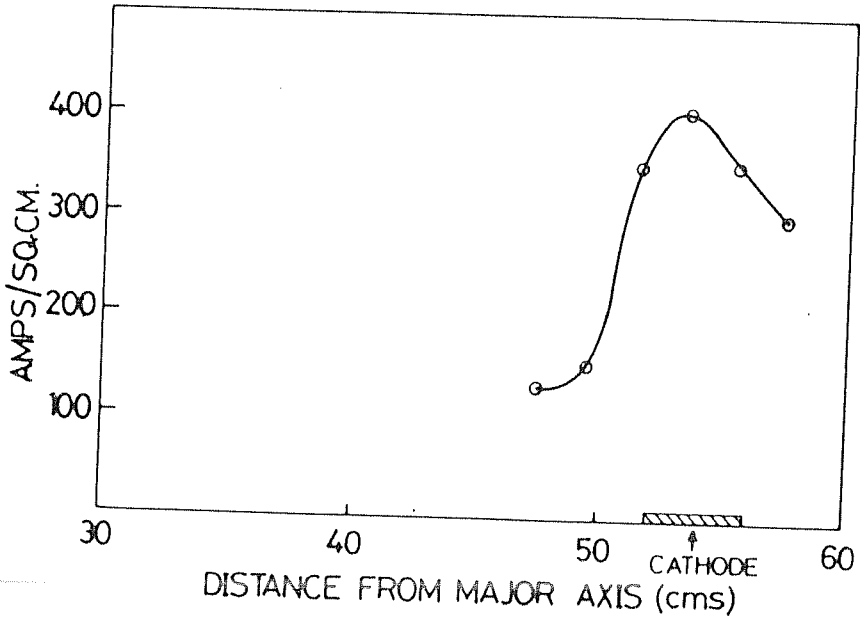

Fig. 3.10: Radial profile of the beam current (foilless cup; low density)

TABLE 3.2

Energy (in keV)	Transmittance(%)
10	2.7×10^{-9}
20	7.1×10^{-3}
30	0.11
40	0.28
50	0.45
60	0.57
70	0.66
80	0.72
90	0.78
100	0.81
110	0.84
120	0.86
130	0.88
140	0.89
150	0.90
160	0.91
170	0.93
180	0.93
190	0.94
200	0.94
210	0.95
220	0.95
230	0.95
240	0.96
250	0.96

density of about 60 Amps/sq.cm. with a duration of about 100 ns. This is higher than that obtained for injection into low density plasma which is about 10 Amps/sq.cm. A profile of this current density is shown in fig. 3.12. This profile also shows a higher current density in the shadow of the cathode compared to that outside the cathode shadow. The total spatially integrated current is about 2.0 kAmps.

TABLE 3.3

Beam energy (in keV)	Energy loss during transmission through foil
30	25.0 kev
50	13.5 kev
100	8.5 kev
200	5.5 kev

When a foilless Faraday cup was used for measuring the forward beam currents, the peak currents and the duration were much different from those measured by the foil covered cup. A typical signal from foilless cup is shown in fig. 3.11(b). These signals have a rise time of 200 - 300 ns. The total duration of these signals is about 2.0 μs. To get the total beam current that is injected, the spatial profiles of the beam current density as seen by the Faraday cup are obtained for different times in front of the cathode. The time evolution of the profiles is shown in figs. 3.13(a) and 3.13(b). These profiles show a high current density in front of the cathode with a sharp fall at the edges of the cathode. This feature is more prominent up to 500 ns. Even within the cathode region the current density peaks at the edge which is nearer to the outer wall up to 200 ns. Beyond this time the

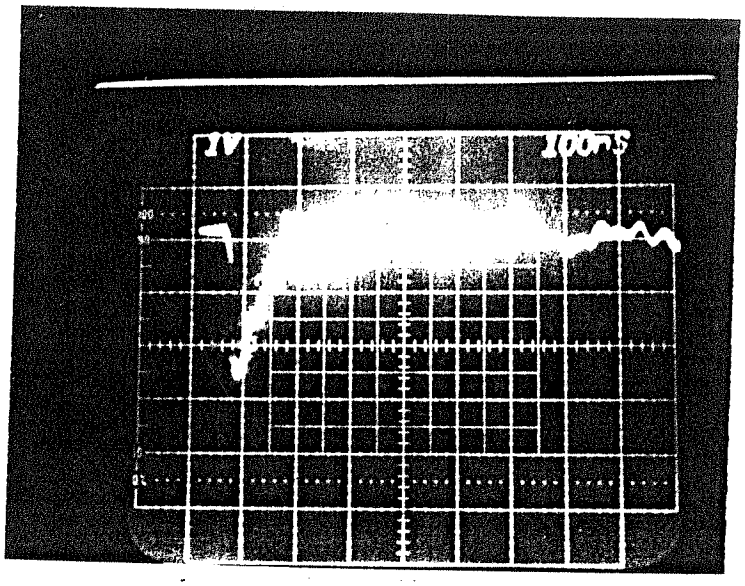

(a) With a foil cover; vertical scale 10 Amps/div.

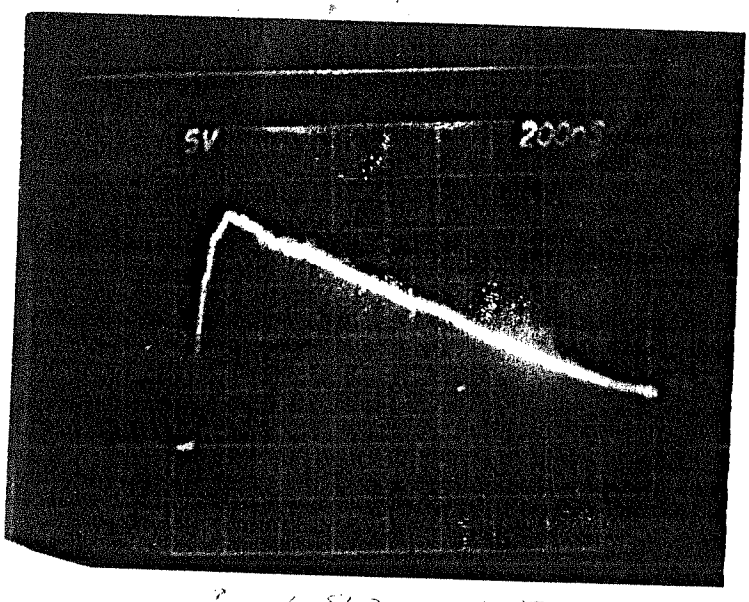

(b) Without a foil cover; vertical scale 50 Amps/div.

Fig. 3.11: Current collected by the Faraday cup (high density)

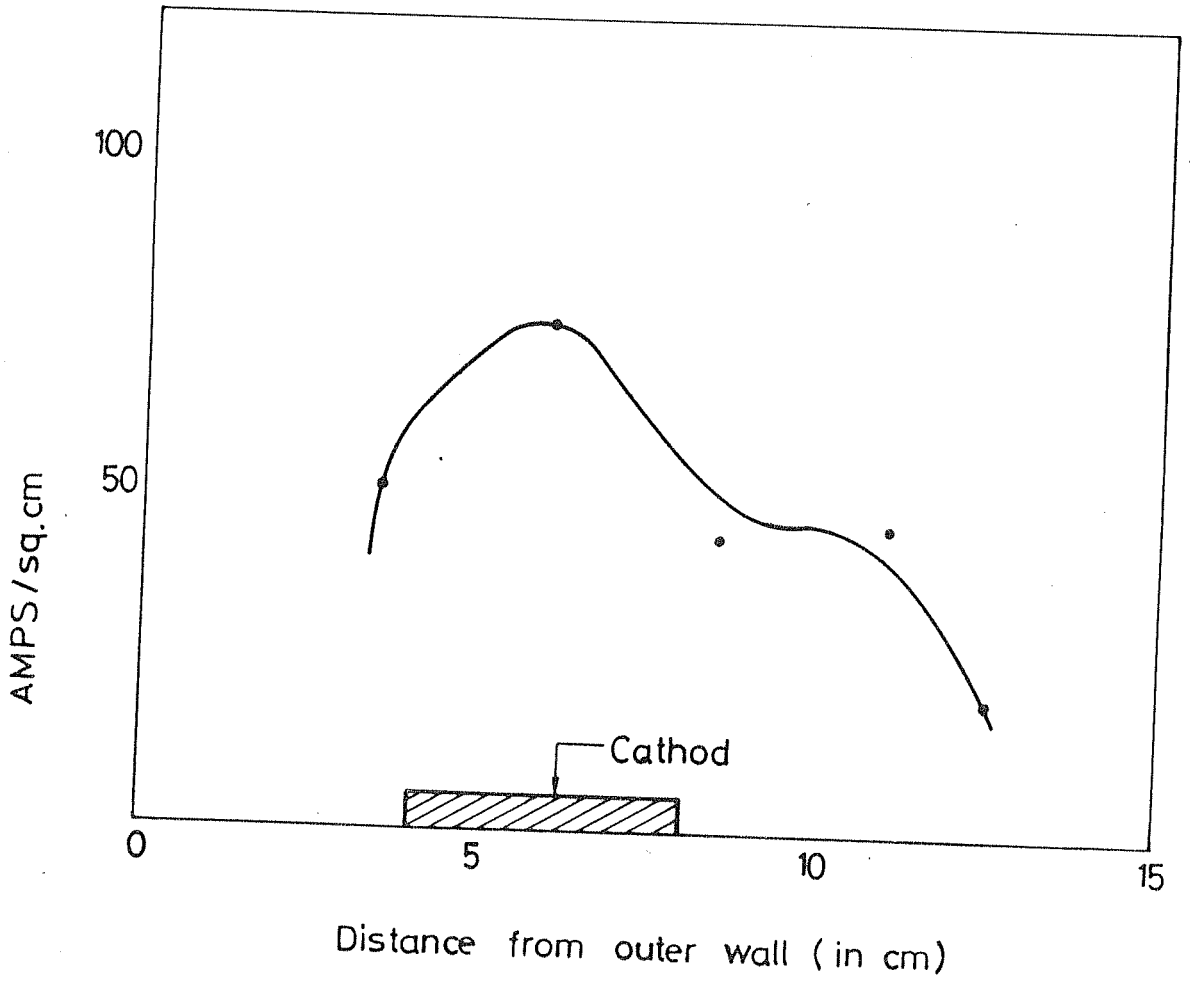

Fig. 3.12: Profile of the beam current density in front of the cathode (foil covered cup)

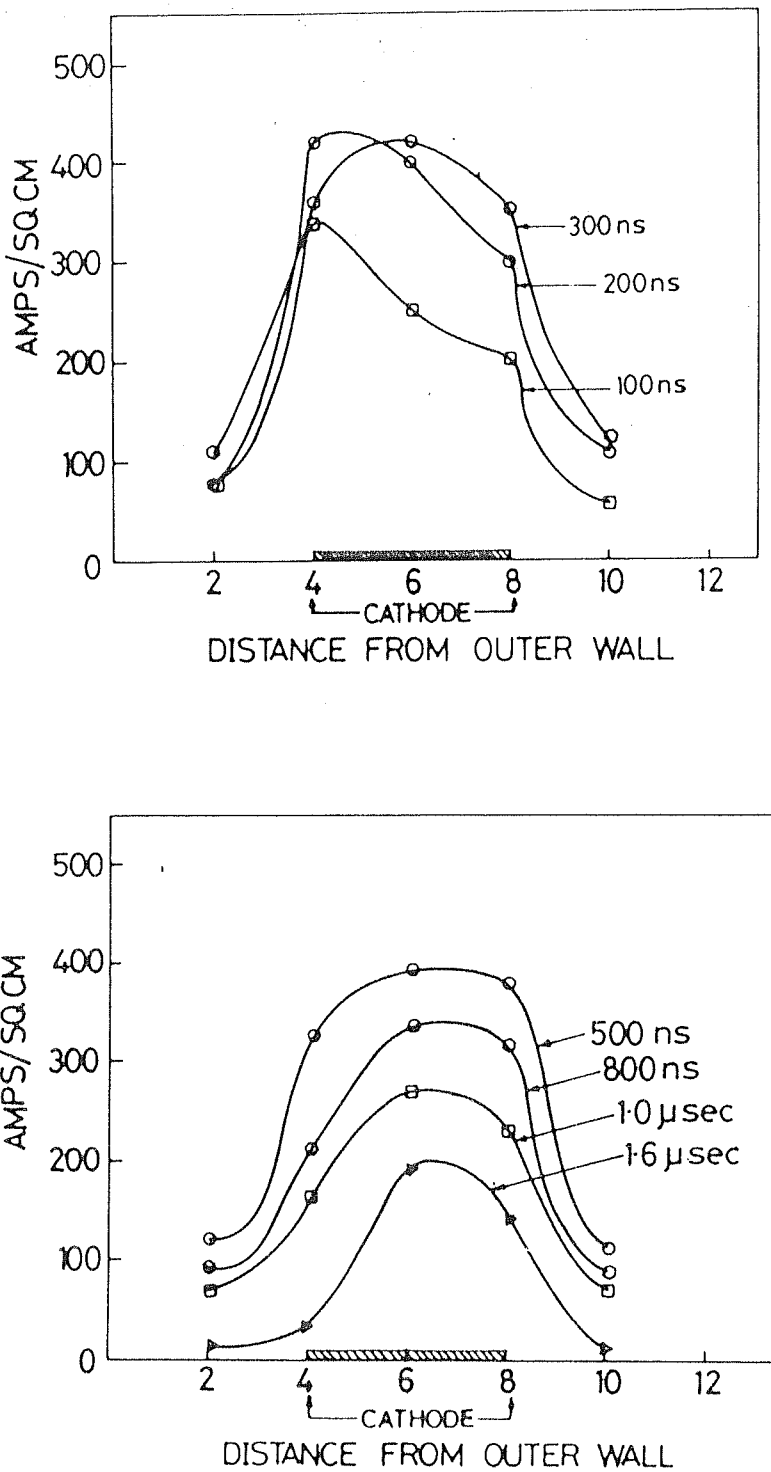

Fig. 3.13: Time evolution of beam current profile in front of the cathode (foilless Faraday cup)

peak of the profile is almost at the centre of the cathode. From the profiles of the current density, the total current injected is obtained and plotted against time (fig. 3.14). This shows a peak current of about 12 kAmps at about 350 ns. The diode current however shows a pulse duration of about 300 ns and a peak current of 12 kAmps (fig. 3.7). The main differences in these two figures (figs. 3.14 and 3.7) is the duration and the rise time. The duration of the current obtained from Faraday cup measurements is much longer (2.0 μs) than the diode current pulse duration (300 ns). The rise time of about 350 ns is also longer in the case of Faraday cup measurements than in the case of diode current.

The difference in the rise times can not be accounted as the beam slowing down as this gives unrealistically low beam energies. This indicates that there is some contribution other than that due to the beam in the foilless Faraday cup signals. A possibility is the Faraday cup collecting the plasma electron current. This view is supported by the fact that the Faraday cup current lasts much longer than the diode current. If the Faraday cup measurement represents the beam current, then after the peak of the diode current, the Faraday cup current should have been like the net current measured by Rogowski coil. Even after adding the trapped net current, a sharp fall is seen in the net current measurement (see fig.3.25), which is not seen in the Faraday cup measurements. A possible explanation for this difference is that the plasma potential is depressed in the beam channel, and the Faraday cup essentially acts like a probe collecting plasma electron current. Because of the high plasma density the plasma potential has to be depressed only by a few tens of volts to account for the high currents collected by the foilless Faraday cup.

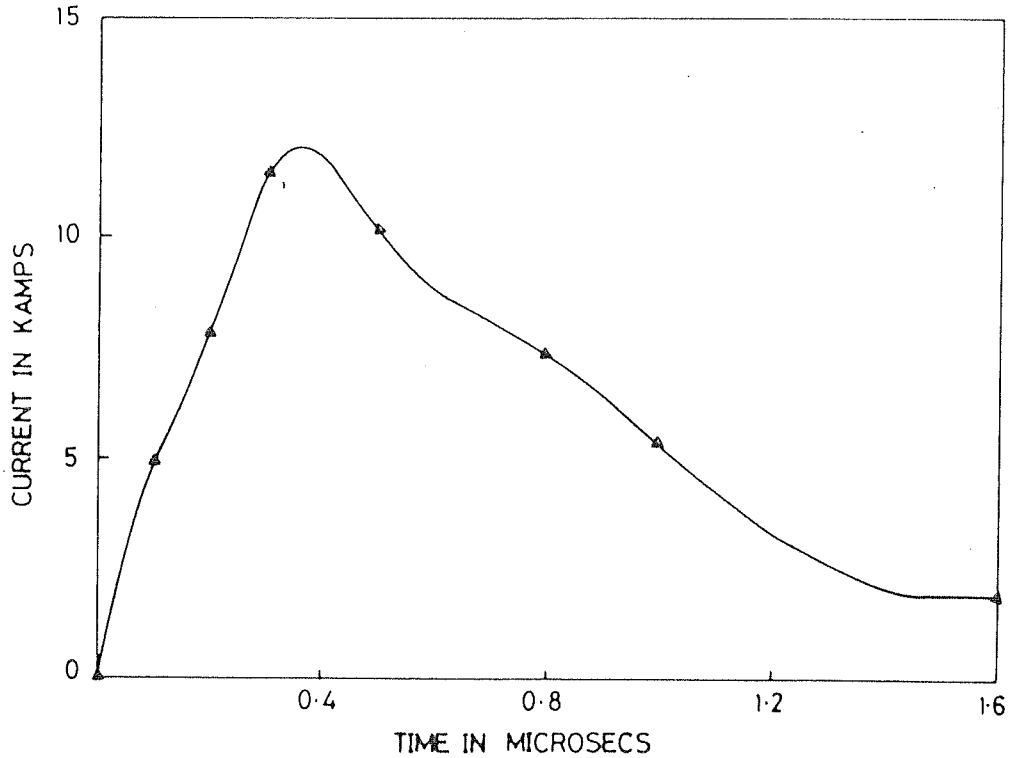

Fig. 3.14: Injected beam current vs. time

Even though there is gross difference in the measurements by the Faraday cup and the diode current, the spatial extent of the current density profile in front of the cathode is nearly same as the cathode dimensions. This indicates a well defined beam being injected into the plasma. The total current obtained from Faraday cup measurements should be treated as an upper limit of the injected beam current. The injected charge is obtained by integrating the injected current with respect to time. The injected charge vs. time for the case of Faraday cup measured currents is shown in fig. 3.15. The diode current also is integrated to get the injected charge and plotted in fig. 3.16. A large difference in the wave forms of these injected charges is clearly evident. Even though the total injected charge at 300 ns (i.e. end of the diode current pulse) is nearly same, the injected charge obtained from diode current shows a saturation, whereas the charge obtained from Faraday cup measurements show a steep increase at this time. This is the result of long lasting Faraday cup signals.

Since the foil covered cups showed a pulse of about 100 ns, the injected charge should be taken as the one at 100 ns. After this time the voltage on the diode is zero and hence there is no beam emission. The injected charge at 100 ns obtained from the Faraday cup measurements is about 0.3 milli Coulombs. This corresponds to a total number of injected particles of 1.9×10^{15}.

3.4 Beam current and the evolution of electron ring

Temporal and spatial evolution of the injected beam electrons as they move toroidally after injection has been studied using radially movable Faraday cups deployed at various toroidal locations at different plasma density

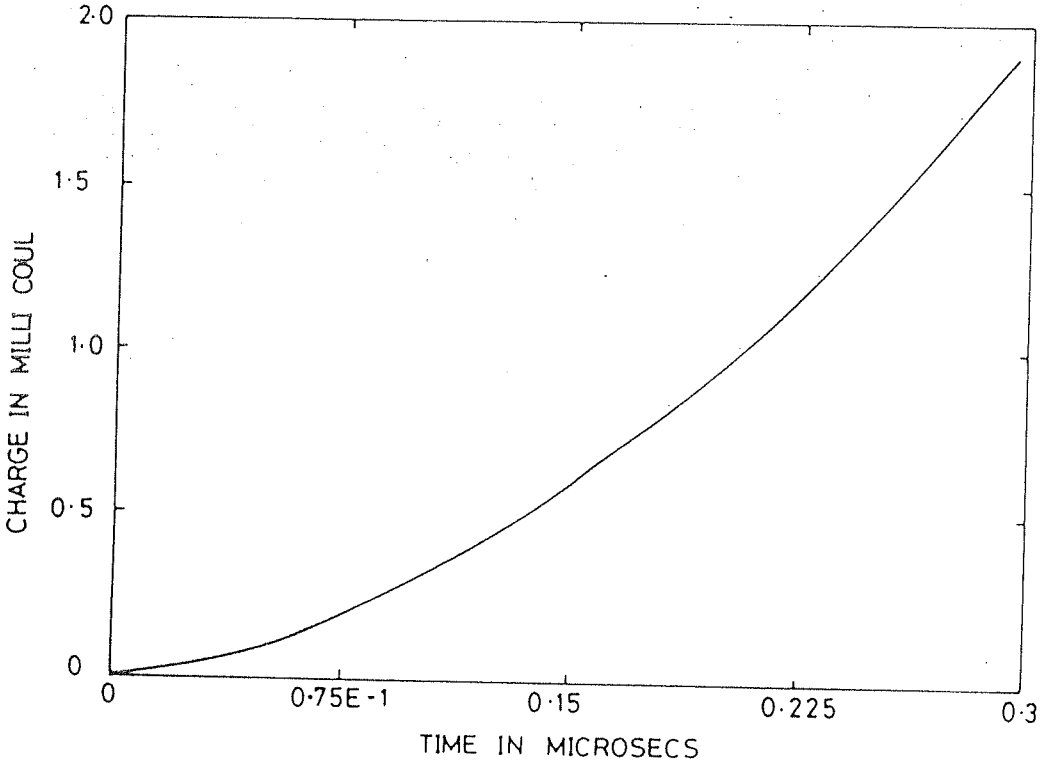

Fig. 3.15: Injected charge (from Faraday cup measurements)

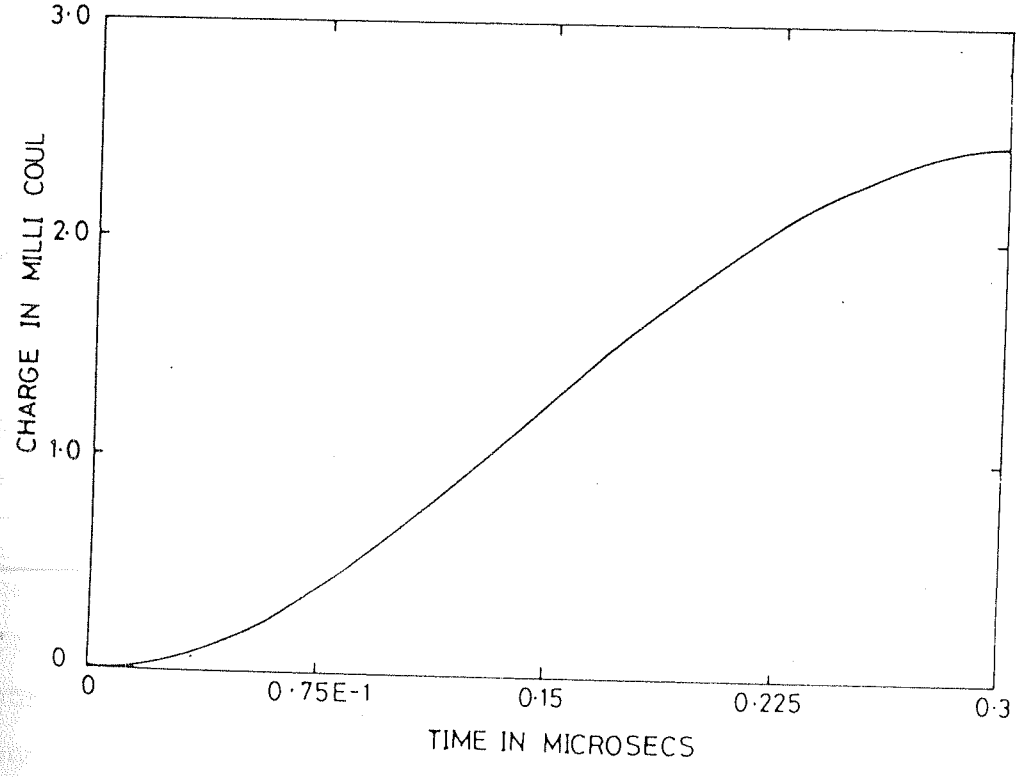

Fig. 3.16: Injected charge (from diode current measurement)

conditions. In addition a small Rogowski coil (15.0 cm diameter) was also used to study the location of the current channel and its development in time.

3.4.1 Injection into low density plasma

Extensive measurements were done with a miniature Faraday cup to locate the beam as it propagates along the toroidal direction. A typical profile of the peak current at $\theta = 337.5°$ obtained with a foilless Faraday cup is shown in fig. 3.17. The total current obtained by spatially integrating this profile is about 6.0 kAmps. Even though the peak current densities are as high as 300 Amps/sq. cm, the peak of the profile occurred always in the shadow of the cathode. At other toroidal locations also, the peak of the profile was found to be in the shadow of the cathode. Even the application of a vertical magnetic field up to 200 gauss could not produce any noticeable shift in the profile.

The net current near the cathode with a large (encircling the whole plasma column) Rogowski coil is shown in fig. 3.18. Typical rise time of this net current is less than 200 ns (the peak of the net current comes at the end of the diode current pulse). The peak currents are in the range of 3-4 kAmps lasting for about 3.0 μs. However no net current was seen at other toroidal locations when the beam was injected into low density plasma irrespective of the operating conditions.

The beam current profile near the back of the cathode indicates that the beam is getting lost by hitting the injector after one transit around the torus. No net current was observed at other toroidal locations indicating a return current decay time much longer than the beam injection duration. The net current observed in front of the cathode has a rise time almost equal to the beam injection duration.

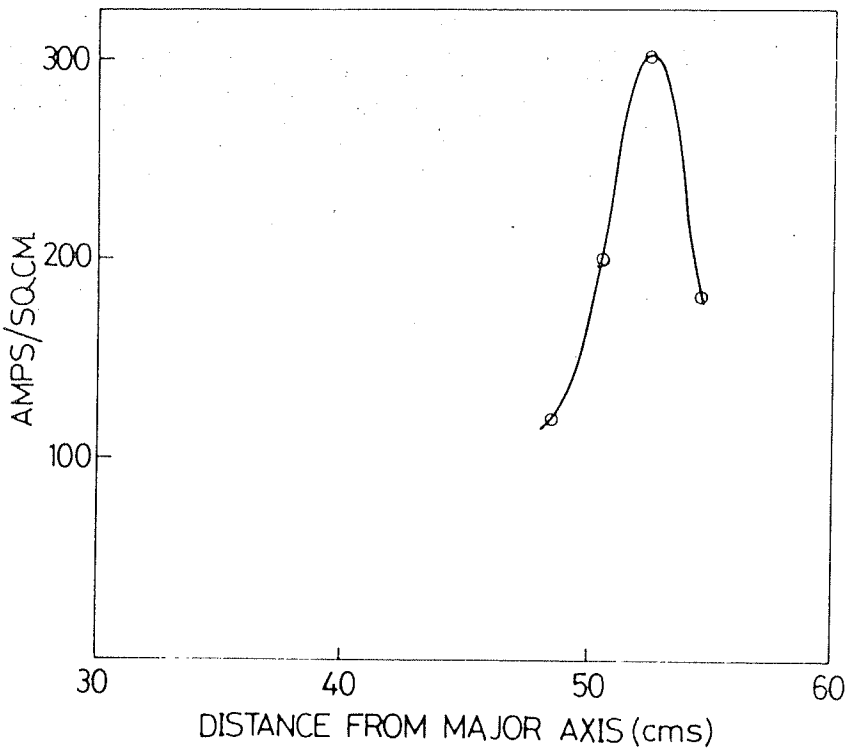

Fig. 3.17: Profile of the beam current at $\theta = 337.5°$ (low density)

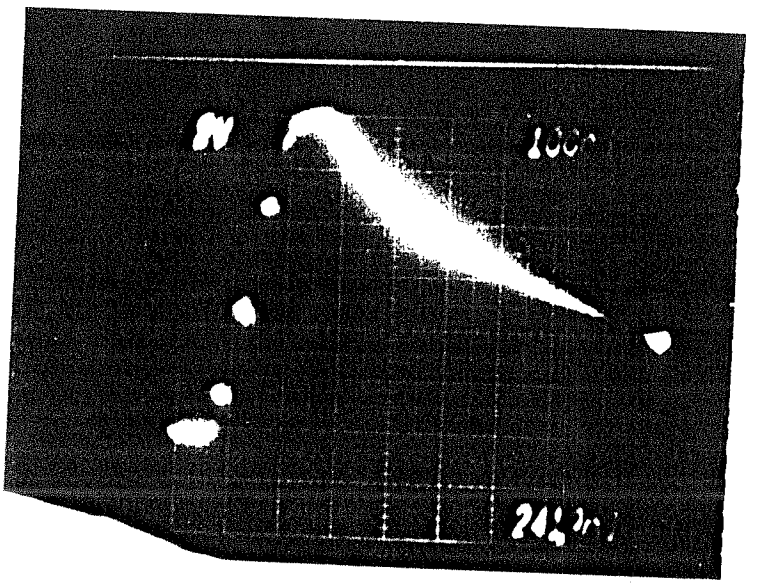

Fig. 3.18: Net current near the cathode (low density)

This also indicates a slow return current decay.

3.4.2 Injection into high density plasma

Faraday cup measurements

As in the case of injection into low density plasma, extensive measurements were done in this case also using a miniature Faraday cup to study the beam evolution.

From the Faraday cup data, beam current density profiles have been obtained near cathode (at θ = 22.5°) and on the back side of the cathode (at θ = 292.5°). The profile at θ = 22.5° is shown in fig. 3.19. This shows a sharp peak at the centre of the cathode (i.e. R = 54.0 cm, R being the major radius) and falls off on both sides of this position, even though the fall is not same on both sides. At θ = 22.5° and R = 50.0 cm, which is not in the shadow of the cathode, a substantial current (≈170 Amps/sq.cm.) is observed. The integrated current (spatial) is about 15.5 kAmps.

The profile obtained on the back side of the cathode is shown in fig. 3.20 and shows the radially inward shift of the peak of the profile. The integrated current at θ = 292.5 is about 7 kA. The peak of the profile occurs at a major radius, R = 50.0 cm on the back side of the cathode, whereas in front of the cathode the radial position of the peak is at R = 54.0 cm coinciding with the cathode location. The peak current is much higher in front of the cathode compared to that observed at the back of the cathode. However, at R = 50 cm, the amplitudes are nearly same at θ = 22.5° and 292.5°. Profiles obtained from Faraday cup signals at θ = 157.5° are plotted in figs. 3.21(a) and 3.21(b) indicating the time evolution of the current density profile. The peak at 100 ns has shifted radially inward by 1 cm. First of all the peaks of the profiles at 100 ns and 200 ns are about 3.0 cm apart. The profiles at later times (after 200 ns) do not show any

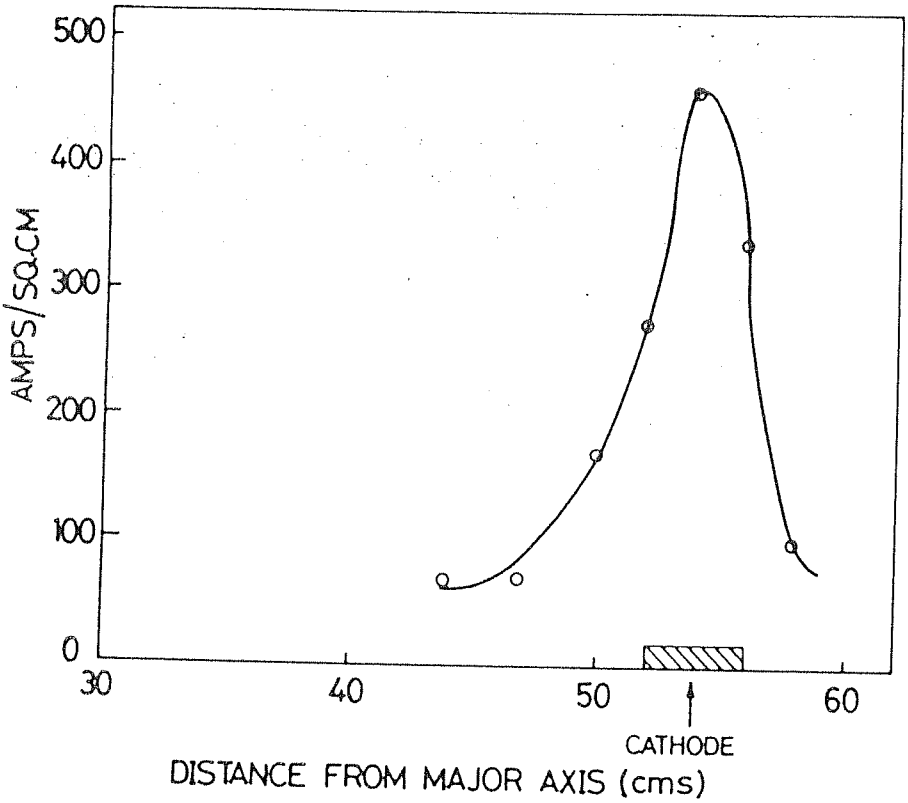

Fig. 3.19: Beam current profile near cathode (hidh density)

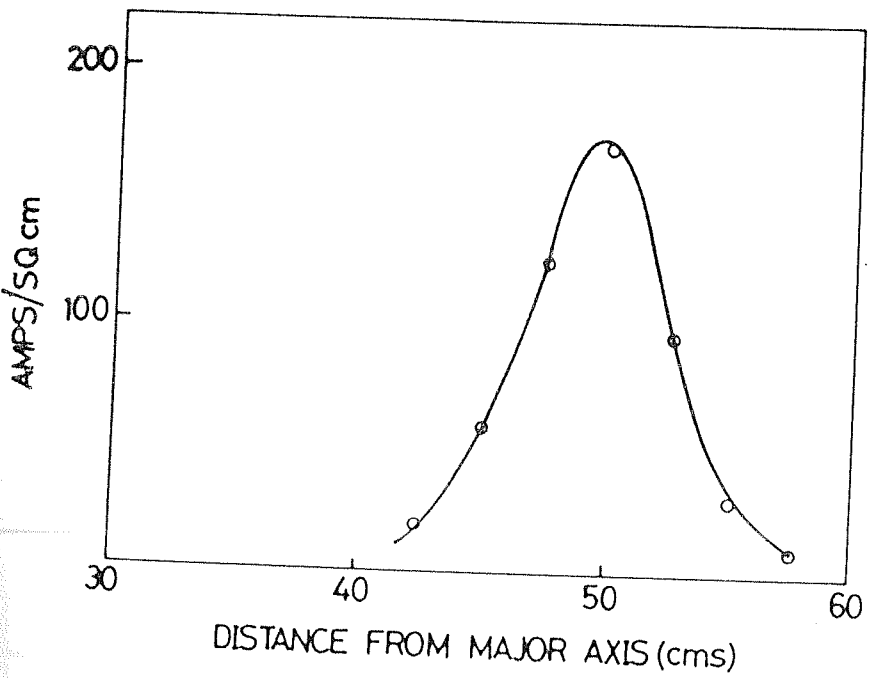

Fig. 3.20: Beam current profile at θ = 292.5° (hidh density)

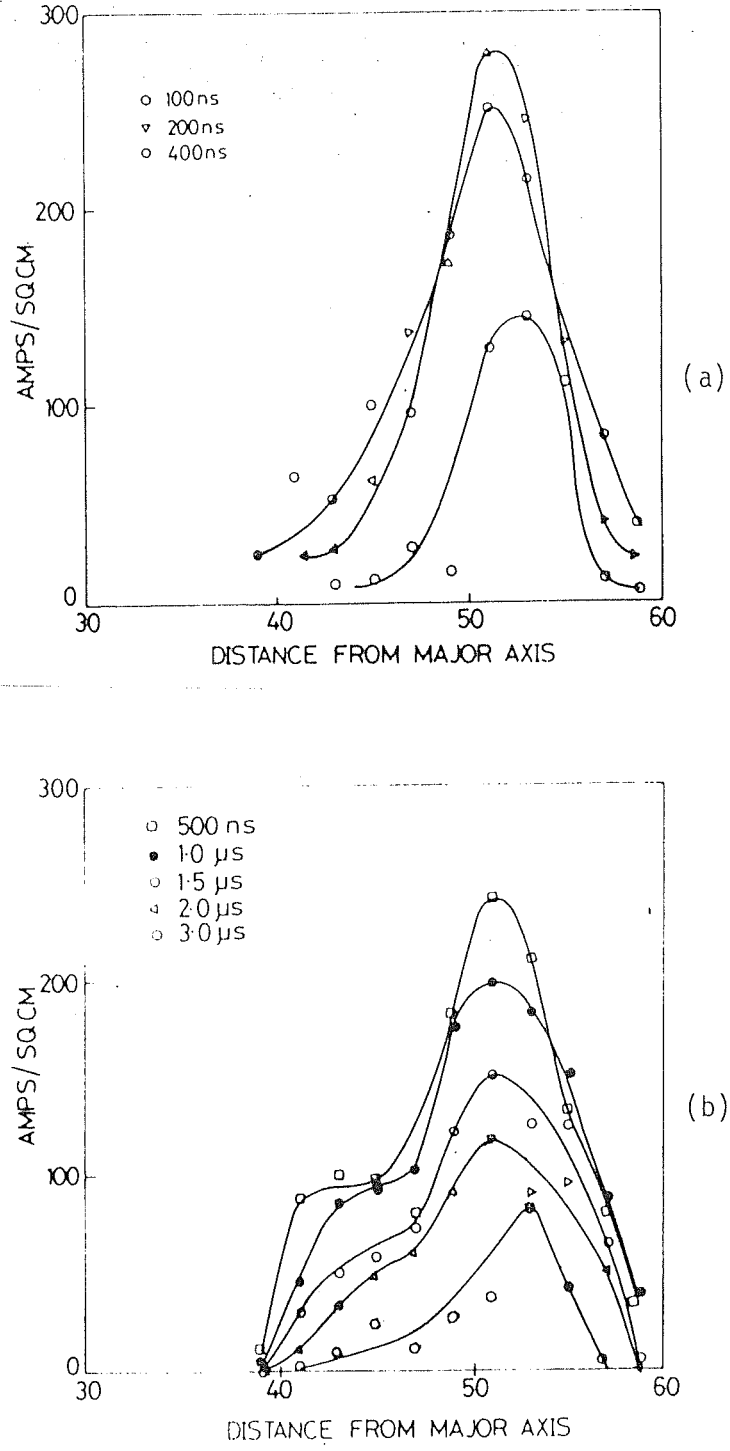

Fig. 3.21: Evolution of beam current profile (high density) at $\theta = 157.5°$

significant shift in the radial position of the peaks. The profile also become increasingly broader as time progresses. Another important feature of these profiles is a fast increase in the peak currents up to 300 ns and a slow decrease thereafter. The total current obtained by integrating these profiles is plotted in fig. 3.22. This shows a peak current of about 13.5 kAmps at 500 ns. Also evident from this figure is a fast rising (less than 500 ns) total current followed by a slow decay.

A comparison of the beam current profile near the cathode and at $\theta = 292.5°$ (figs. 3.19 and 3.20) shows that the beam shifts inward clearing the injector as it propagates around the torus. The time evolution of the beam profile at $\theta = 157.5°$ (fig. 3.21) also show that the beam moves inward as it makes rotations along the toroidal direction and finally launches on an equilibrium orbit.

Measurements with a small Rogowski coil

A small Rogowski coil with a diameter of 15.0 cm is used for space resolved measurements of the net current. The Rogowski coil is movable along the major radius. Because of the fairly large dimension of the Rogowski coil, it is not possible to get the net current distribution but at the same time gives a good picture about the current channel i.e. major radial location and its shift with time.

Figs. 3.23(a), (b) and (c) show the Rogowski signals when the Rogowski coil (i.e. the centre of the Rogowski coil) is at a major radius of R = 52.5 cm (cathode centre is at R = 54.0 cm), 45.0 cm and 37.5 cm respectively.

The Rogowski signal at R = 52.5 cm (fig 3.23(a)) shows a fast rising signal (rising to its peak within 300 ns) and a fast fall immediately after the peak followed by a slower decay. The Rogowski signal at R = 45.0 cm (i.e. at the minor

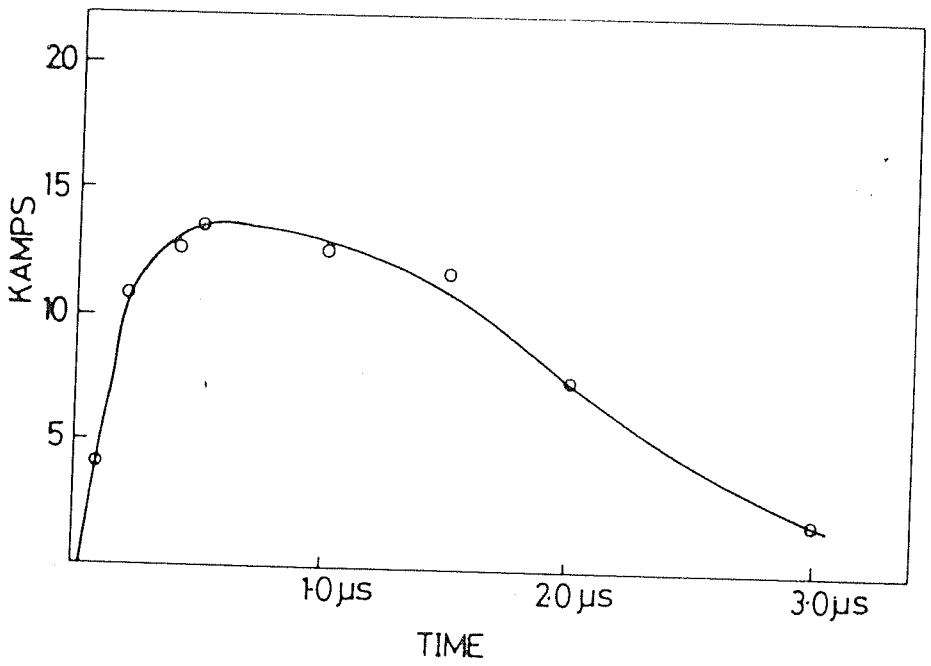

Fig. 3.22: Total beam current as a function of time

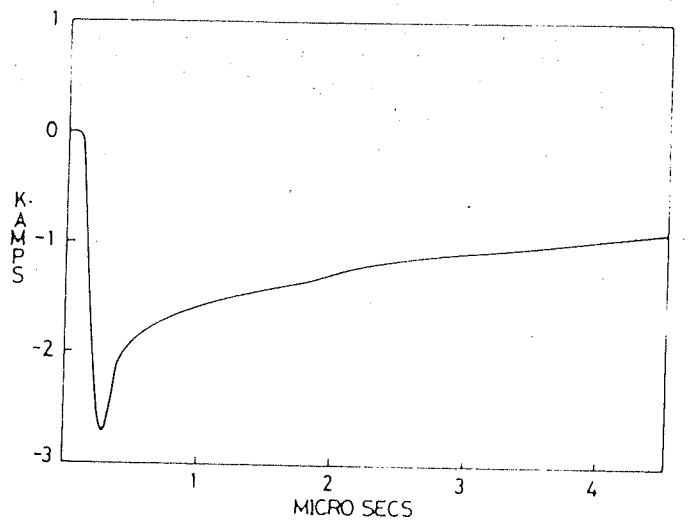

(a) R = 52.5 cm

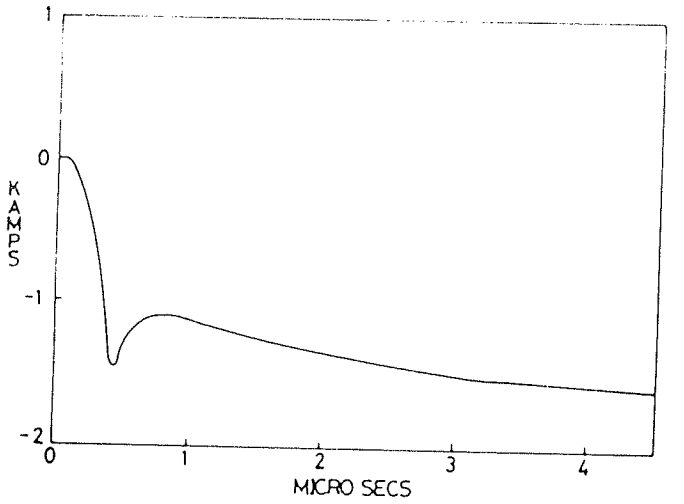

(b) R = 45.0 cm

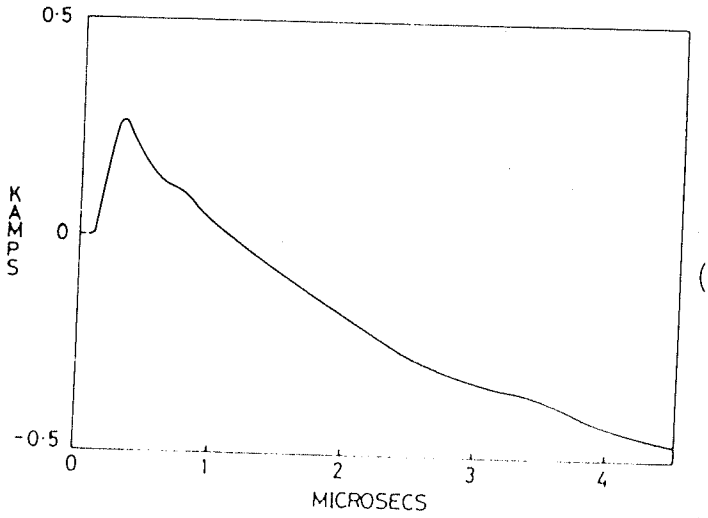

(c) R = 37.5 cm

Fig. 3.23: Net current from small Rogowski coil.

axis) is distinctly different from that of at R = 52.5 cm. The peak occurs at 500 ns (at R = 52.5 cm it occurs at about 300 ns). Even though there is a fast decay immediately after this peak, like in the previous one, there is no slow decay (unlike the one at R = 52.5 cm, where a slow decay is observed). Instead there is an increase in the net current as seen by the Rogowski coil at this location, though the increase is not too appreciable. The Rogowski signal at R = 32.5 cm is even more strikingly different from the earlier two. To start with there is a net current opposite to the beam current for about 1.0 μs, which reverses and becomes in the same direction as the beam current and continues to be so. The magnitude of the current keeps on increasing.

These signals are shown in fig. 3.24 along with the circumference (inner circles) of the Rogowski coil used. The outer circle shows the location of the vessel wall. The difference in the waveforms shown in this figure and the earlier ones (fig. 3.23) is that in fig. 3.24 the Y-scale is same in all the waveforms.

From the net current measurements by small Rogowski coil, we can understand its gross temporal and spatial behaviour. The rising part of the wave form in fig. 3.23(a) and (b) and the initial net current behaviour of fig. 3.23(c) indicate that the main current channel is in circle 1 of fig. 3.24 (the one nearer to the outer wall). The magnitudes of signals in circles 1 and 2 (fig. 3.24) are not equal during the injection phase, and this may be due to the current channel not being entirely in the intersection of circles 1 and 2 or due to a return current which is present in circle 2. The peak current in circle 1 occurs at 300 ns, while it occurs at 500 ns in circle 2. This observation and a current in the opposite direction to that of beam current in fig.

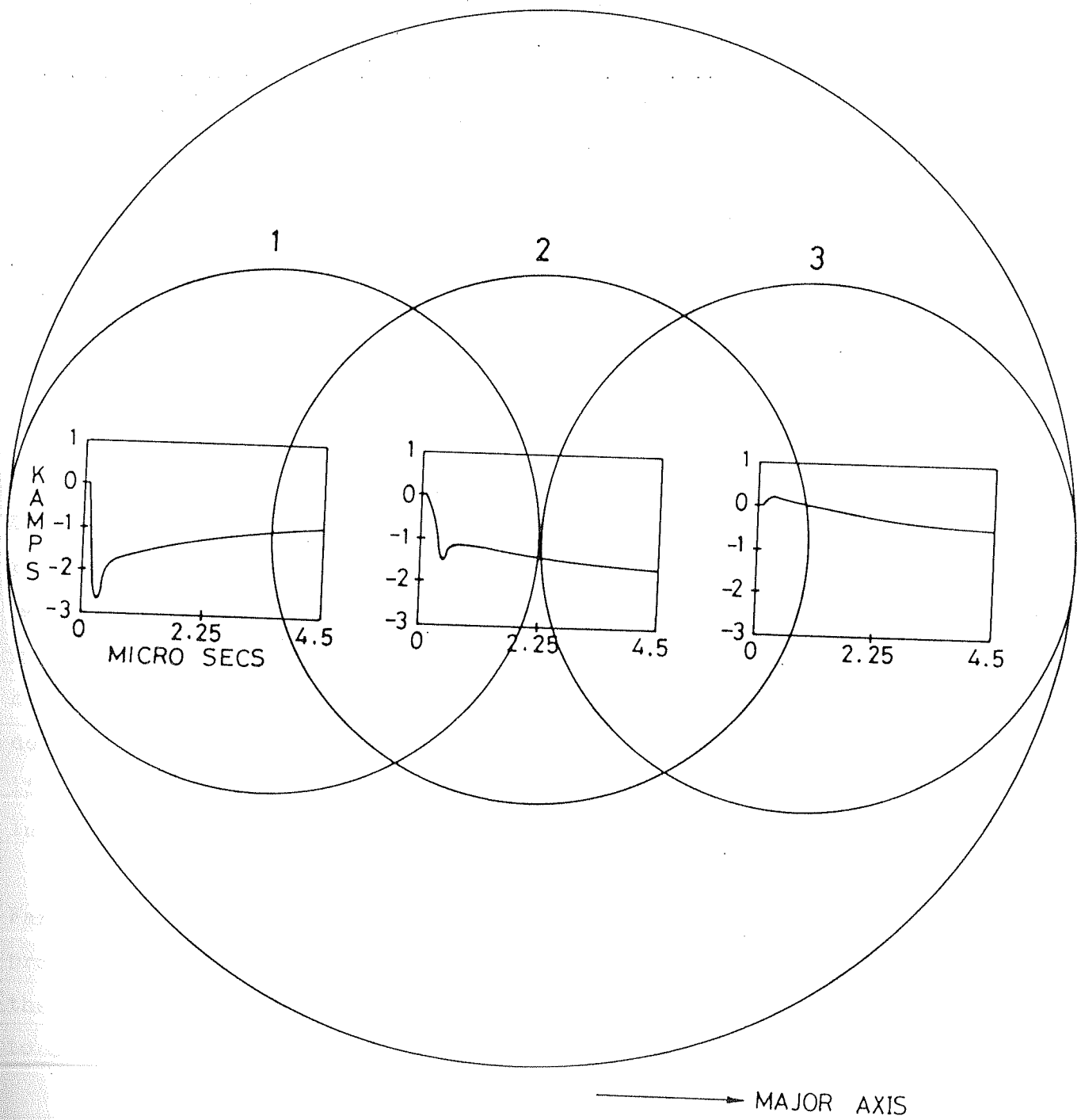

Fig. 3.24: Net current distribution in the poloidal cross-section

3.23(c) during the initial phase indicate a difference in the return current behaviour at various locations (basically the temporal evolution of the return current distribution). The initial slow rise of the net current in circle 2 compared to the rise of the net current in circle 1 may indicate a current channel moving towards the major axis.

The current near to the inner wall fig. 3.23(c) is opposite to the direction of the beam current initially. The current at this location changes sign after 1.0 μs. This can be due to a slow decay of the return current and/or return current being induced in the same direction due to the decay of the net current. But since the appearance of net current is much faster compared to the decay of the net current, the induced current due to the decay should be much smaller. This indicates another possibility, which is as follows. The main current channel continues to shift towards the major axis and hence the Rogowski near the inner wall partly intercepts this current and hence starts showing a current in the same direction as that of the beam current as soon as this dominates the return current. The same will be observed even if the current channel becomes broad (even without shift) and intercepted by the Rogowski coil.

Since no shift is seen by the magnetic probes and Faraday cup after 1.0 μs and actual broadening of this profile is seen by both these measurements, the behaviour of the waveform in fig. 3.23(c) can be safely assumed to be due to the broadening of the current channel.

After the initial fast rise of the net current, the current starts decaying in fig. 3.23(a), while that in fig. 3.23(b) starts increasing (though marginally). The net current in fig. 3.23(c) also shows an increase of current in the direction of the beam current. Since the variations in

the net currents at these three locations is not significant after the initial 1.0 μs and considering the global nature of the measurement, we can conclude that a stable current ring is formed in the location marked by circle 2 (fig. 3.24).

To understand the net current distribution in the system, let us compare the magnitudes of these currents from figs. 3.23(a), (b) and (c) at 4.5 μs. The net current in circle 2 is 1.5 kAmps, in circle 3 it is 0.5 kAmps and in circle 1 it is about 1.0 kAmp. A rather simple physical picture will be enough to explain this distribution. A net current channel whose current distribution is such that the net current in intersection of circles 1 & 2 is more (1.0 kA) than the net current in the intersection of 2 and 3 (about 0.5 kAmps). From this we can say that the current is predominantly in between the minor axis and outer wall though it is inside of the injector.

From the foregoing discussion one can conclude that the net current shifts towards the major axis during the beam injection phase and stays at an equilibrium position without any major poloidal motion.

3.5 Net circulating current after beam injection

Net current in the system was measured by large Rogowski coils, which were deployed at different toroidal locations. From these measurements at different toroidal location it was found that the net current waveforms at $\theta = 100°$ and beyond are identical for any given shot. However the net current near the cathode (i.e. $\theta = 10°$) showed marked difference during the beam injection phase.

Fig. 3.25 and 3.26 show typical waveforms obtained at $\theta = 10°$ and $\theta = 202.5°$ respectively. As can be seen from these two figures, there is a large difference during the

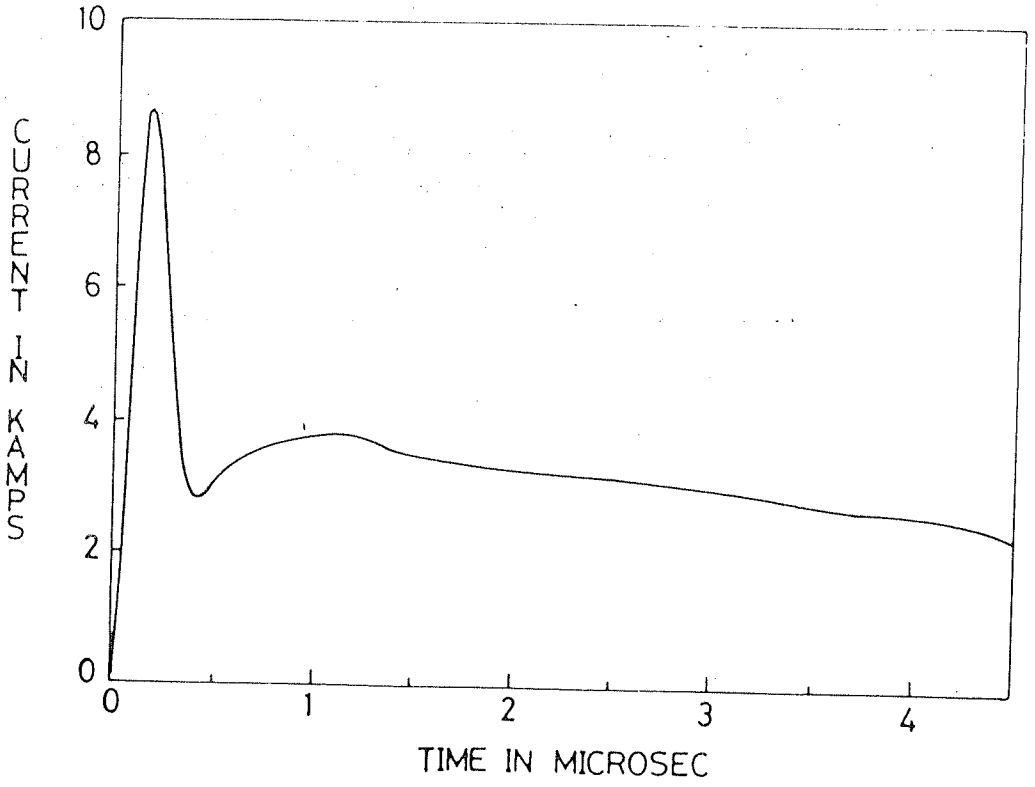

Fig. 3.25: Net current at $\theta = 10°$

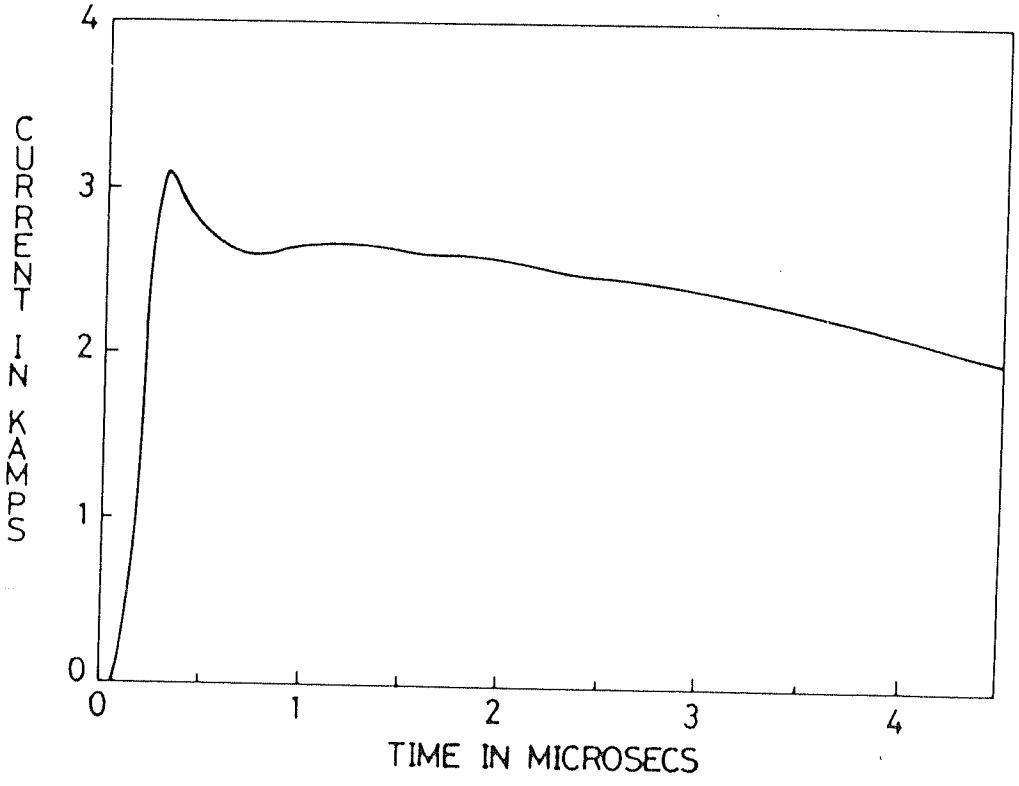

Fig. 3.26: Net current at $\theta = 202.5°$

beam injection. The net current in front of the cathode sharply rises to its peak value of about 9.0 kAmps at about 200 ns. Immediately after this peak there is a sharp fall and the net current after this sharp fall is about 3.0 kA and rises again within 1 μs followed by a slow decay. The waveform at $\theta = 202.5°$ shows a sharp rise to about 3 kAmps followed by a slow decay. The apparent difference in the magnitude after the injection is over, in the two figures, is due to shot to shot reproducibility problem.

The trapped current in a well tuned condition is shown in fig. 3.27 which shows a peak current of about 5 kA and falls smoothly to zero in about 32 μs. The oscillogram of which fig. 3.27 is obtained is shown in fig. 3.28(a). The negative portion of the signal is due to inadequate RC integration.

For some shots the trapped current showed a sudden drop just after the peak as shown in the oscillogram of fig. 3.28(b). Again negative part in the oscillogram is due to the inadequate RC integration.

Now let us compare the trapped beam and trapped net currents as measured by Faraday cup and Rogowski coils. These currents are shown in fig. 3.22 and 3.27 respectively. Here also the rise time from the Faraday cup measurements (≈500 ns) is larger than net current rise time and injected pulse duration (≈300 ns). This can not be explained as transit time effect, as this would have been reflected in the net current measurement as well. The total current from the Faraday cup measurements is much higher (≈13 kAmps) than the net currents (≈5 kAmps). At 500 ns, when the beam injection is over and the return current has died down, the difference is unexplained if we assume that whatever measured by the Faraday cup is the beam current. This difference is due to

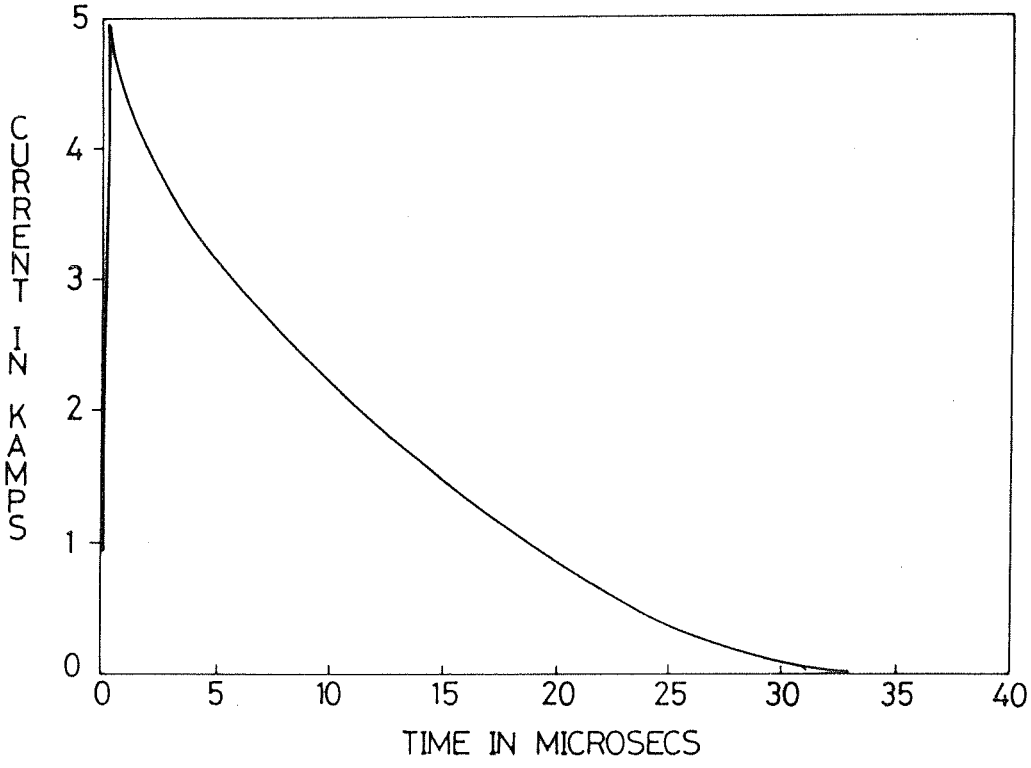

Fig. 3.27: Net current at $\theta = 202.5°$

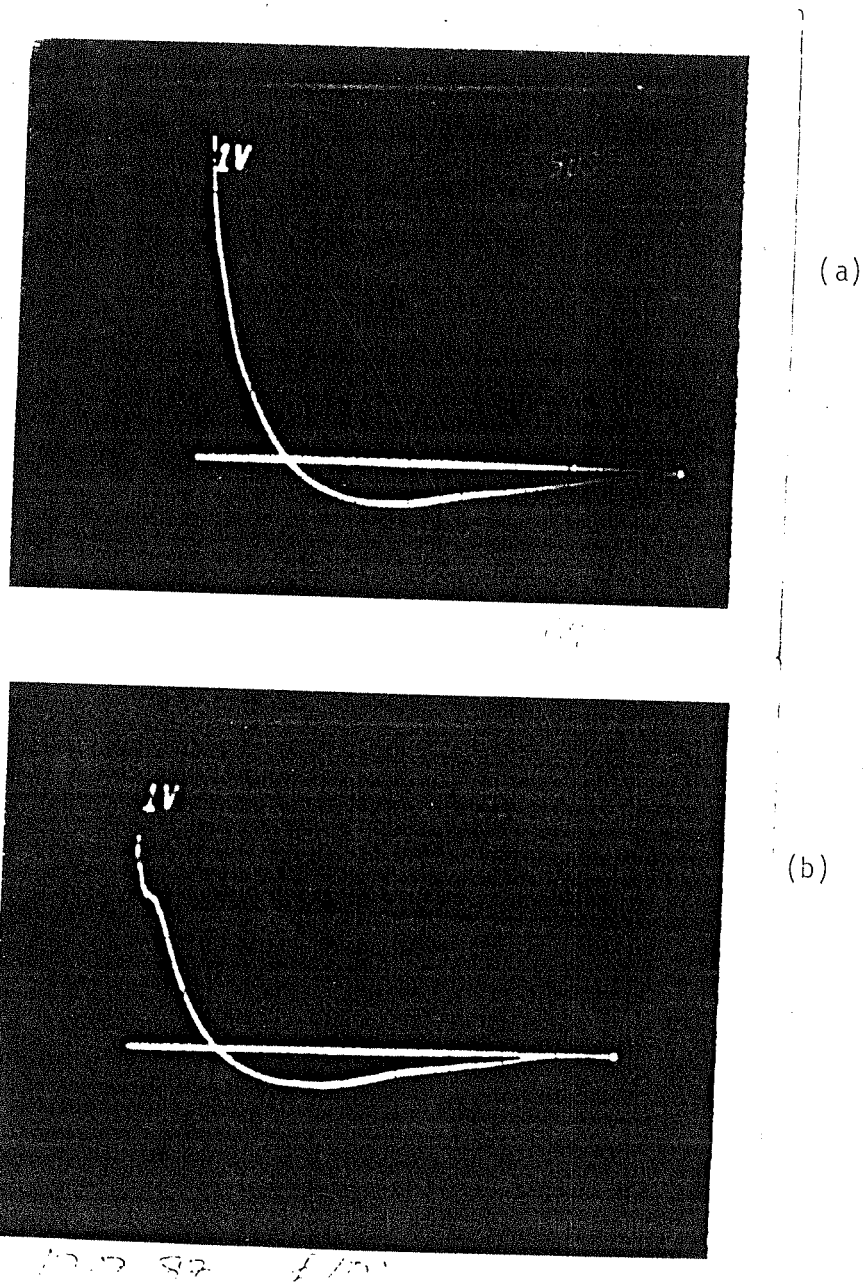

Fig. 3.28: Oscillograms of net current with 5μs RC integrator

the contribution from the plasma to the Faraday cup acting as a simple probe biased to collect plasma electrons.

Since the net current near the cathode is not rising all through the injection pulse, it is clear that the beam stacking is rather poor. However a definite beam stacking can be seen from the net trapped current (fig. 3.27). Since this current rises all through the injection duration, there is a stacking, however low the stacking factor may be. The rising part of this net current is shown in fig. 3.29. If all the charge injected goes into building up of the net current, then the slopes of the injected charge (fig. 3.15) and the slope of the net current during the rise time (fig. 3.29) should have been same at all times. As is clear from these two figures, where the slopes are not same, the conclusion is that either all the injected charge does not participate in the net current build up and/or the charge injected at different times gets decelerated to different extents. This is possible as the beam front is known to get decelerated more than the rest of the beam.

3.5.1 Ring current

The net current measured by large Rogowski coils at different toroidal locations indicate whether there is a continuous current ring or not. The current measured near the cathode is not necessarily the ring current. During the injection phase (i.e. first 300 ns), the Rogowski coil near the cathode measures the trapped current and the instantaneous injected current and hence will be more than the trapped current. This is clearly seen in our experiments (fig. 3.25 and 3.26). However, from the time when injection is complete, the net current at all toroidal locations is identical. This shows a continuous current ring formation.

If a beam of current I_b is injected for a duration, t to

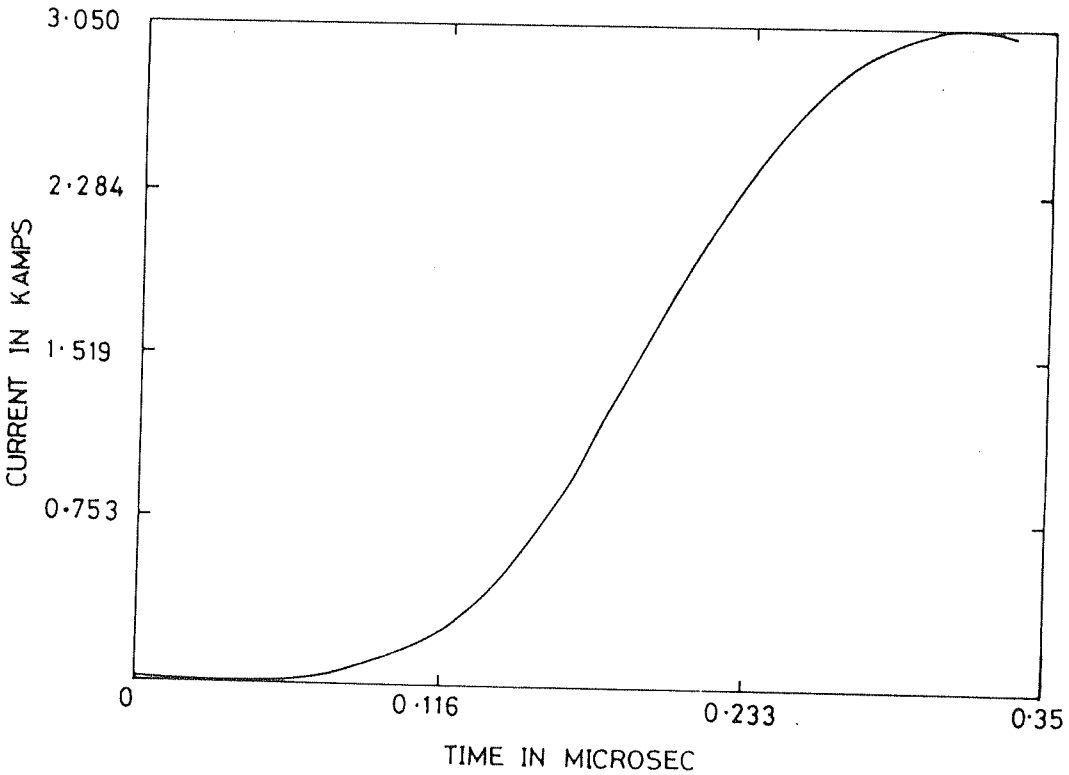

Fig. 3.29: Rising part of the net current

form a current ring, the ring current I_r will be given by (with no return currents)

$$I_r = \frac{v_b}{2\pi R} I_b t \qquad (3.13)$$

where v_b is the velocity of beam particles at injection and R is the major radius of the ring. This relation, however will be valid only if all the injected particles without any loss of energy participate in the building up of ring current. This will also be valid in the case of an ultra relativistic beam even if the beam losses energy, since the loss of energy does not appreciably reduce the velocity ($\delta v_b/v_b \approx \delta\Gamma/\Gamma^3$). In such a case the ring current rises faster than the beam current (if $t > 2\pi R/v_b$). This can be readily seen by differentiating eq. (3.13)

$$\frac{dI_r}{dt} = \frac{v_b}{2\pi R} t \frac{dI_b}{dt} + \frac{v_b}{2\pi R} I_b \qquad (3.14)$$

i.e. $$\frac{dI_r}{dt} > \frac{dI_b}{dt} \qquad (3.15)$$

But in the case of low energy beam, the loss of beam energy due to plasma heating and setting up of self electromagnetic fields reduces the beam velocity and hence limits the attainable ring currents.

The maximum attainable ring currents have been calculated by Narihara (1981 and 1982) under two extreme conditions, namely: (1) the injection pulse width is much smaller than the return current decay time and (2) there is no return current at all. The maximum ring current in the two cases is given by

and $$I_r < \frac{1}{2}\left(\frac{F}{g}\right) I_\alpha \left(\Gamma^2-1\right)^{1/2} \equiv I_{max} \qquad (3.16)$$

$$I_r < \frac{1}{2g} I_\alpha \ln[1 + \frac{ct}{\pi R} (\frac{gI_b}{I_\alpha})] \equiv I_{max} \qquad (3.17)$$

respectively, where F and g are geometrical factors of the order of unity, I_α = 17000 Amps. In deriving eq. (3.17), the loss of beam energy due to setting up of self magnetic field alone is considered. In the actual experimental situations, the beam energy loss due to plasma heating will further restrict the attainable ring currents.

Since the injection energy of beam particles is of the order of 100 keV and about half of this energy appears as plasma perpendicular energy (estimated from diamagnetic measurements), it is reasonable to assume that the energy of the particles in the ring is about 50 keV. This is in good agreement with the estimated energy using the observed ring positions and the net currents.

Using the reduced energy, the maximum attainable ring current as given by eq. (3.16) is about 4.0 kAmps. Since a ring current of 5 to 6 kAmps is realized, the condition for eq. (3.16) (i.e. the return current decays in a time longer than the injection pulse width) is not satisfied and hence higher ring currents are observed. The conclusion reached from the net current rise times, that the return current decay time is much shorter than the injection duration, is in support of the above observation. The maximum ring current attainable from eq. (3.17) is about 20 kAmps. Even though this is a maximum limit, the observed currents are much less than the maximum current of 20 kAmps. This is possibly because of the reduced beam energies when the ring is formed. A realistic estimate should take into account the energy loss due to other mechanisms as well.

In the case of beam injection into a linear system, the beam enters the system from one end and leaves from the other

end. The beam current is assumed to be as shown in fig. 3.30(a). Now if the induced return current decays much faster than the beam current rise time, then the net current will be nearly same as the beam current. In the other extreme when the return current decay time is longer than the beam pulse width, then the net current rise time will be same as the beam pulse width. Return current and net current are shown in fig. 3.30(b) and 3.30(c) respectively for this case. The same is true in the case of a beam injection into a toroidal device, if the beam is lost within one transit around the torus.

In the case of injection into a toroidal system, the trapped beam current rise time is same as the injected beam pulse width. Here also we shall follow the same ordering as above, namely (1) the return current decay is much faster than the injected beam current rise time or injected beam pulse duration (since the trapped beam rise time is the pulse duration) and (2) the return current decay time is longer than the injected pulse duration. If the return current decay time is much faster than the trapped beam current rise time, then the net current will be same as the trapped beam current (as shown in fig. 3.31(a)). If the return current decay is longer than the beam pulse duration (injected) (see fig. 3.31(b)), then the net current rise time will be longer than the injected beam pulse duration (fig. 3.31(c)).

In view of the above discussions, return current decay can be inferred from the observed net current behaviour. First we shall consider the beam injection into a low density plasma.

In this case no net trapped current is observed. Hence the net current measured near the cathode (fig. 3.18) has no contribution of this component. The rise time of the net

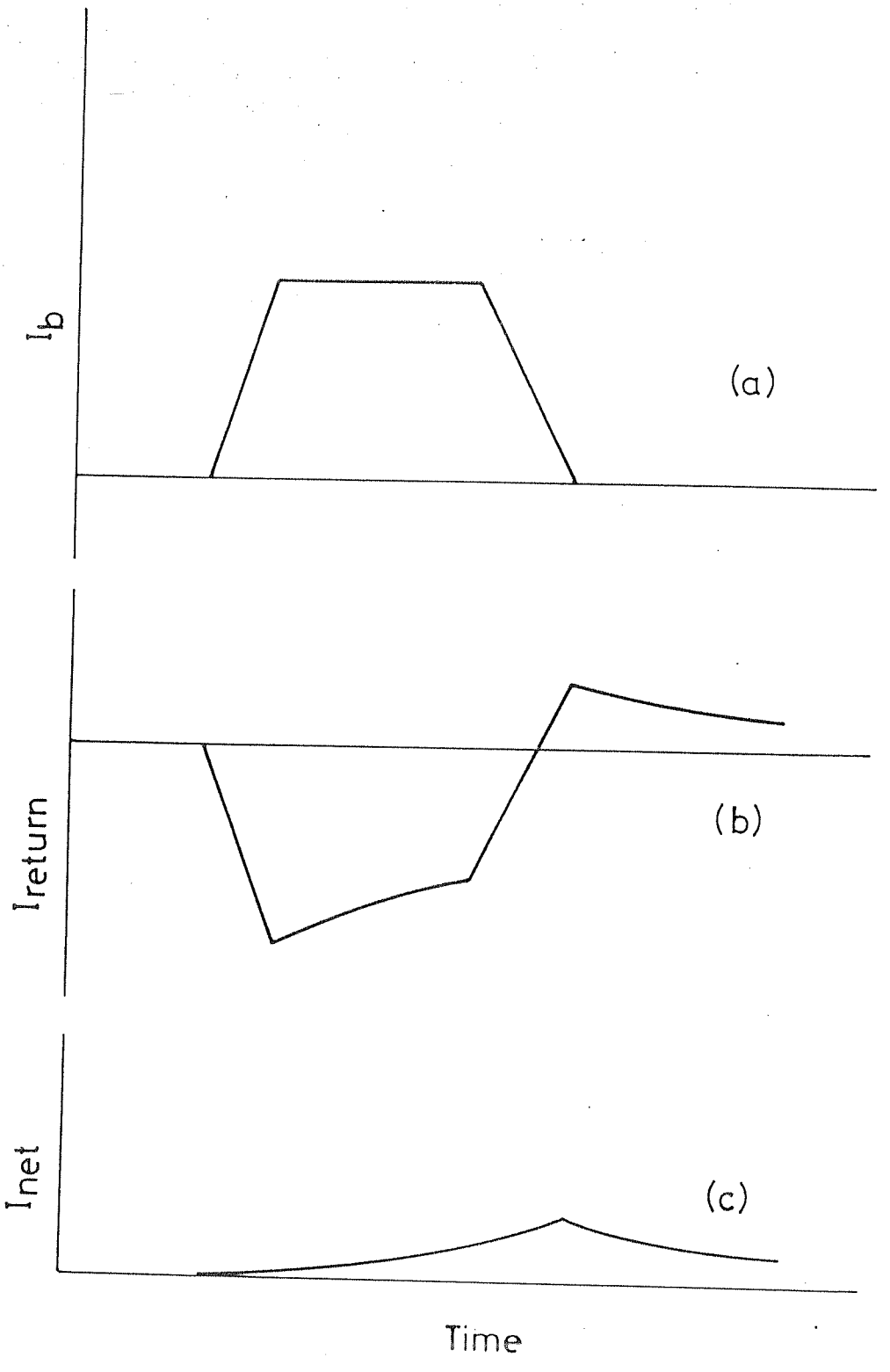

Fig. 3.30: Temporal evolution of (a) Beam current,
(b) Return current, (c) Net current in a linear system

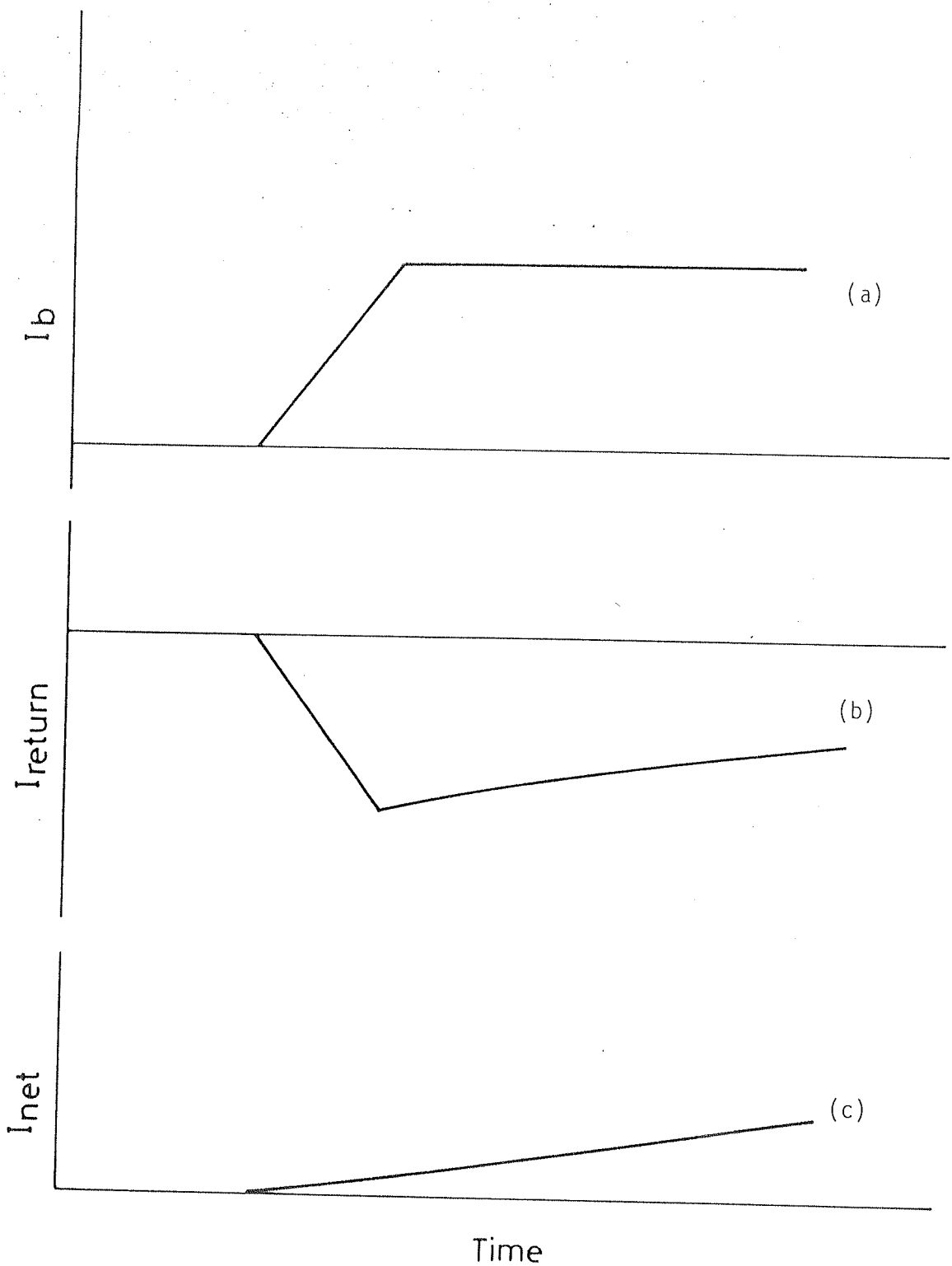

Fig. 3.31: Temporal evolution of (a) Beam current,
(b) Return current, (c) Net current in a toroidal system

current is same as the injected beam pulse (fig. 3.6) width. This is the case shown in fig. 3.30(c). Comparing the net current rise time with that of the diode current, we can readily conclude that the return current decay time is much longer than the beam pulse duration. The peak net current of 4 to 5 kAmps compared to 15 kAmps of diode current also indicates the slow decay of return current.

In the case of the beam injection into a high density plasma, there is a net trapped current (i.e. circulating current or ring current). The net current near the cathode is shown in fig. 3.25. The peak current of 8 - 9 kAmps comes at the same time as the peak of the diode current (fig. 3.7). The peak diode current of 10 - 12 kAmps is however higher than the injected net current. The injected net current is less than 8 - 9 kAmps, since this consists of the trapped net current as well. The trapped net current rise time (fig. 3.27) is nearly same as the injected pulse duration. If there is a return current and decays slowly compared to the beam injection duration, then the net currents should have much longer rise times than the observed rise times. Since the observed net current rise times are smaller than the injection pulse duration near the cathode and are same as the injection pulse duration at other toroidal locations, we can conclude that the return current decay times are much smaller than the injected beam rise time (≈150 ns).

The return current decay time due to Coulomb collisions alone is more than 1.0 μs. Therefore, the fast decay of the return current necessitates some mechanism other than the Coulomb collisions in the case of beam injection into high density plasma. One such mechanism is ion-acoustic instability (Lee and Sudan, 1971; Lovelace and Sudan, 1971). The necessary condition for ion acoustic instability is $c_s <$

$v_d < v_{te}$, where c_s is the ion sound velocity, v_d (= $n_b \cdot v_b / n_p$; where n_b and n_p are the beam and plasma densities) is the drifting electron velocity due to the return current) and v_{te} is the electron thermal velocity. In our experiment this condition is satisfied for the high density case, since $c_s \approx 2 \times 10^6$ cm/s, $v_d \approx 8.0 \times 10^7$ cm/s and $v_{te} \approx 1.0 \times 10^8$ cm/s. Due to this instability, the return current decay time, T is given by (Lee and Sudan, 1971)

$$T = \tau^* \left(\frac{r_p^2}{\lambda_\epsilon^2}\right) \qquad (3.18)$$

(where r_p is the radius of the plasma column, $\lambda_\epsilon = c/w_{pe}$ is the electro-magnetic skin depth, w_{pe} is the electron plasma frequency and τ^* is a phenomenological relaxation time (Lee and Sudan, 1971) given by (Sagdeev, 1967)

$$\tau^* \approx 10^2 \left(\frac{T_i}{T_e}\right) \left(\frac{v_{te}}{v_d}\right) \frac{1}{w_{pe}} \qquad (3.19)$$

$$\approx (0.1\ w_{pe})^{-1} \approx 5.6 \times 10^{-11}\ s$$

The decay time, T, predicted by this theory is about 35 ns, which is smaller than the beam injection duration (≈300 ns), and explains the observed net current rise times.

In the low density case the necessary criteria for the ion acoustic turbulence ($c_s < v_d < v_{te}$) is not satisfied and hence there is only the normal collisional decay.

These conclusions have another implication on beam trapping. For a successful beam trapping, a fast appearance (within the beam injection time scale) of a net current is essential. In the low density case, where there is no appearance of net current during the beam injection time scale is the reason for no beam trapping. In the high density case a net current appears during the beam injection time.

Hence the conducting wall sees the net current and pushes the beam inward and the beam is trapped. This is consistent with the drift injection models proposed by Mohri et al., (1975; 1982); Masuzaki et al., (1975) and Benford et al., (1974b)

3.6 Self magnetic field of the beam and the net current Profiles

The poloidal magnetic field measured in the mid plane at different major radial locations is shown in figs. 3.32(a)-3.32(d). Fig. 3.32(a) is the poloidal field evolution at a major radius of R = 54.0 cm. Poloidal field at this location is negative (only for reference purpose, since no poloidal field is present prior to the beam injection) through out the time with a rise of about 250 ns, followed by a slow decay. Fig. 3.32(b) is the signal obtained at R = 50.0 cm. This signal shows a small positive pulse for about 200 ns duration followed by a change in the polarity of the signal which remains negative for the rest of the time. The change in polarity occurs within 200 ns from start and the duration of change (from positive peak to negative peak) is less than 100 ns. The same behaviour is observed when the probe is at R = 52.0 cm location also.

The probes at other locations for example (R = 46.0 cm and R = 38 cm; figs. 3.32(c) and (d)) show a unipolar signal like the one at R = 54.0 cm, but the polarity of the signal being opposite to that of at R = 54 cm and with different rise times. Probes at R = 38.0 cm show a large rise time compared to that of at R = 46.0 cm.

The time evolution of the radial profile of the poloidal magnetic field is shown in figs. 3.33(a) to 3.33(m). The solid line is a polynomial fit to the experimental data. The

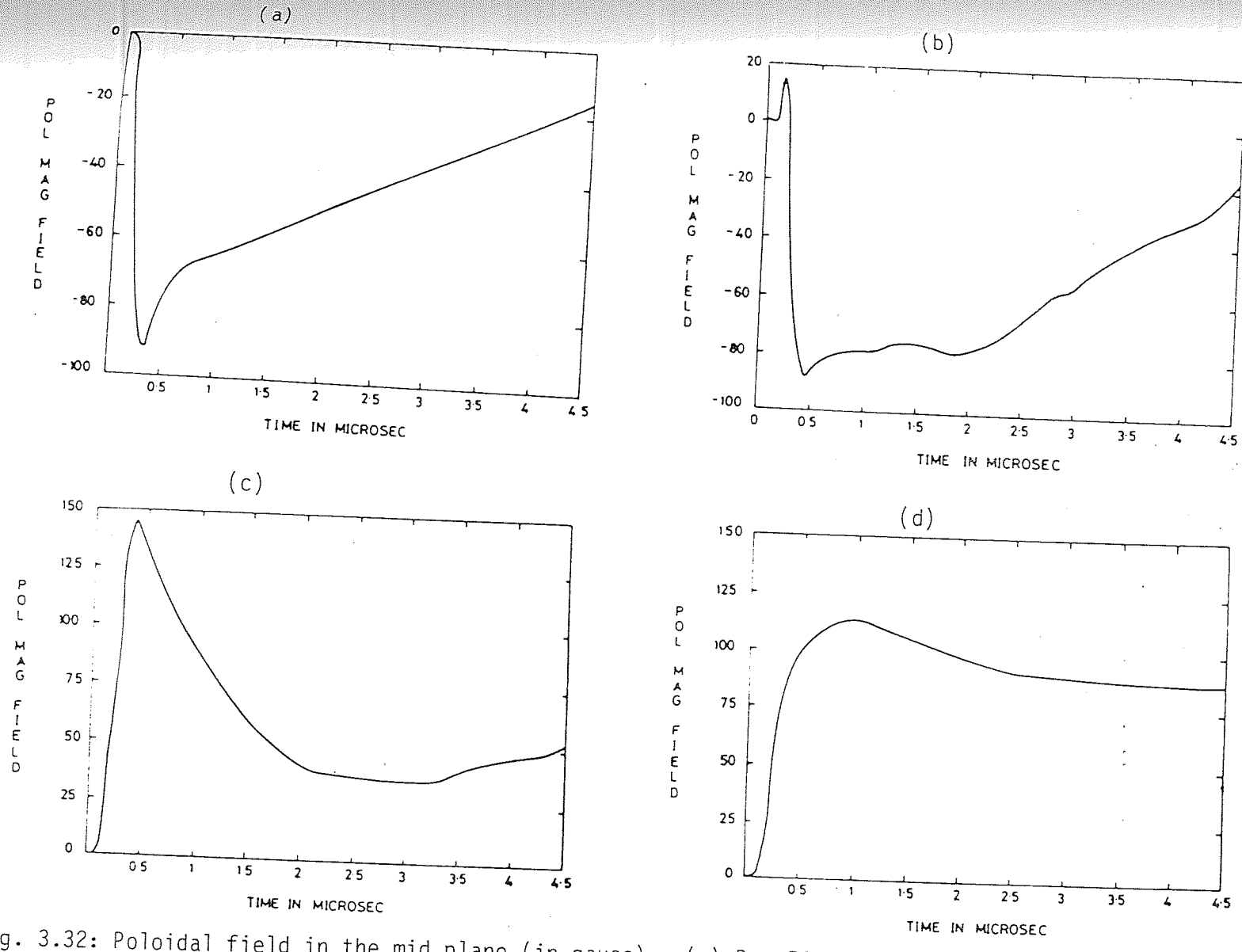

Fig. 3.32: Poloidal field in the mid plane (in gauss) : (a) R = 54.0 cm; (b) R = 50.0 cm; (c) R = 46.0 cm; (d) R = 38.0 cm

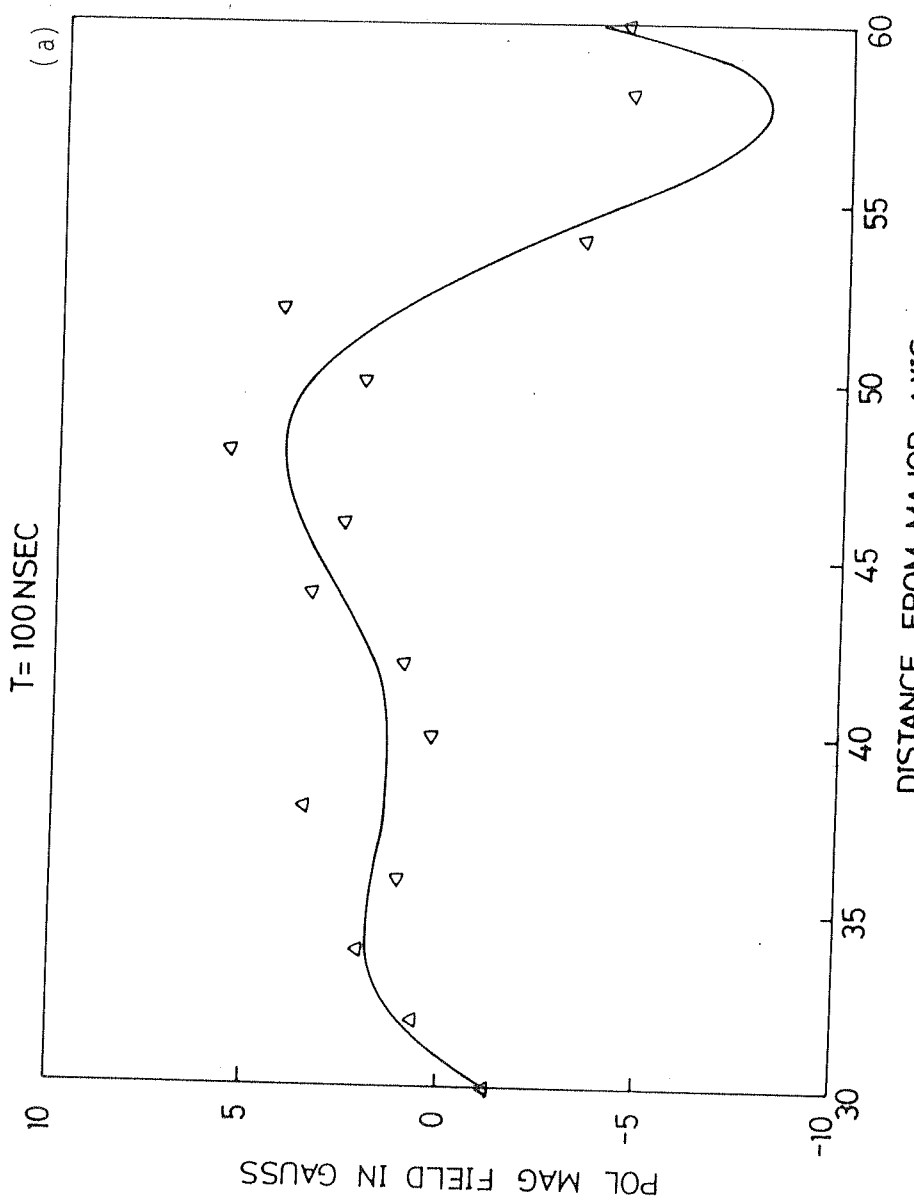

Fig. 3.33: Time evolution of radial profile of poloidal field.

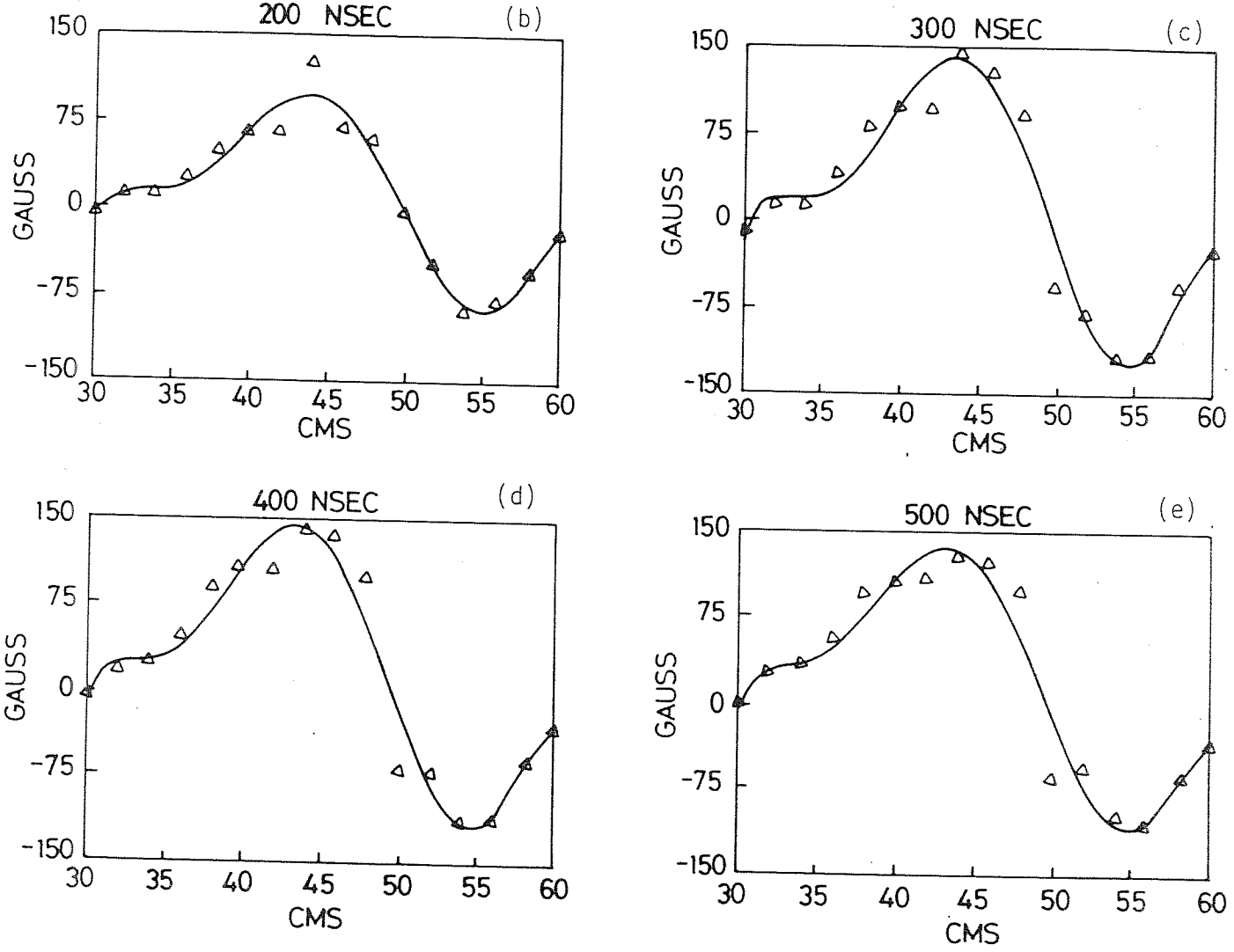

Fig. 3.33: Time evolution of radial profile of poloidal field.

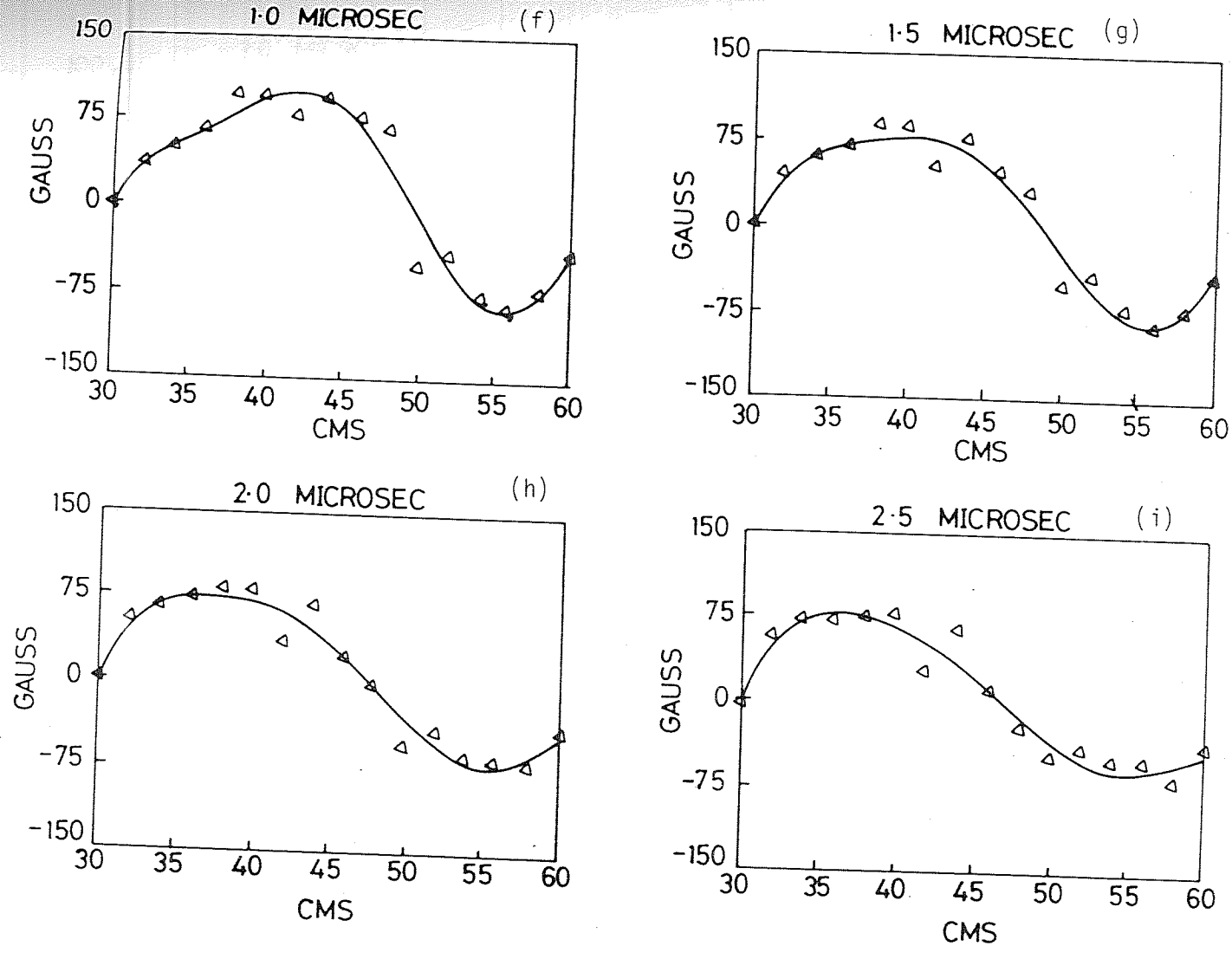

Fig. 3.33: Time evolution of radial profile of poloidal field.

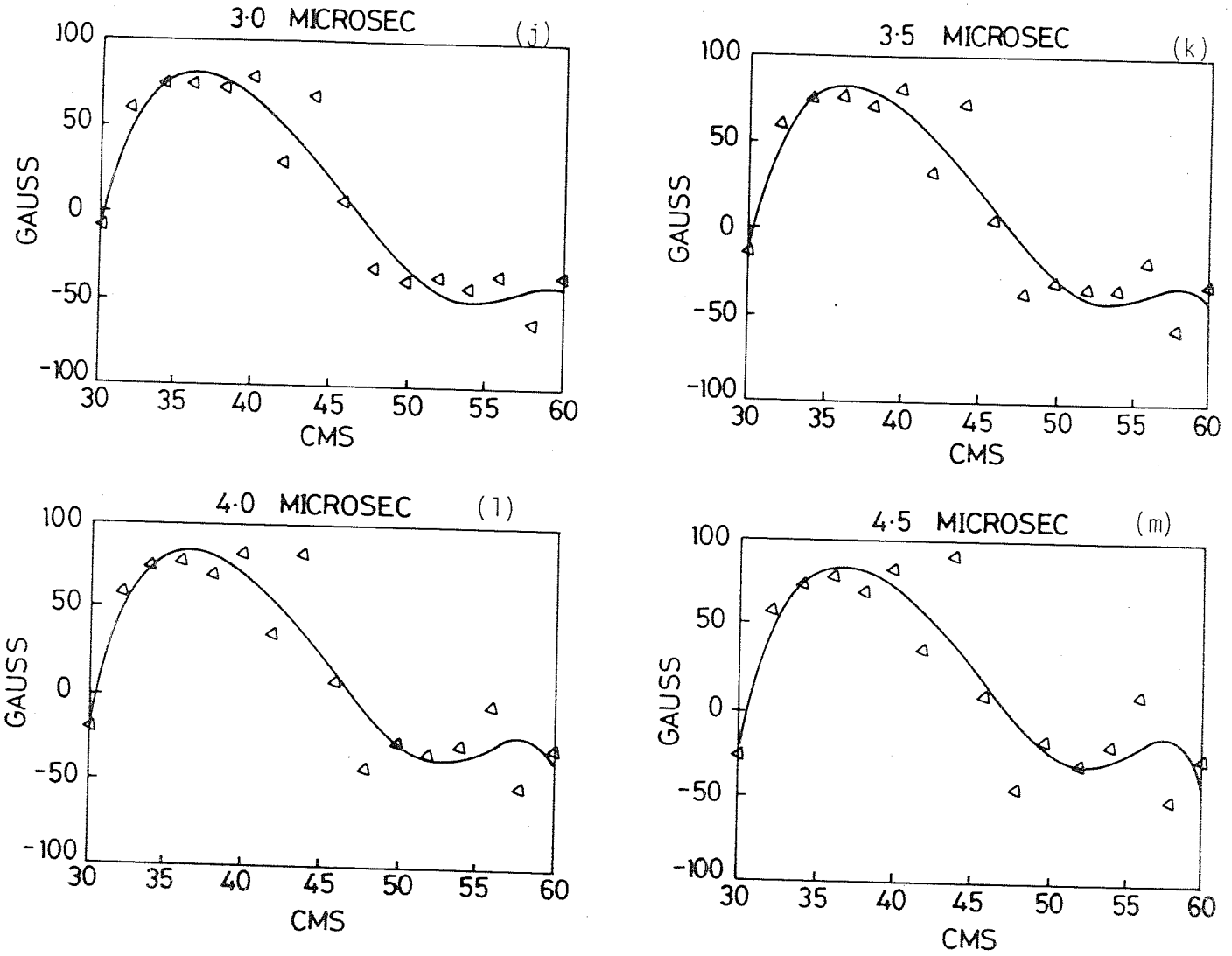

Fig. 3.33: Time evolution of radial profile of poloidal field.

zero crossing of the poloidal magnetic field is near 53.0 cm at 100 ns. The maximum poloidal field at this time being about 10 gauss as shown in fig. 3.32(a). But at 200 ns the position of the minimum shifts to R < 50 cm and the maximum poloidal field is about 100 gauss. The minimum of the magnetic field (i.e. zero crossing) continues to stay at around the same radial location (i.e. near R = 48.0 cm) without any appreciable shift up to about 1.0 μs, with maximum poloidal fields coming at about 300 ns. After 1 μs, the minimum is shifted further inward and the field starts decreasing all along the radius. The apparent asymmetry in the poloidal field profiles after 500 ns is due to errors which crept in during the digitization. The signal levels before digitization (i.e. before the correction is added and not the actual poloidal fields) are low after 500 ns, because of which the errors in digitization are more after this time. However, in the case of vertical profiles of the poloidal field and in the measurements of δB_t, where the signals have longer rise time and lasts for longer time with high signal levels, the errors due to digitization are negligible. Another observation regarding these profiles is the steepness of the gradient at the minimum. The sharp gradient at the minimum of the field at 300 ns becomes more shallow at 1.0 μs and later.

Typical poloidal field observed at a major radius of 45.0 cm along a chord parallel to the major axis (i.e. vertical profile) is shown in figs. 3.34(a) and 3.34(b). Fig. 3.34(a) shows a typical signal at a distance of 6 cm above the mid plane, which shows a rise time of about 350 ns followed by a slow decay. Fig. 3.34(b) is a signal obtained at a distance of 9 cm below the mid plane. This shows a rise time of about 400 ns, followed by a slow decay.

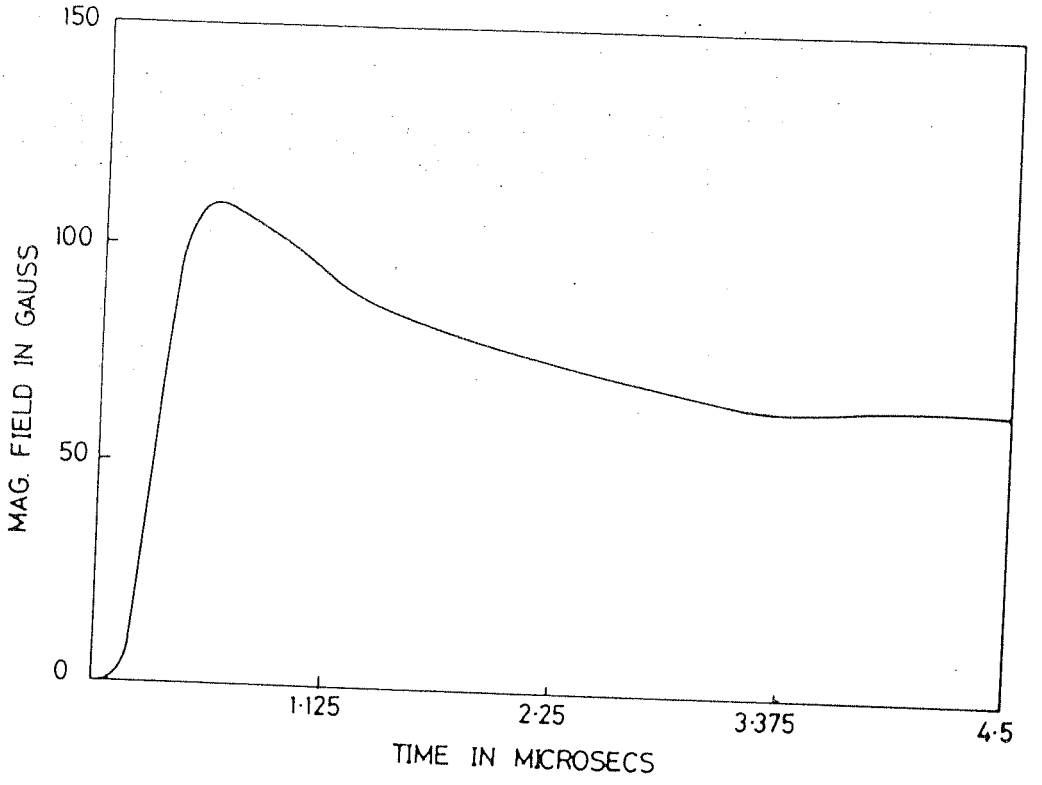

(a)

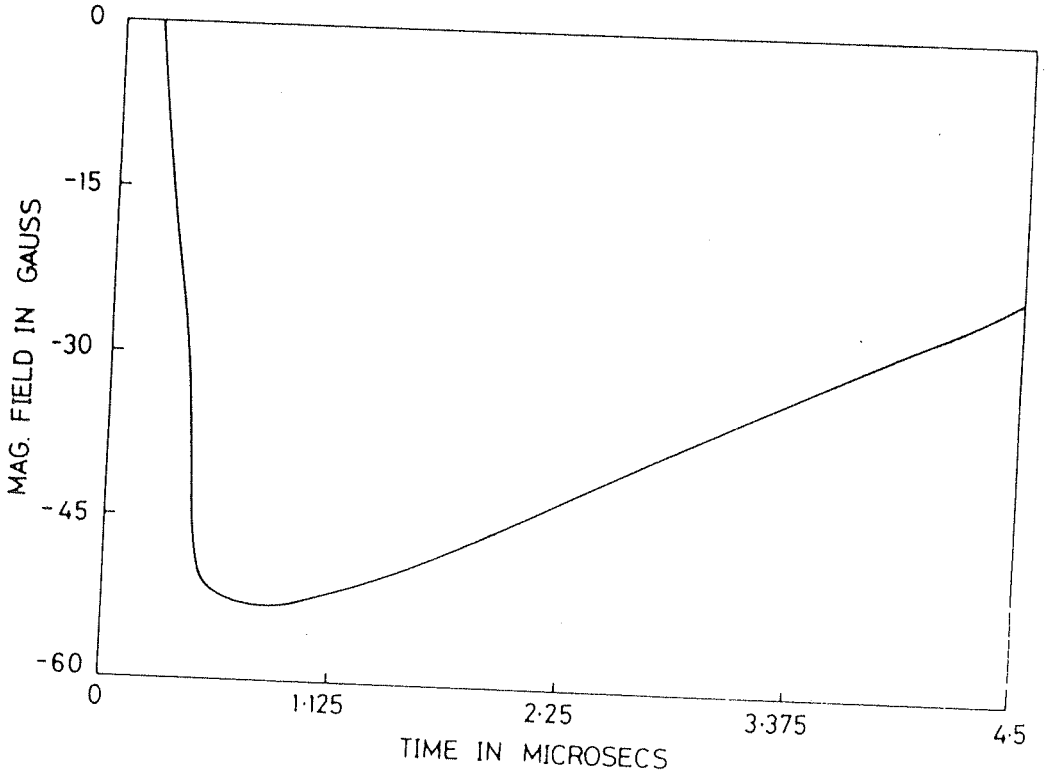

(b)

Fig. 3.34: Poloidal field at R = 45.0 cm
(a) z = +6.0 cm; (b) z = -9.0 cm

The time evolution of the vertical profile of the poloidal field is plotted in fig. 3.35(a) to 3.35(m). As can be seen from these figures, a flat profile at 100 ns (where B_ϕ is less than few gauss)evolves into a symmetric one about the mid plane at 200 ns and remains symmetric thereafter. with the peak of the magnetic field coming between 300-400 ns. These profiles also show a sharp gradient in the field near the minimum up to about 500 ns, which becomes more and more shallow at and after 1.0 μs, like the radial profiles. Unlike the radial profiles these profiles show no appreciable shifting of the minimum.

The poloidal magnetic field is a measure of the net current and its location. If the location of the current channel is independent of time then the magnitude of this field gives the net current. Since in our experiment the current channel location is not fixed (especially during the beam injection), the time evolution of the magnetic field profile will be needed for calculating the current profiles. Besides, the time evolution of the magnetic field will be useful in evaluating the self magnetic energy and in calculating the equilibrium and stability of the system. Firstly, the field near the outer wall rises fast within 250 ns (almost same as the net current rise time) and starts decaying but remains of same polarity. The decrease of the field after the peak can be due to a decrease in current or shift of the current channel away from the outer wall or both. Since the decay of the field is faster than the net current decay, we can infer that the shift of the net current is responsible for the observed fast decay of the poloidal field near the outer wall. (The actual field is comprised of two parts viz. (1) the field due to net current in the torus and (2) the field due to wall currents). The magnetic field

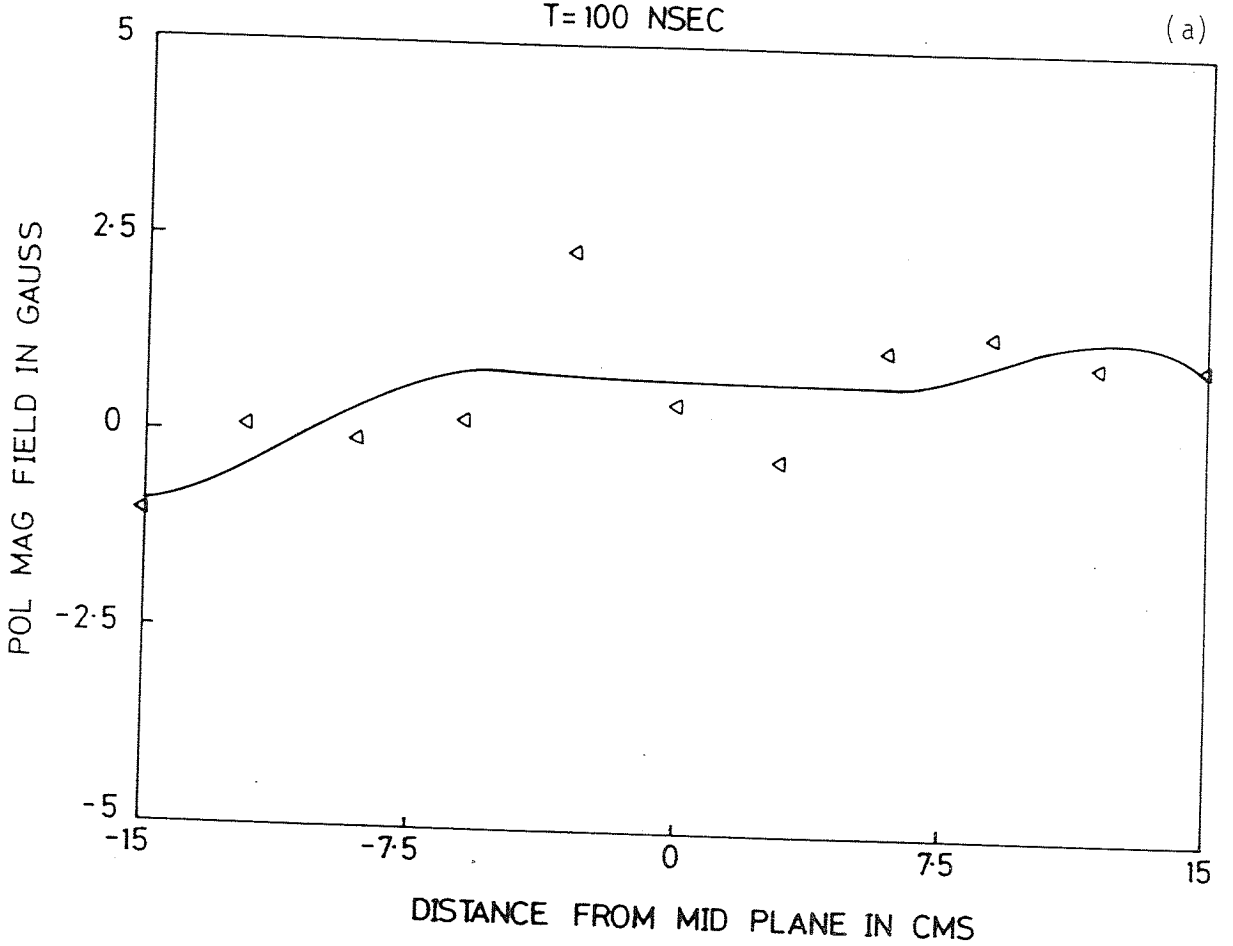

Fig. 3.35: Time evolution of vertical profile of poloidal field

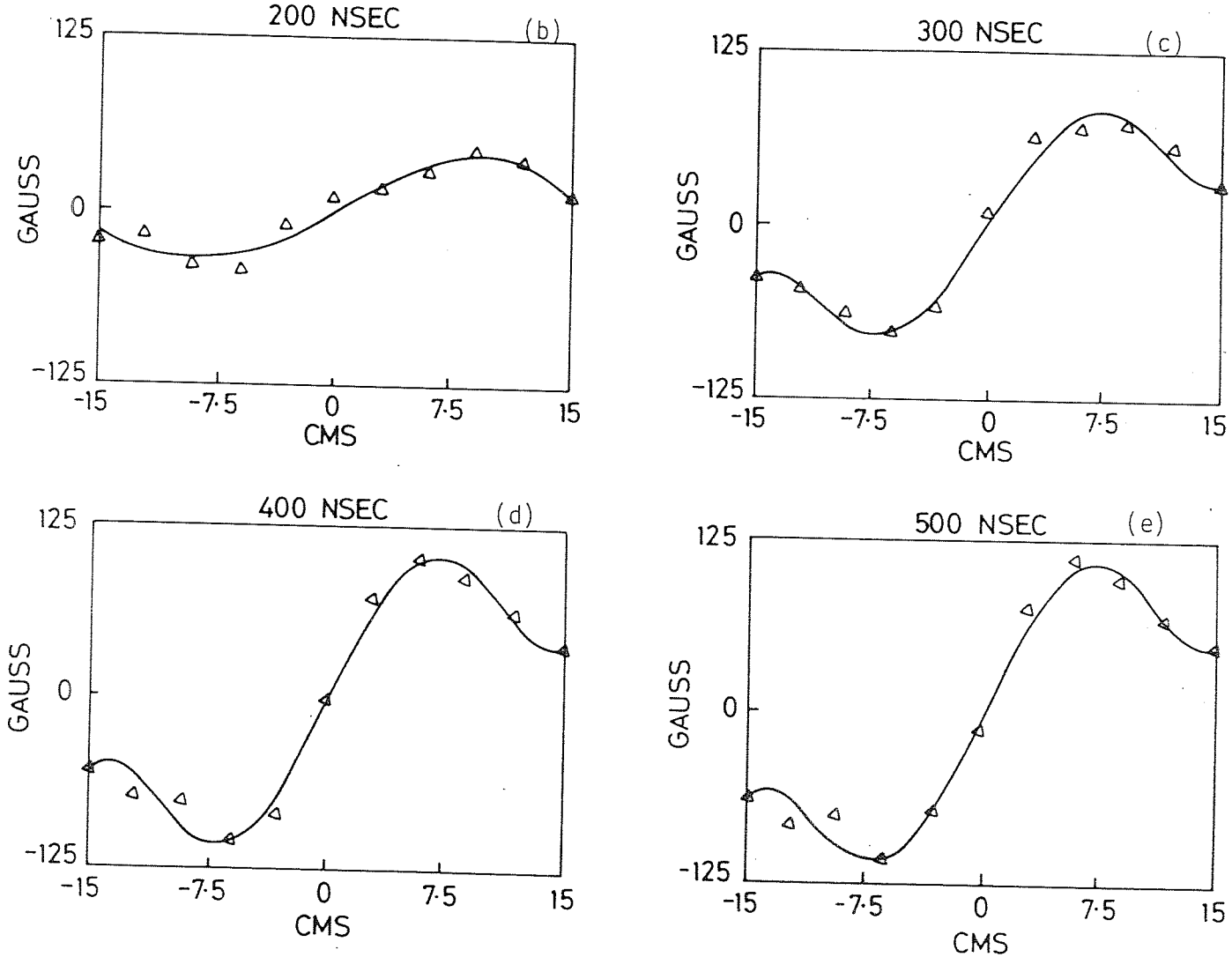

Fig. 3.35: Time evolution of vertical profile of poloidal field

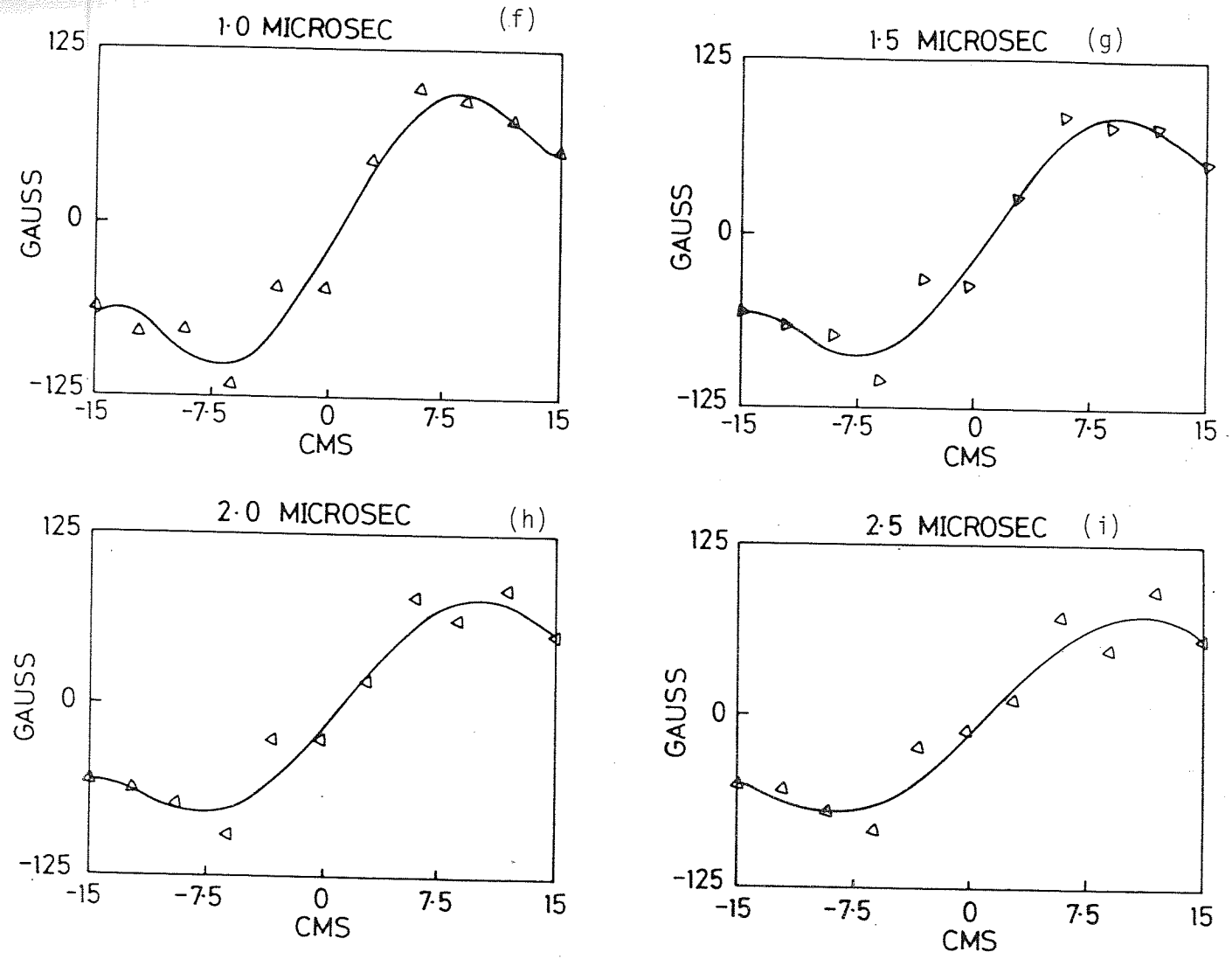

Fig. 3.35: Time evolution of vertical profile of poloidal field

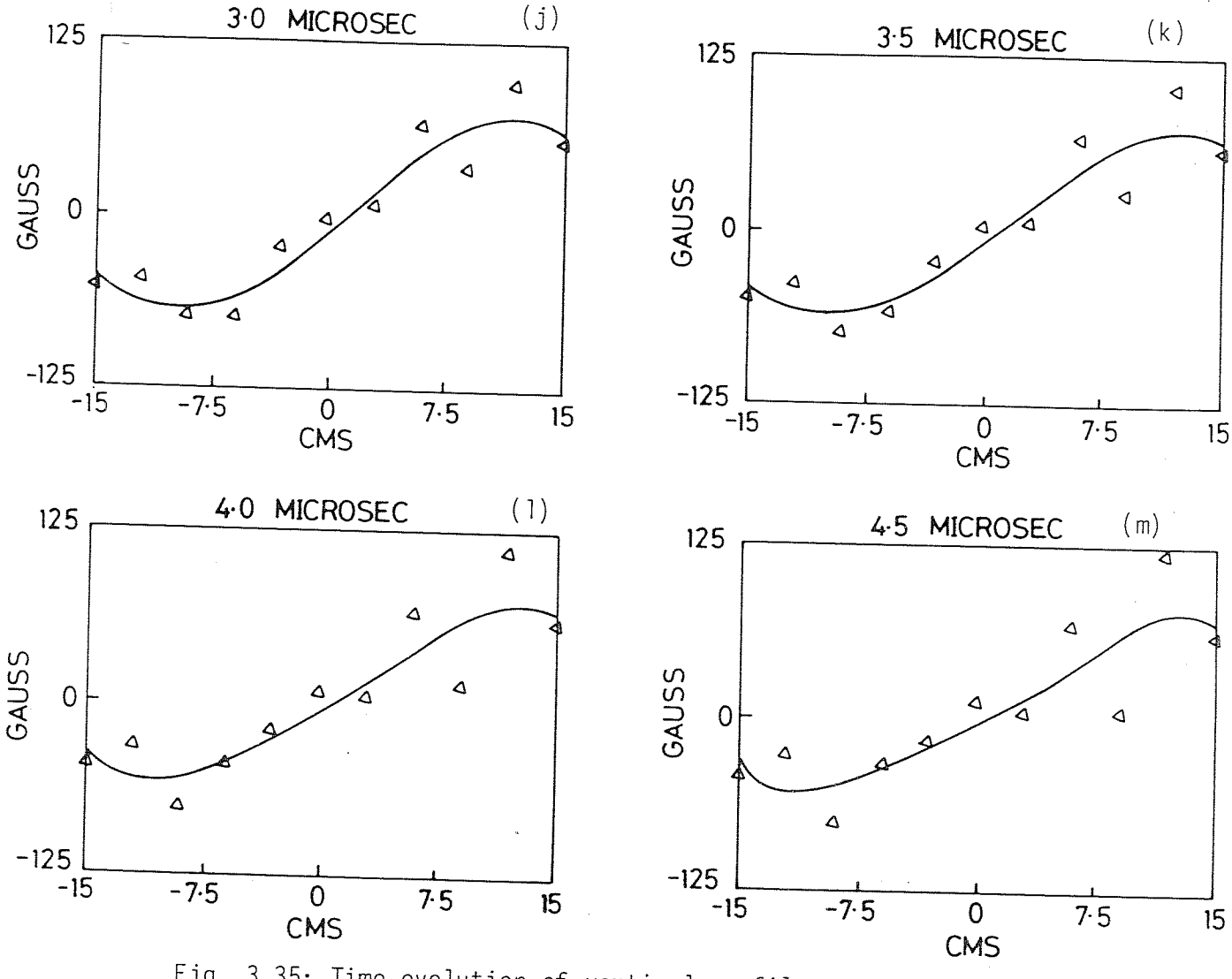

Fig. 3.35: Time evolution of vertical profile of poloidal field

from R = 48.0 cm to R = 52.0 cm (R is the major radius) shows an interesting feature. The field is initially of opposite polarity to that of the field near the outer wall but quickly changes sign (fig. 3.32(b)) and remains without any further change in polarity. This indicates that the beam arrives at this location nearer to the outer wall but later on moves near to the minor axis reversing the direction of the magnetic field. Since the magnetic field at the minor axis and inward remains unidirectional throughout the time, it can be concluded that the current channel did not shift inward beyond the minor axis.

The time evolution of these poloidal field profiles (fig. 3.33) indicates a clear shift of the zero crossing (which is roughly the current centre). During the net current rise time (i.e. beam injection phase) these profiles show sharp rise in the field all along the radius as well as shift of the zero crossing of the field towards the major axis. This can be clearly understood as the building up of the net current and also the shift of the current channel inward simultaneously. The near similarity of the profiles between 200 ns and 500 ns indicates the establishment of an equilibrium current ring. After 1.0 μs the profile starts flattening indicating a current decay.

The poloidal field along the major axis at a major radius of 45.0 cm, shows rise times similar to the rise time observed at R = 45.0 cm while measuring the radial profiles. This shows no measurable motion along the vertical direction. The time evolution of the vertical profile (fig. 3.35) showed no change of polarity. These profiles are symmetric with respect to mid plane all through the time indicating no gross vertical motion of the current channel.

Comparison of radial and vertical profiles of the

poloidal field shows a clear structure in the radial profile at 100 ns. No such structure could be seen in the vertical profile at this time, indicating a current channel away from minor axis (nearer to the outer wall). The steep gradient of this profile near the zero crossing at early times (less than 500 ns) becomes shallower indicating a decay in the net current.

From the discussion of the small Rogowski coil measurements and the poloidal field measurements, we can qualitatively understand that the beam moves major radially inward from the point of injection and the net current rises simultaneously.

To understand this behaviour more quantitatively, time and space resolved Faraday cup measurements and the net current density profiles obtained from the poloidal field profiles are discussed here.

3.6.1 Effect of wall currents on the calculation of current profiles:

When a beam is injected and trapped in a torus for times shorter than the magnetic diffusion time of the vessel, image currents are induced in the vessel wall in the opposite direction to that of the net current in the vessel. The magnitude of this image current is same as that of the net current. If the net current channel is centered at the minor axis and with a symmetric net current distribution, the poloidal magnetic field measured can be used to calculate the current distribution from the $\nabla \times \mathbf{B}$ equation. For the current density in the toroidal direction, we can write (assuming $R/a \gg 1$)

$$\frac{1}{r}\frac{\partial}{\partial r}(rB_\phi) - \left(\frac{1}{r}\frac{\partial B_r}{\partial \phi}\right) = \mu_o J_\theta \qquad (3.20)$$

where ϕ and θ are the poloidal (about the current centre) and toroidal directions respectively and r is the minor radius (measured from the current centre). Assuming symmetry about ϕ, we can neglect the second term on the L.H.S. and the above equation reduces to

$$\frac{1}{r}\frac{\partial}{\partial r}(rB_\phi) = \mu_o J_\theta \qquad (3.21)$$

The above equation assumes that 1) the toroidal effects are negligible ($R/a \gg 1$) and 2) B_r is symmetric about the current centre.

However in the experiment, even if we neglect the toroidal effects, the beam is not at the minor axis, thus forcing a non uniform wall currents, and the neglecting of the $\partial/\partial\phi$ term in eq. (3.20) is not justified. This difficulty can be overcome if we use the major axis as the cylinder axis and calculate the toroidal current using the following equation

$$\frac{\partial B_R}{\partial z} - \frac{\partial B_z}{\partial R} = \mu_o J_\theta \qquad (3.22)$$

From the above equation we can see that we need to measure B_z as a function of R to obtain the second term on the L.H.S and B_R as a function of z at many radial locations to obtain the first term on the L.H.S. The important point is that current calculated from this equation does not involve any assumption.

The poloidal magnetic field profile and the current density calculated using eq. (3.21) are shown in fig. 3.36(a) and 3.36(b) respectively. As can be seen from this figure the peak current density is less than 75 Amps/sq.cm. The current density obtained from eq. (3.22) is shown in fig. 3.36(c) whose peak current density is more than 100 Amps/sq.cm. These

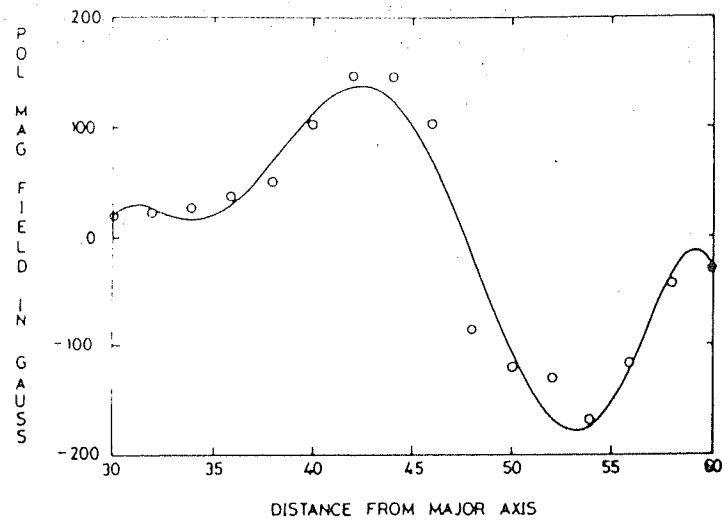

(a) Poloidal field profile

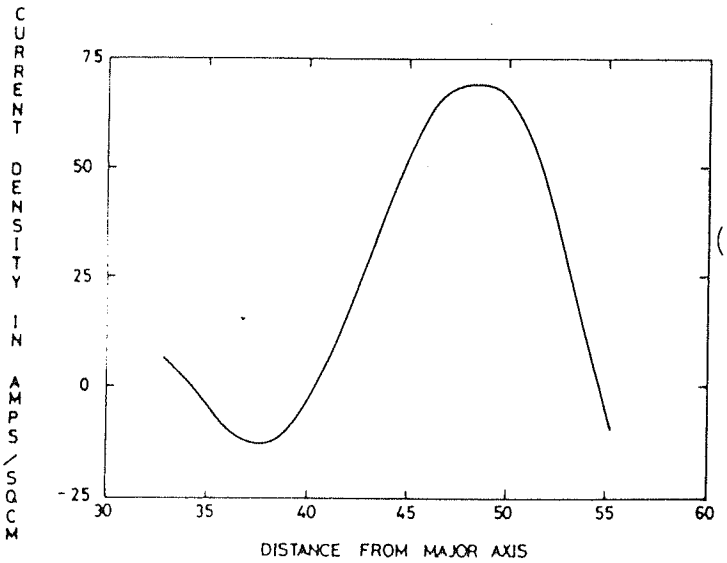

(b) Current profile (with assumption)

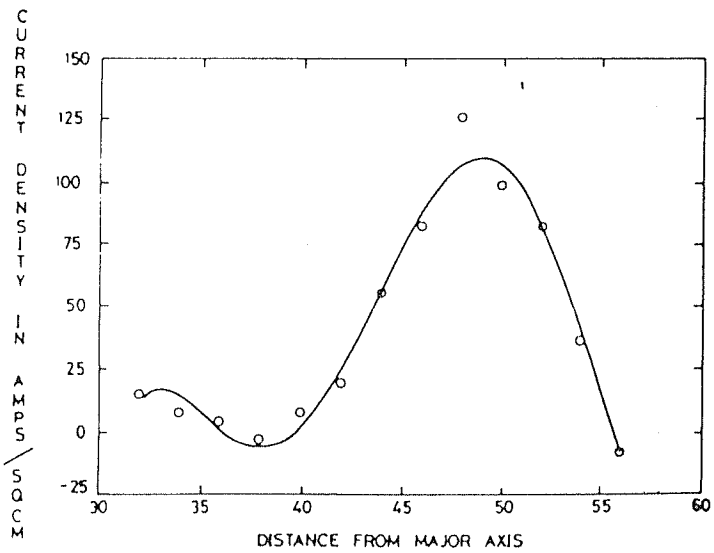

(c) Current profile (without assumption)

Figure 3.36

profiles are at the time of the peak net current, which corresponds to the time after the beam had reached the equilibrium. The difference can be even more during the initial phase, where the beam is more to one side of the minor axis.

3.6.2 Net current profile and its time evolution

The profiles of net current density calculated from the radial profiles of the poloidal magnetic field are shown in figs. 3.37(a) - 3.37(m). One important thing to remember is that these currents are calculated from least square polynomial fit for the experimental points. Because of the finite number of terms in the polynomial, to some extent, there is always a smoothing. This will reduce the gradients and hence while calculating the current densities, the calculated peak current densities could appear as less than the actual peak current densities. The discontinuity at the peak of the current is due to interpolation which is to be done to avoid infinities in calculating current densities using $J_\theta = 1/r \ \partial(rB_\phi)/\partial r$ at $r = 0$.

In obtaining the time evolution of these net current density profiles (fig. 3.37(a) - 3.37(m)) only an approximate formula (eq. (3.21)) was used as discussed earlier. Therefore, it is not necessary that these profiles are the actual profiles. However comparison of the correct profile (fig. 3.36(c)) with the one obtained from the approximated formula (fig. 3.36(b)) shows a good agreement in the shape. But the magnitude of the correct profile is nearly 1.6 times the approximate one. This comparison is when the current channel is away from the wall. Hence the current profile at 100 ns (fig. 3.37(a) may not be the correct profile, but the profiles at 200 ns and later can be safely assumed to be the real profiles with a factor (of about 1.6) multiplying the Y-

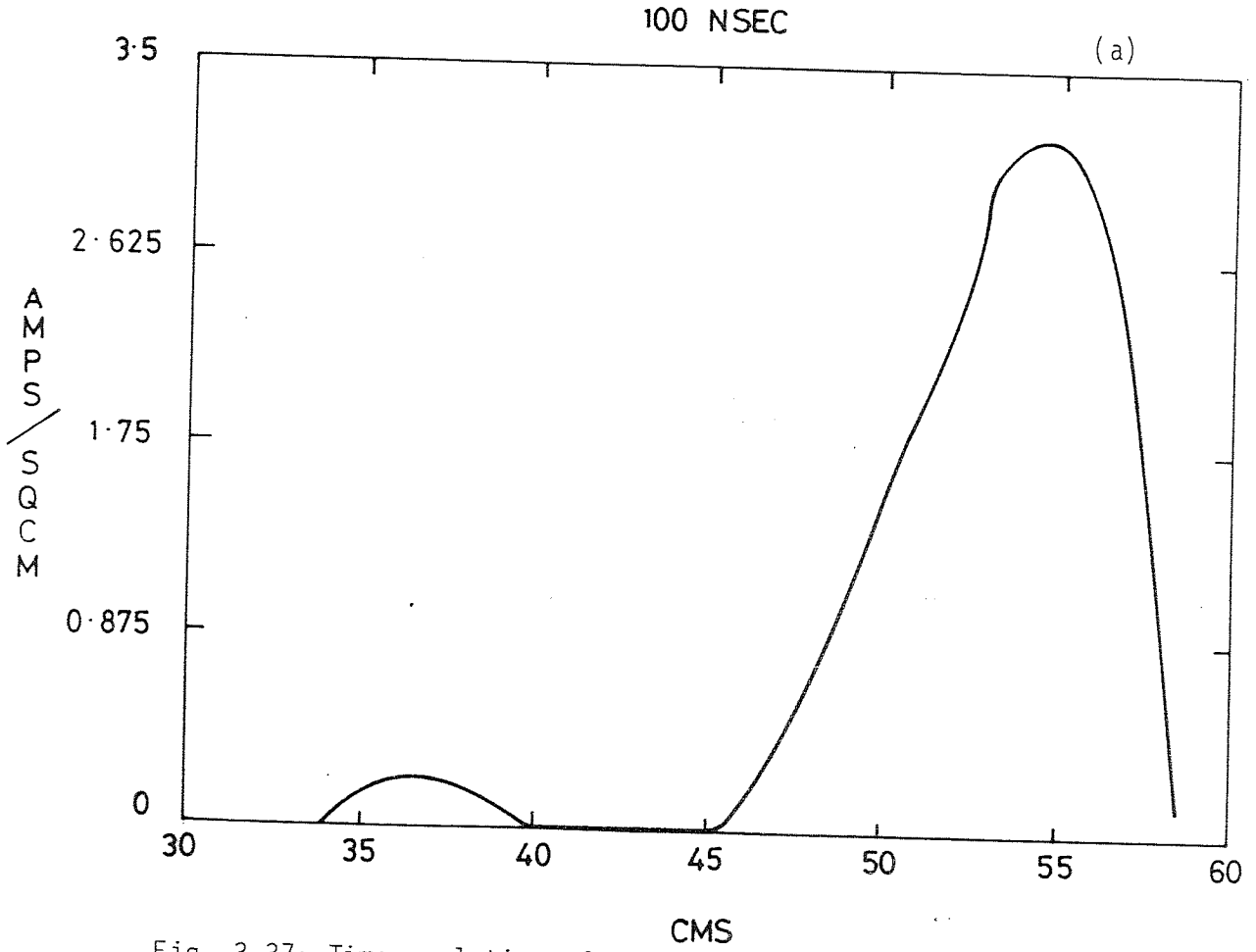

Fig. 3.37: Time evolution of net current profile

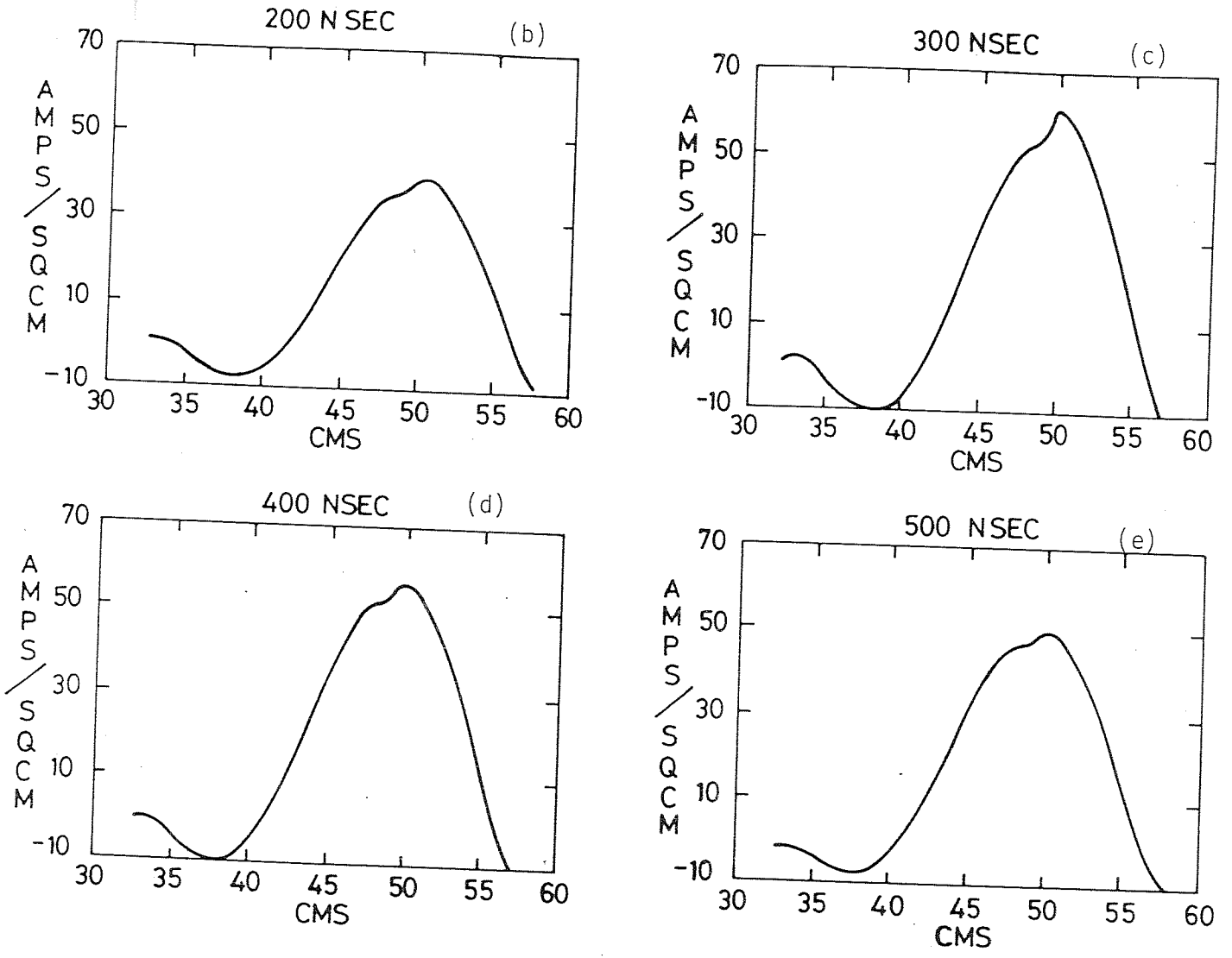

Fig. 3.37: Time evolution of net current profile

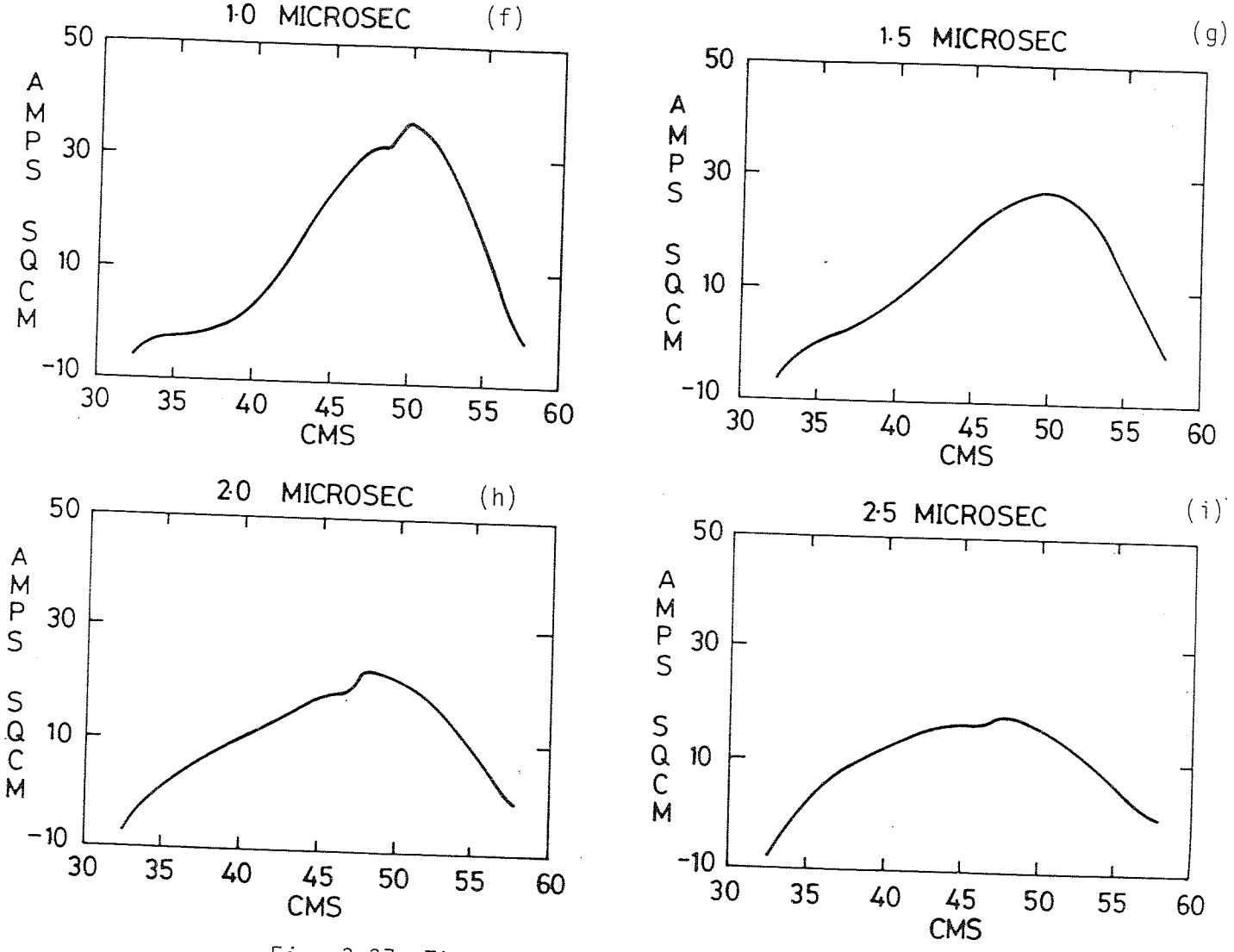

Fig. 3.37: Time evolution of net current profile

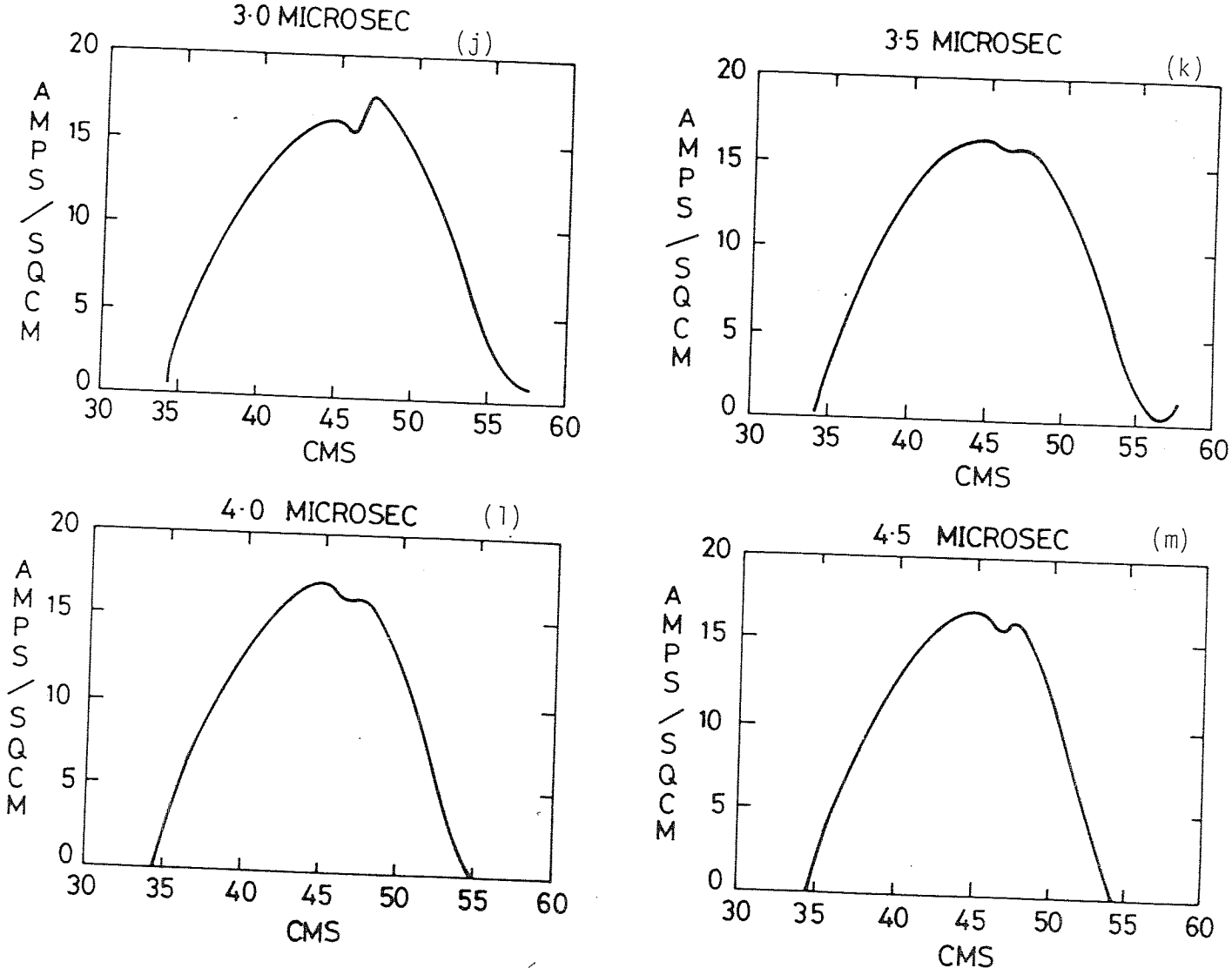

Fig. 3.37: Time evolution of net current profile

scale in the profiles shown in figs. 3.37(b) to 3.37(m). The beam current profiles obtained from the Faraday cup measurements are shown in figs. 3.21(a) and 3.21(b).

As expected from the poloidal field profiles, the net current density profiles showed an inward shift with time during the first 300 ns. Faraday cup profiles also show an inward shift (fig. 3.21(a)). However, the position of the peak of the profiles and their magnitude are different in both these measurements. In the case of the net current profiles the peak current density is 125 Amps/sq.cm and its position is at a major radius of R = 48.0 cm. In the case of Faraday cup measurements they are 250 Amps/Sq.cm and R = 51.0 cm respectively.

The difference in the peak amplitudes is most likely due to two reasons. (1) Faraday cup does not register any return current and (2) it collects plasma electrons as well (as it is not covered with a foil). Both these effects make the Faraday cup measurements to show higher current densities than the net current profiles.

If the return current decay calculations (decay time of 35 ns) and the values inferred from the net current measurements (decay time should be less than the net current rise time $\approx$300 ns) are any indication, then the high Faraday cup current densities are to be understood as the contribution from plasma. The total current obtained from the net current density profile (fig. 3.36(c)) is about 5300 Amps and in good agreement with the net current measured by Rogowski coil (5.0 kAmps). This is only to be expected, since this is without any assumption. However the profiles shown in figs. 3.37(b) to 3.37(m) show lesser total net current, but when multiplied by the factor (1.6), give nearly the currents observed by Rogowski coil.

Comparison of the Faraday cup profiles (fig. 3.21(b)) with net current profiles [figs. 3.37(f) - 3.37(m)] at later times (after 500 ns) also show a difference in their magnitude but are in agreement in their spatial extents.

Comparison of the net current density profiles with that of the small Rogowski coil measurements is interesting. A simultaneous decrease and increase in the net current measured by the small Rogowski coil, when the Rogowski coil is near the outer wall and at centre respectively, shows a net current channel shifting towards the centre of the chamber (i.e. towards the minor axis). This is in agreement with the current profiles obtained from Faraday cup and also from the magnetic fields. An important observation in the net current profiles is the existence of a current opposite to that of the beam current near the inner wall. This feature persists for nearly 1.0 μs. A negative current is seen when the small Rogowski coil is kept near the inner wall (fig. 3.33(c)). This also persisted for about 1.0 μs. Two independent (though magnetic in nature) measurements agree well to substantiate that there is a current opposite to that of the beam current at this location. The location of the return current incidentally is at a location where the plasma density is low before the beam injection. This may be because of slow decay of the return current in the low density region.

One important aspect of the study during the beam injection is the motion of the beam in a poloidal cross-section. We shall neglect the Larmor motion of the beam particles in this discussion. In the presence of a toroidal field alone, the beam particles undergo the familiar curvature and gradient drifts, which is in the vertical direction (i.e. parallel to the major axis). Adding a

betatron type field to the toroidal field produces an elliptical orbit in a poloidal plane (projection of the beam particle trajectory on a poloidal plane), the major and minor radii and the ellipticity depending on the magnitude and the field index of the applied betatron field (Linhart, 1960) and Benford et al., 1974b). The beam motion in a conducting toroidal vessel in the presence of an external toroidal and vertical magnetic field is analyzed by Mohri et al., (1977a). This analysis showed that the beam trajectory (projected on a poloidal plane) is a periodic oscillation about an equilibrium position. The amplitude of this oscillation was shown to decrease with increasing net current. Partial beam energy loss also was predicted to produce the same effect. In the presence of a conducting wall and only toroidal field (no vertical field), the beam particle trajectory is a closed orbit in the poloidal plane. The equilibrium position lies inside this orbit (Kusse and Lockner, 1974).

From the above observations, we can conclude that in the presence of a conducting wall the beam particle trajectory is a closed orbit and the amplitude of this periodic motion about the equilibrium will be inversely proportional to the net current and beam energy loss.

The above discussion is valid for a single particle in the applied and wall induced fields. Since the beam self fields produce only a rotation of the beam about its own axis, the beam (centre) trajectory will be same as the single particle trajectory in the applied and wall induced fields (Bailey et al., 1982).

Experimentally, closed orbits were inferred from the REB current drive experiments in the macrotor tokamak by Bailey et al., (1982). A good beam penetration from outside wall into the plasma column has been reported (Proulx, 1981).

Experimental confirmation of a wall induced field acting on the beam to effect its trajectory has been reported by Benford et al., (1974a). In the SPAC experiments, the wall induced fields have been used to launch the beam on an equilibrium orbit (Mohri et al., 1982).

In our experiment, we have not observed any vertical motion of the beam. Instead, the beam swiftly moves inward from a major radial launch position of R = 54.0 cm to an equilibrium position of R = 48.0 cm. This can be understood as follows. Fast net current rise induces a current in the wall. This in turn produces a magnetic field at the centre of the beam. This magnetic field interacts with the current and forces it radially inward to an equilibrium position determined by the force balance. As pointed out by Mohri et al., (1977a), the amplitude of the periodic motion decreases as the net current increases. Now, if the amplitude is smaller than the beam radius, then we will not be able to see any vertical motion of the beam.

3.7 Plasma diamagnetism

The changes in toroidal field, δB_t is monitored following the beam injection. An important observation in these measurements is the δB_t behaviour near the outer wall. δB_t at this location is paramagnetic (positive) initially for about 700 ns, which later becomes diamagnetic and stays diamagnetic as shown in figs. 3.38(a) and 38(b). Fig. 3.38(a) show the δB_t evolution at R = 58.0 cm and fig. 3.36(b) shows the same thing at R = 54.0 cm. From these figures it is clear that initially a paramagnetic field with a rise time of less than 500 ns stays paramagnetic for about 700 ns, beyond which it becomes diamagnetic. The change in polarity occurs (peak to peak) in about 300 ns.

Figs. 3.38(c) and 3.38(d) show δB_t at R = 50.0 cm and at R = 46.0 cm. These signals show a diamagnetic field all through the time (up to 1.5 μs) tending to become paramagnetic after 1.5 μs. The δB_t profiles on the mid plane are shown in fig. 3.39(a) to 3.39(p) and 3.40(a) to 3.40(l). As these profiles show, the diamagnetic signal starts appearing near the minor axis at about 100 ns, the signal near the inner and outer walls being paramagnetic. This kind of profile persists for about 600-700 ns, beyond which time δB_t remains paramagnetic near the inner wall and changes to diamagnetic in nature near the outer wall. The simultaneous maximum values of diamagnetic and paramagnetic fields in the profile appearing at about 400 ns. The consistency in the behaviour of δB_t near the outer wall can be gauged from fig. 3.41, where the signal at R = 54.0 cm is taken from two consecutive shots when the probe is rotated through 180° for the second shot.

Similarly, the profiles of δB_t along the vertical direction are plotted in figs. 3.42(a) to 3.42(p) and 3.43(a) to 3.43(l), where it can be seen that the signal is in general diamagnetic above the mid plane and paramagnetic below the mid plane. This trend remains the same almost throughout the time.

Unlike the poloidal field signals, reproducibility of δB_t is rather poor (except near the outer wall, which is well reproducible).

A common diagnostic tool used for measuring the plasma perpendicular energy in the presence of an externally applied magnetic field in REB-plasma interaction experiments is the diamagnetic loop (Abrashitov et al., 1974; Ekdahl et al., 1974, Miller and Kuswa, 1973; Greenspan et al., 1980; Kapetanakos et al., 1975 and Sethian, 1976). When a plasma

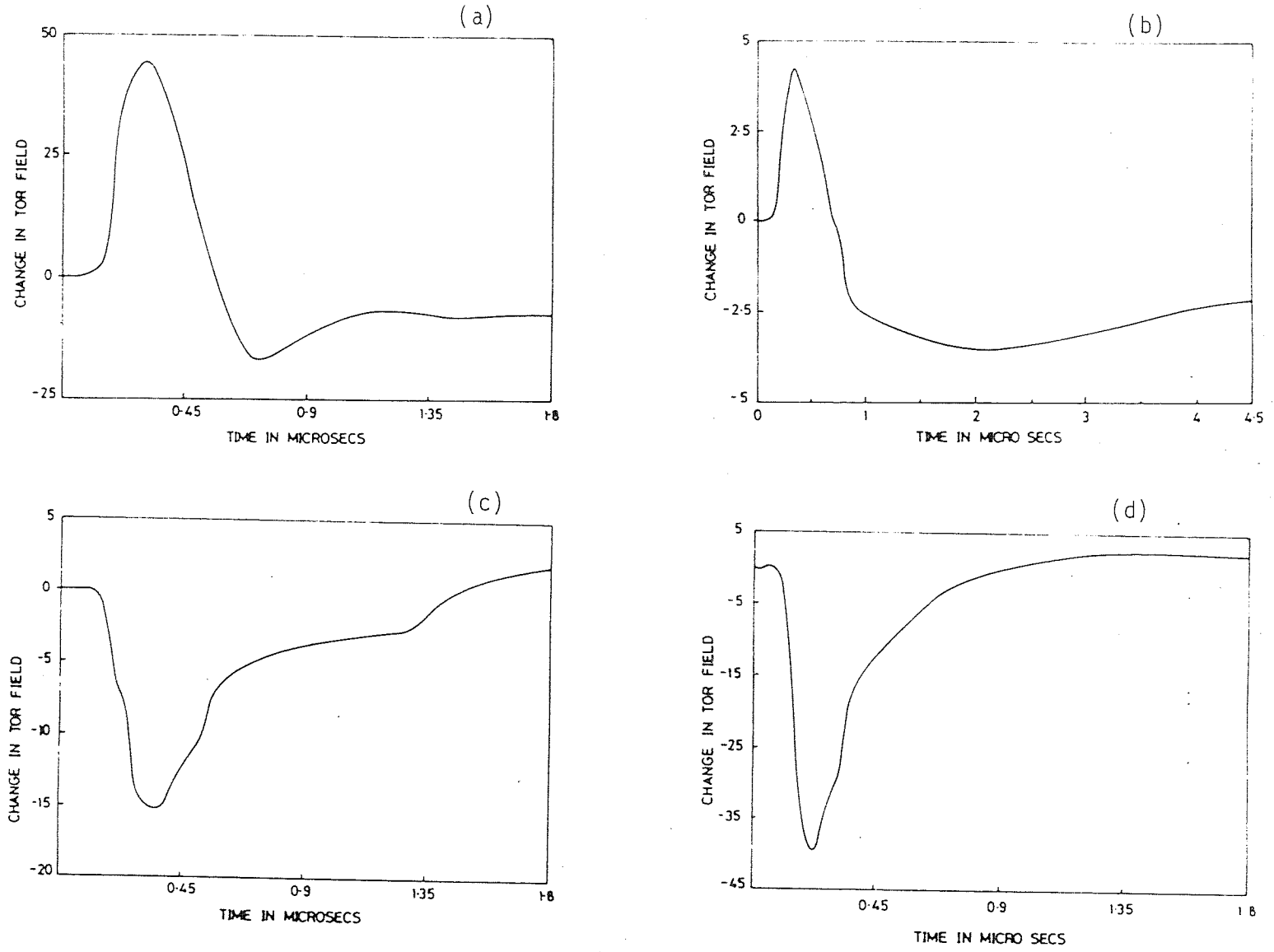

Fig. 3.38: Change in toroidal field (δB_t) in the mid plane
(a) R = 58.0 cm; (b) R = 54.0 cm; (c) R = 50.0 cm; (d) R = 46.0 cm

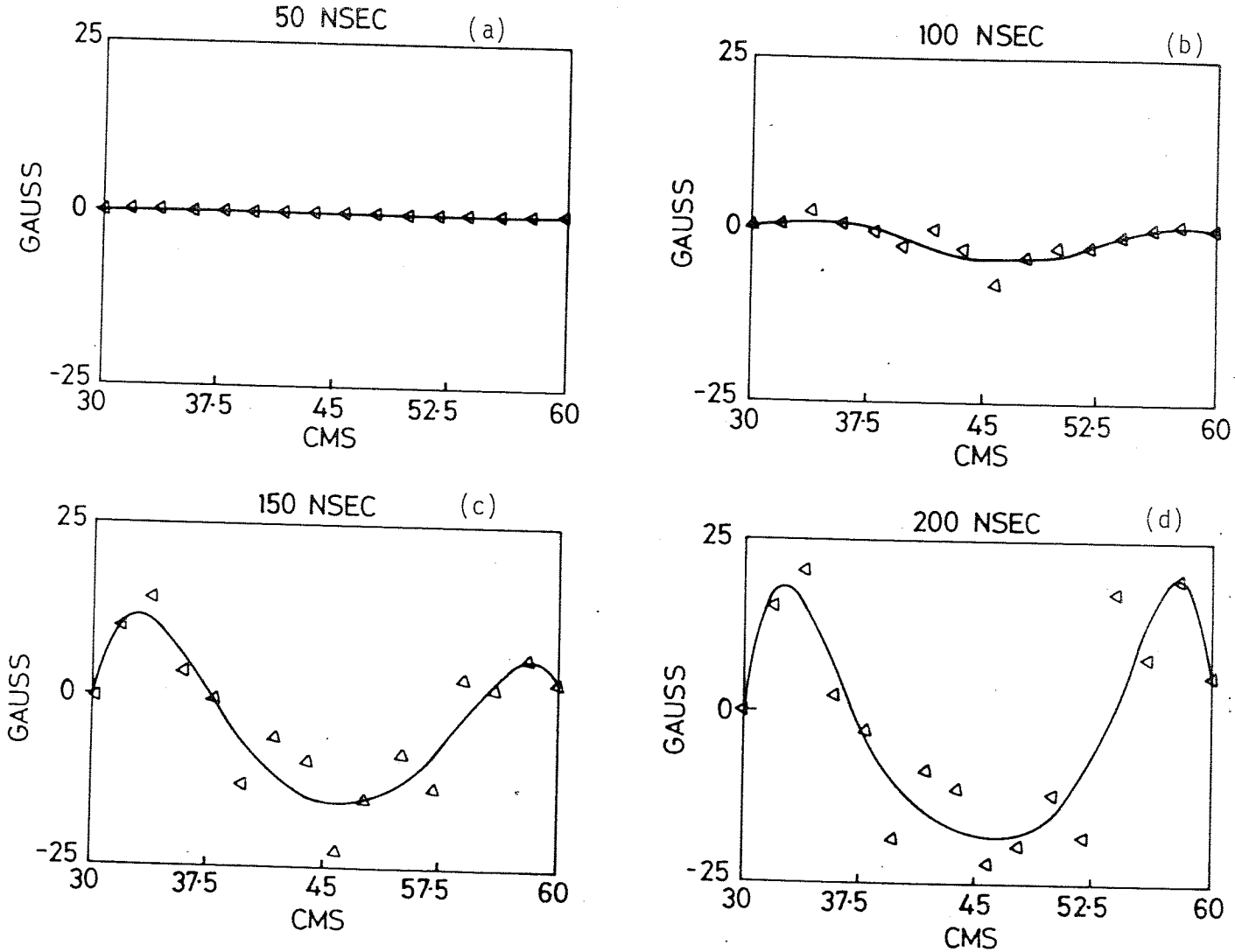

Fig. 3.39: Time evolution of radial profile of δB_t

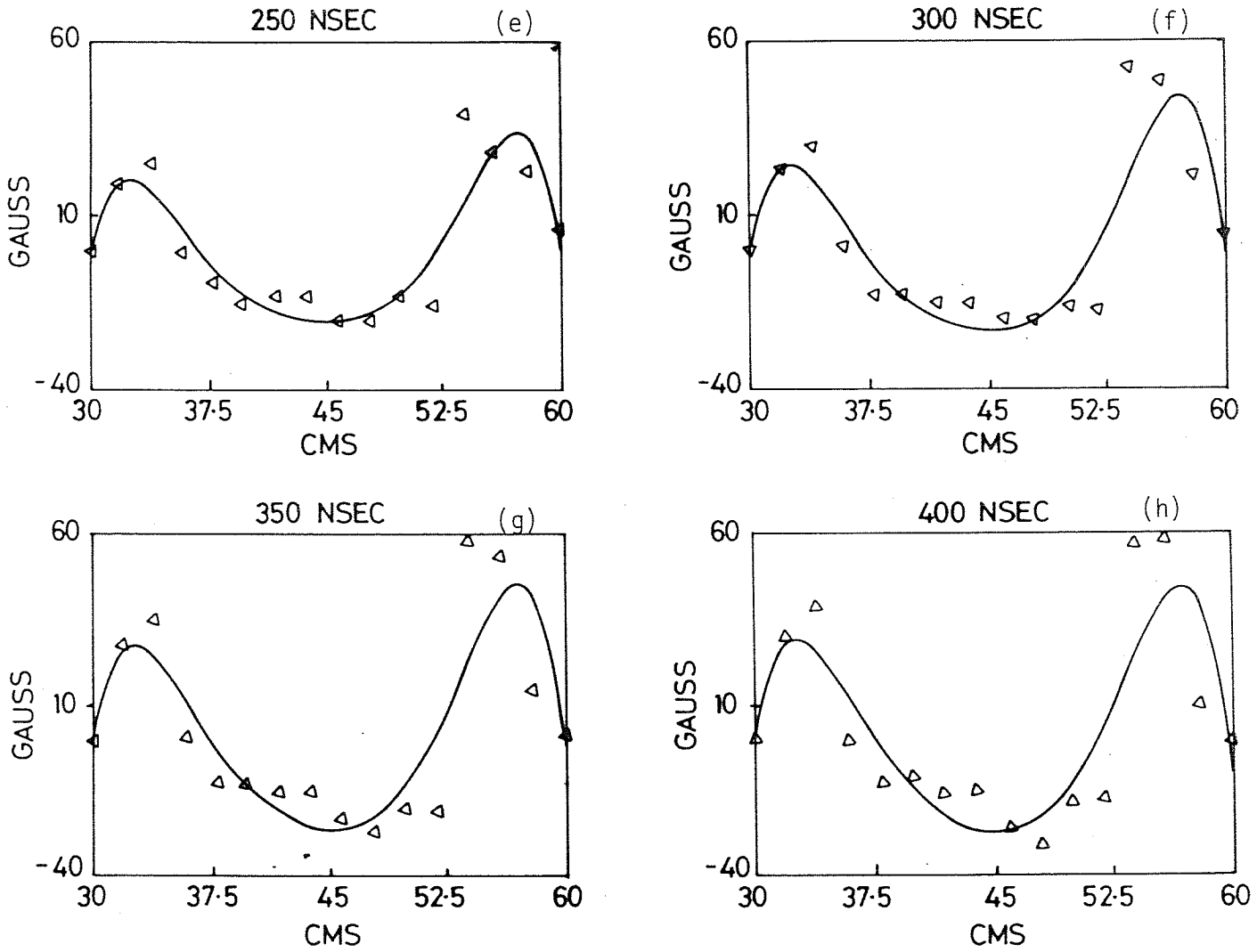

Fig. 3.39: Time evolution of radial profile of δB_t

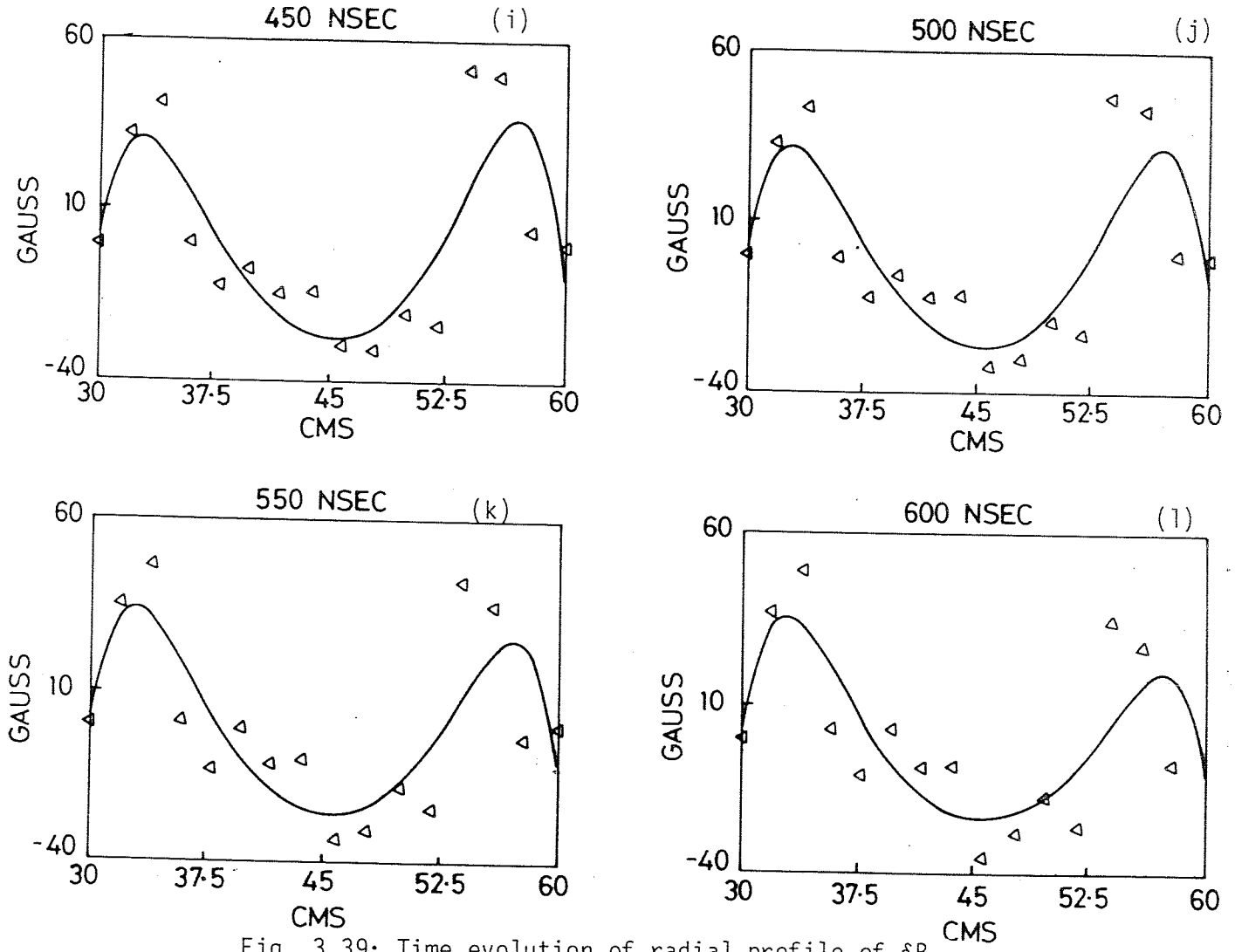

Fig. 3.39: Time evolution of radial profile of δB_t

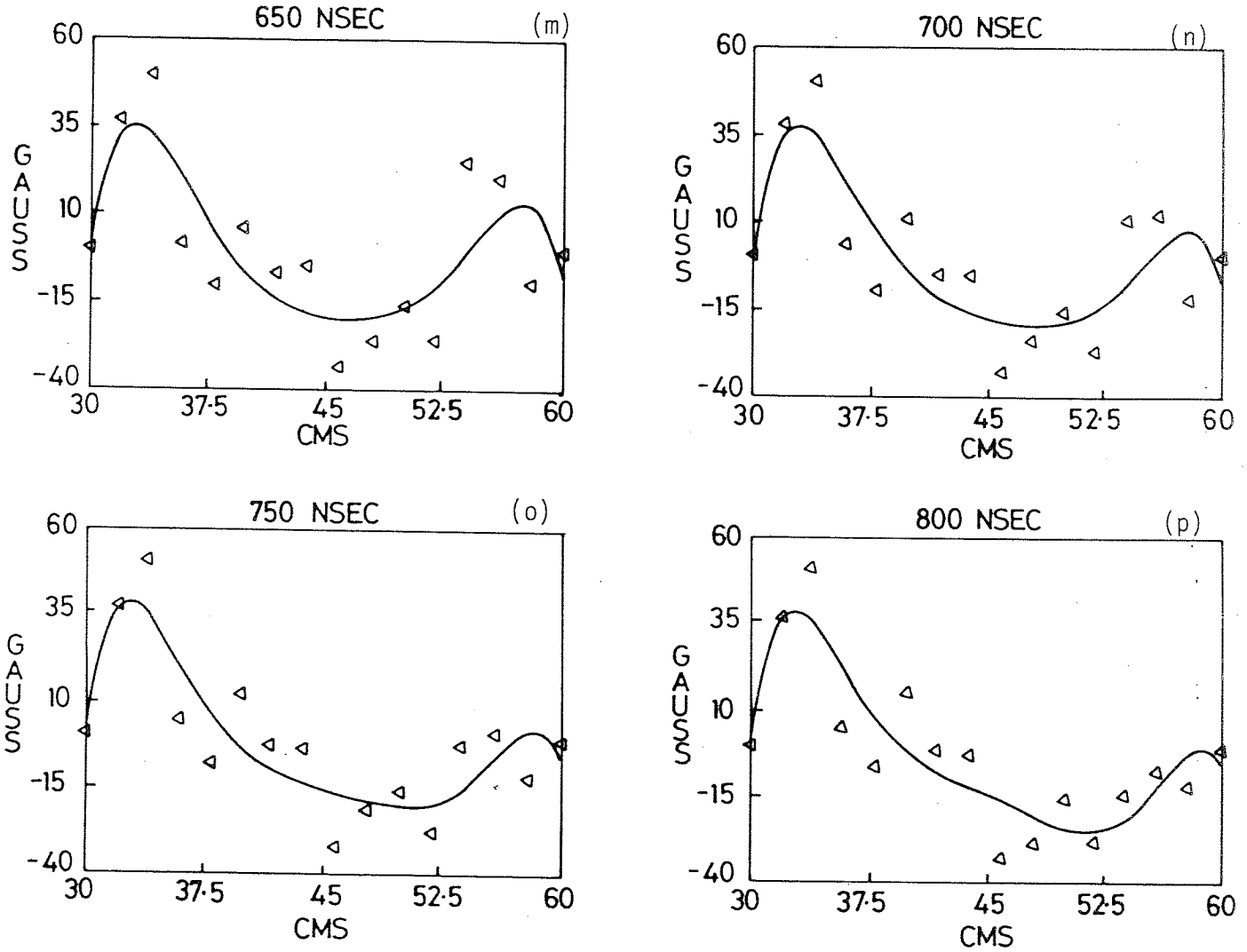

Fig. 3.39: Time evolution of radial profile of δB_t

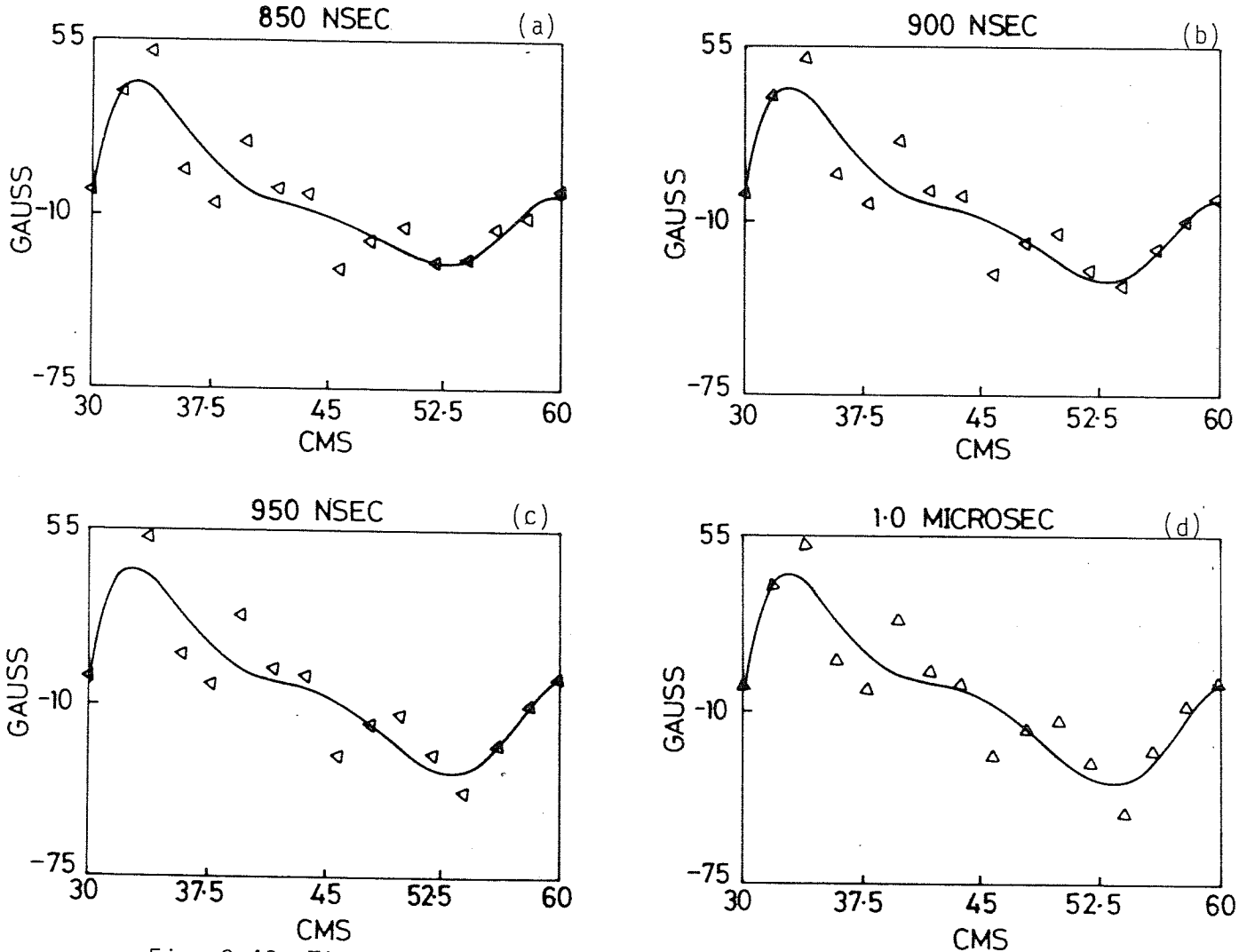

Fig. 3.40: Time evolution of radial profile of δB_t

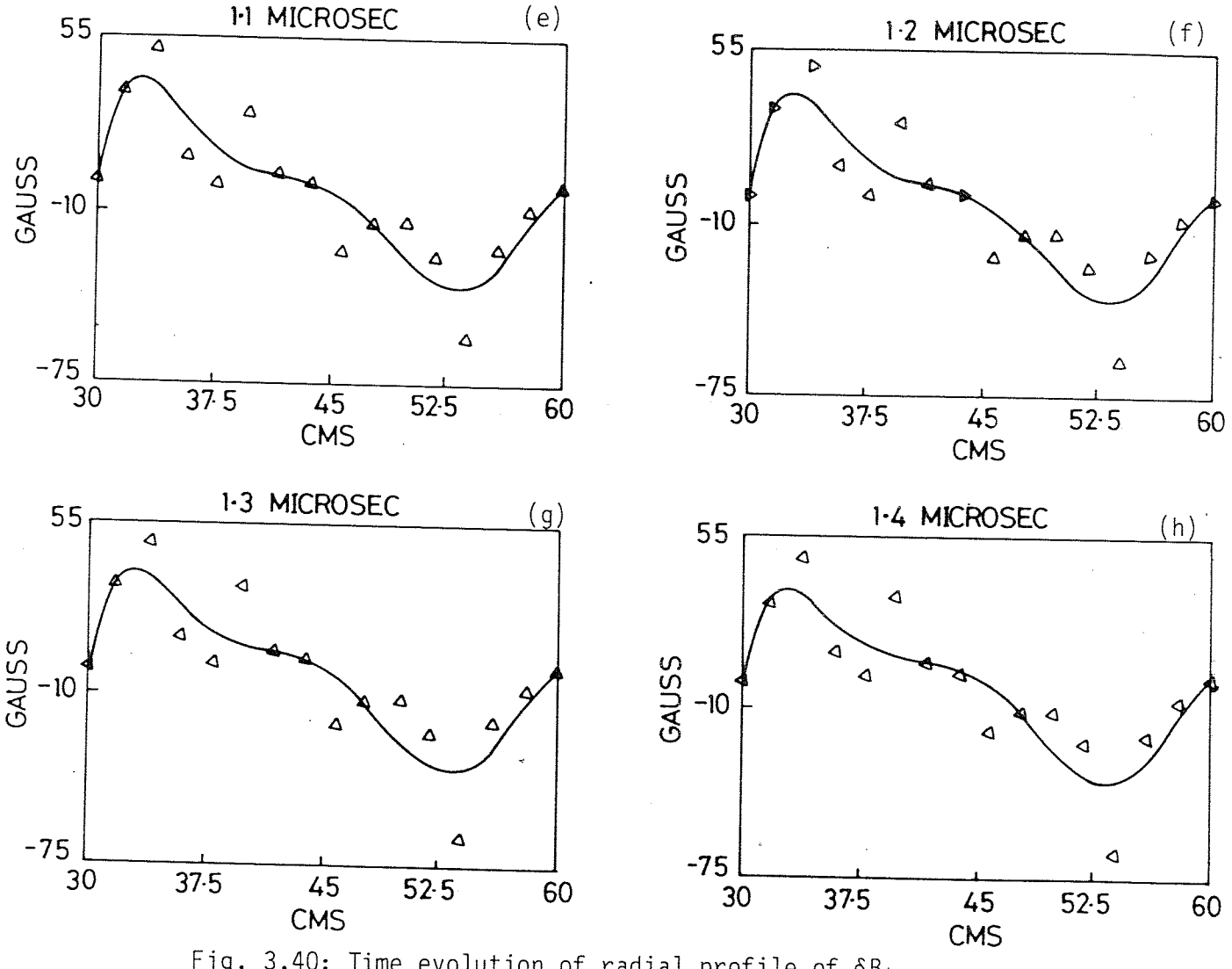

Fig. 3.40: Time evolution of radial profile of δB_t

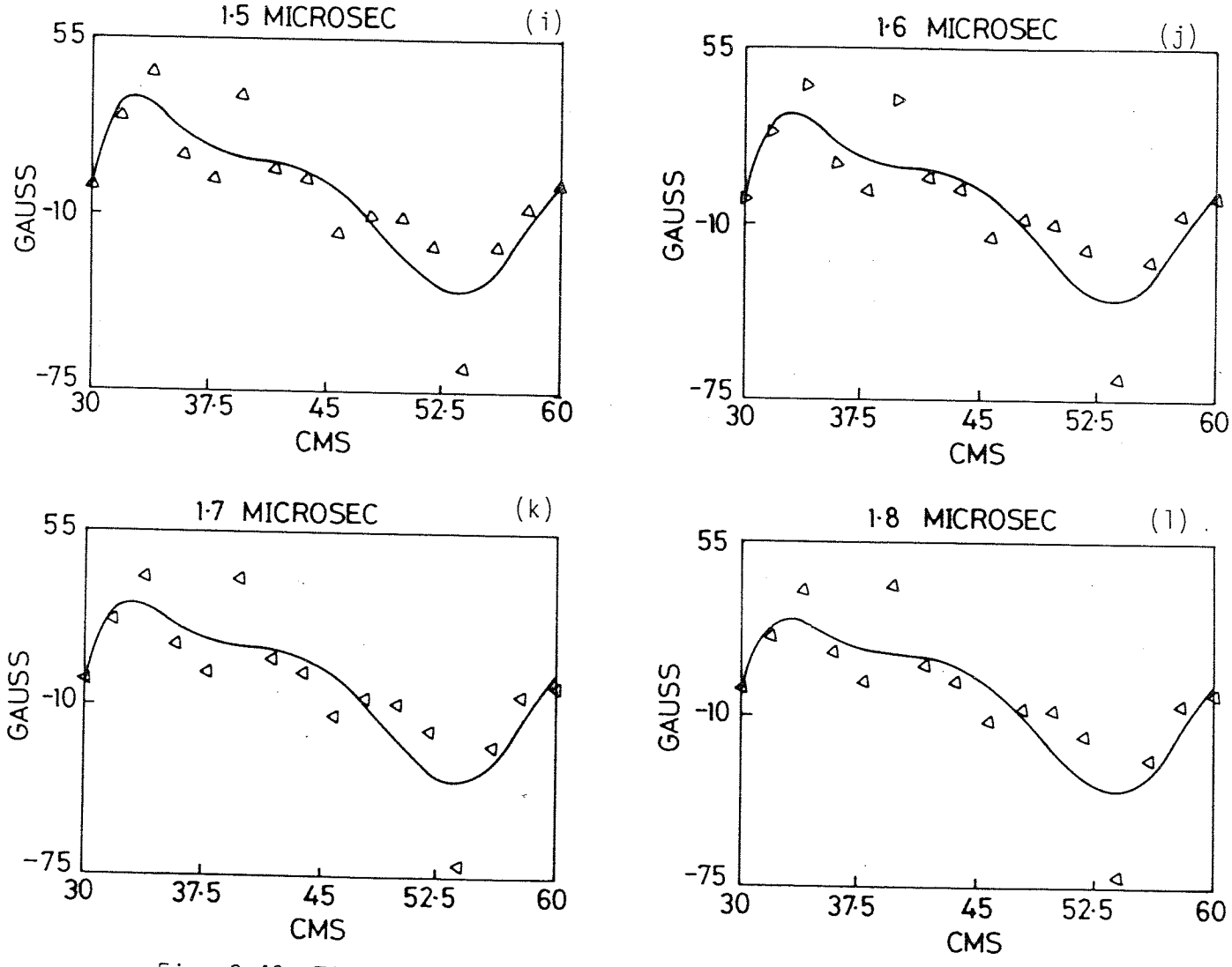

Fig. 3.40: Time evolution of radial profile of δB_t

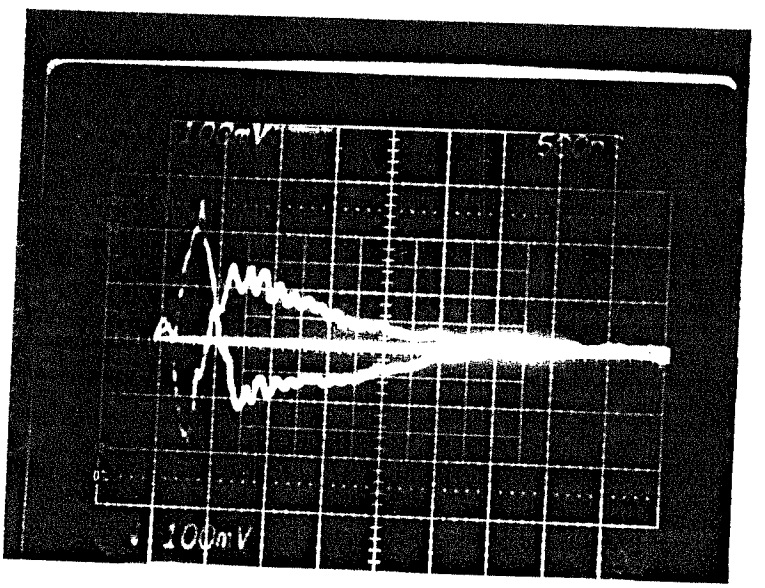

Fig. 3.41: δB_t at R =54.0 cm and z = 0

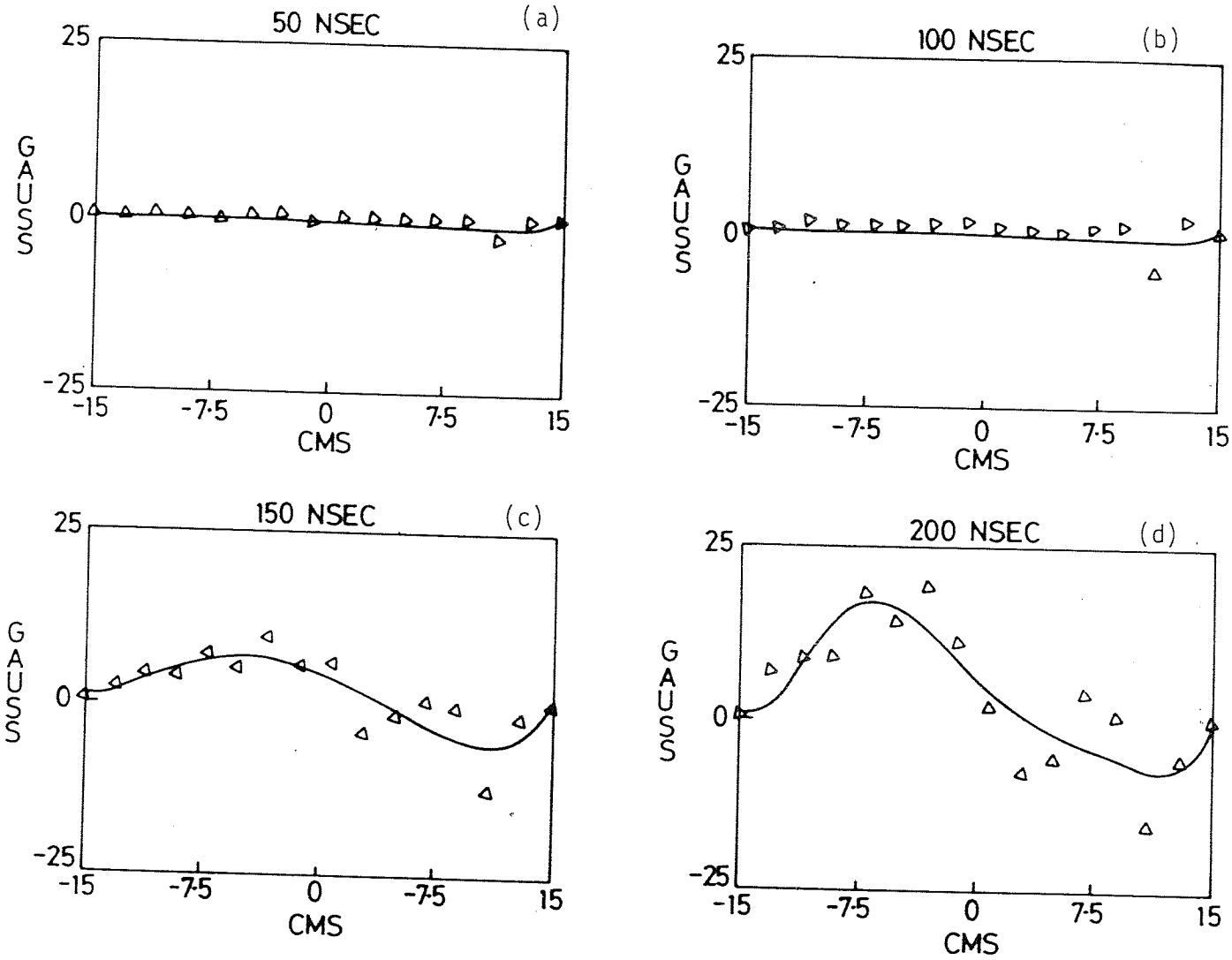

Fig. 3.42: Time evolution of vertical profile of δB_t

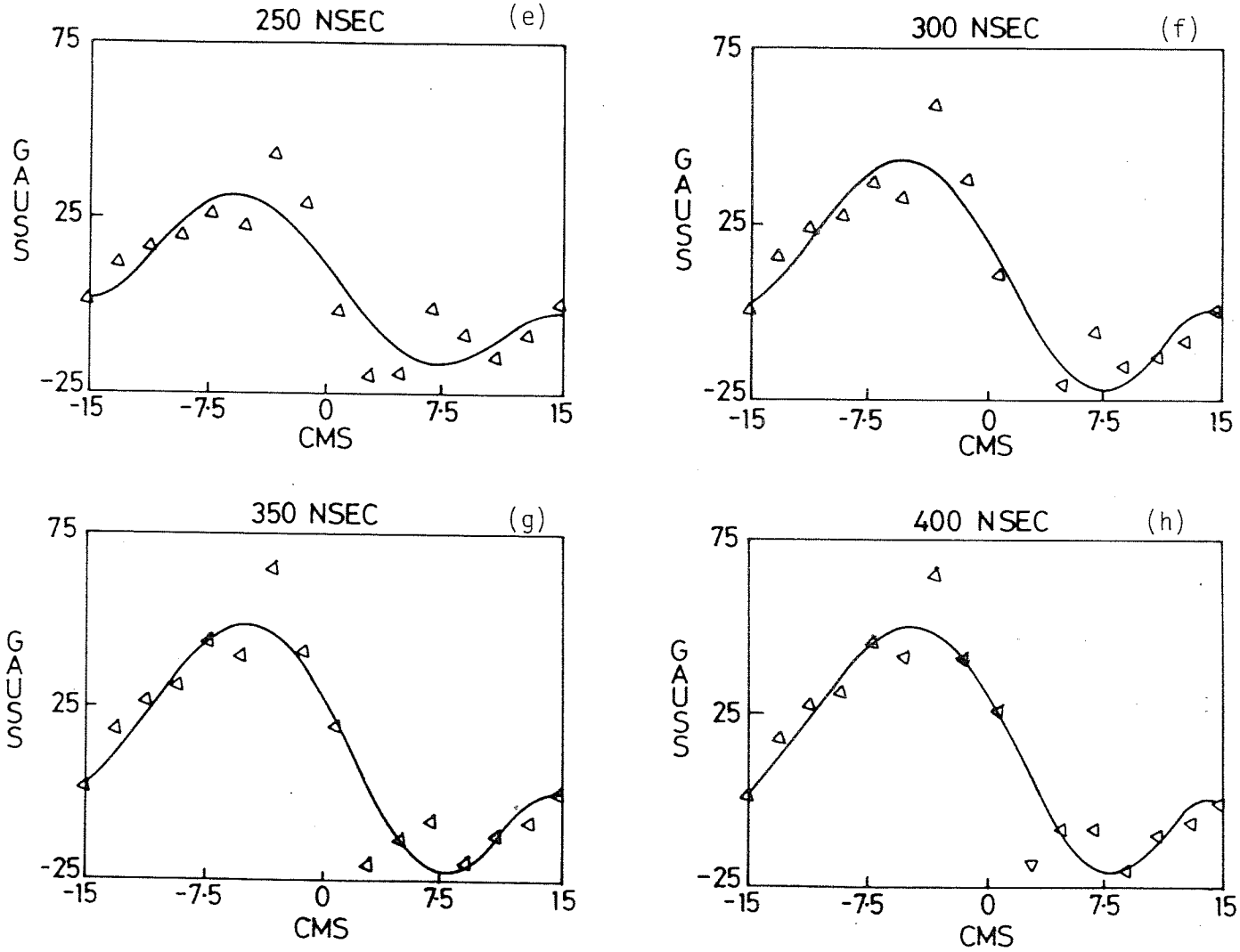

Fig. 3.42: Time evolution of vertical profile of δB_t

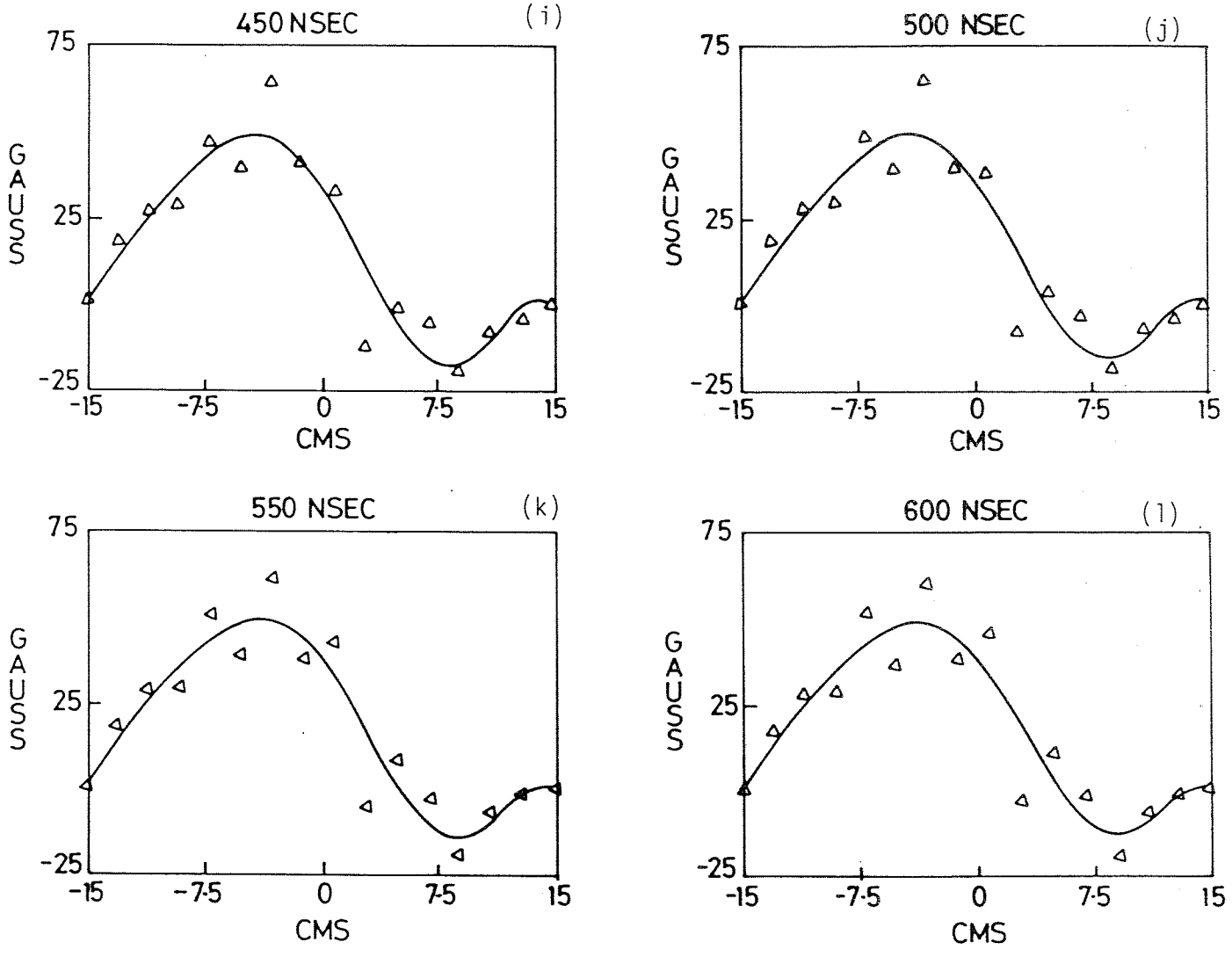

Fig. 3.42: Time evolution of vertical profile of δB_t

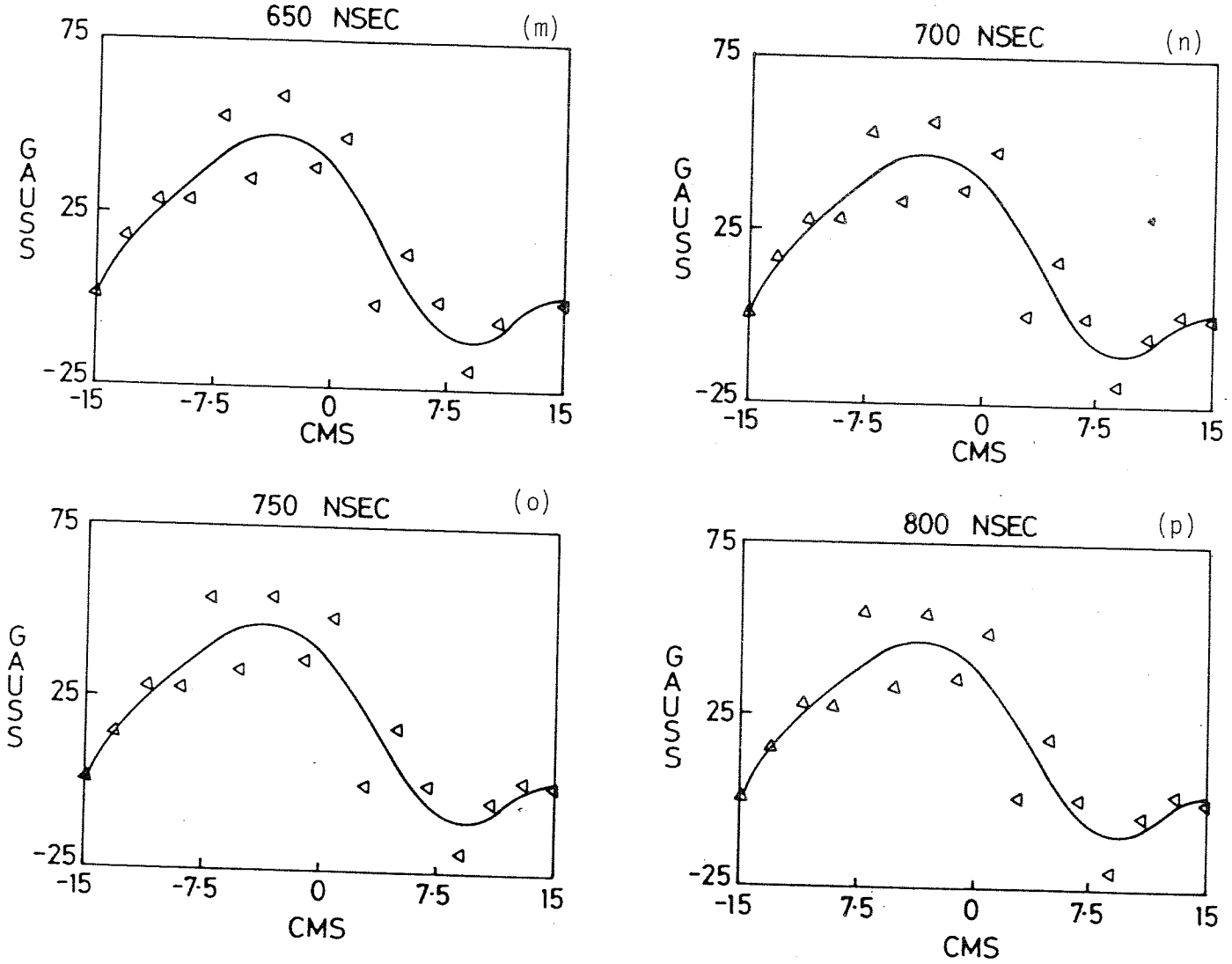

Fig. 3.42: Time evolution of vertical profile of δB_t

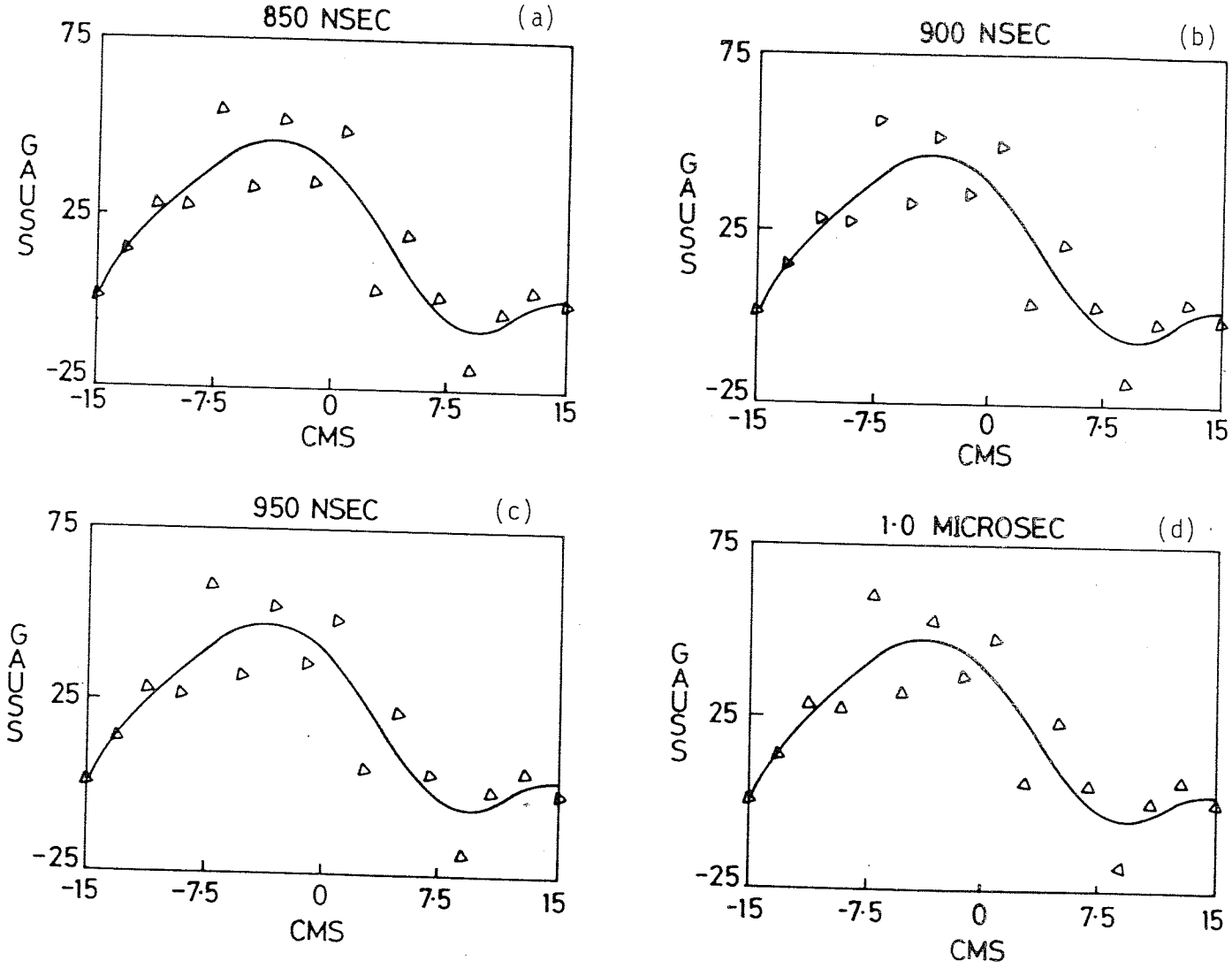

Fig. 3.43: Time evolution of vertical profile of δB_t

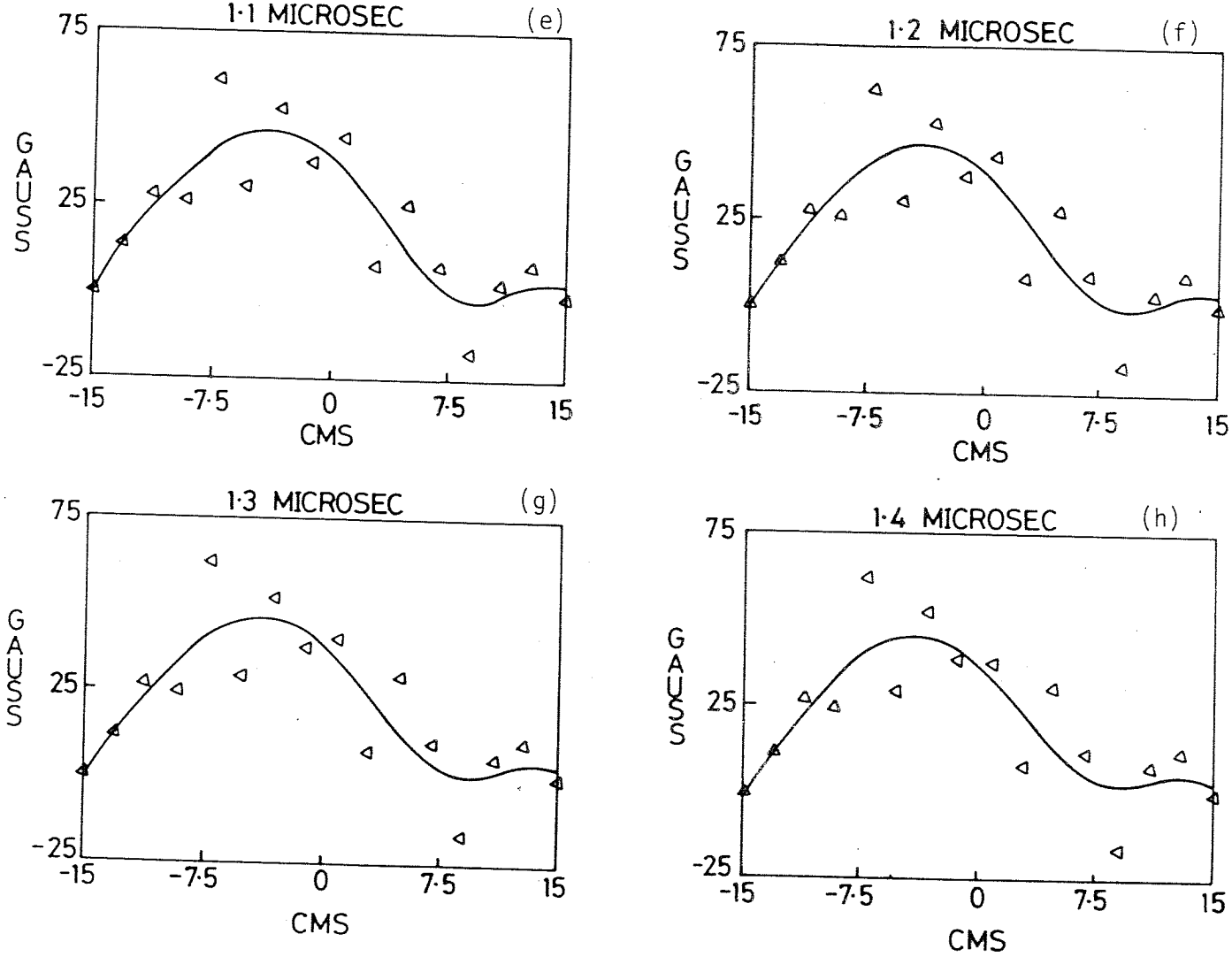

Fig. 3.43: Time evolution of vertical profile of δB_t

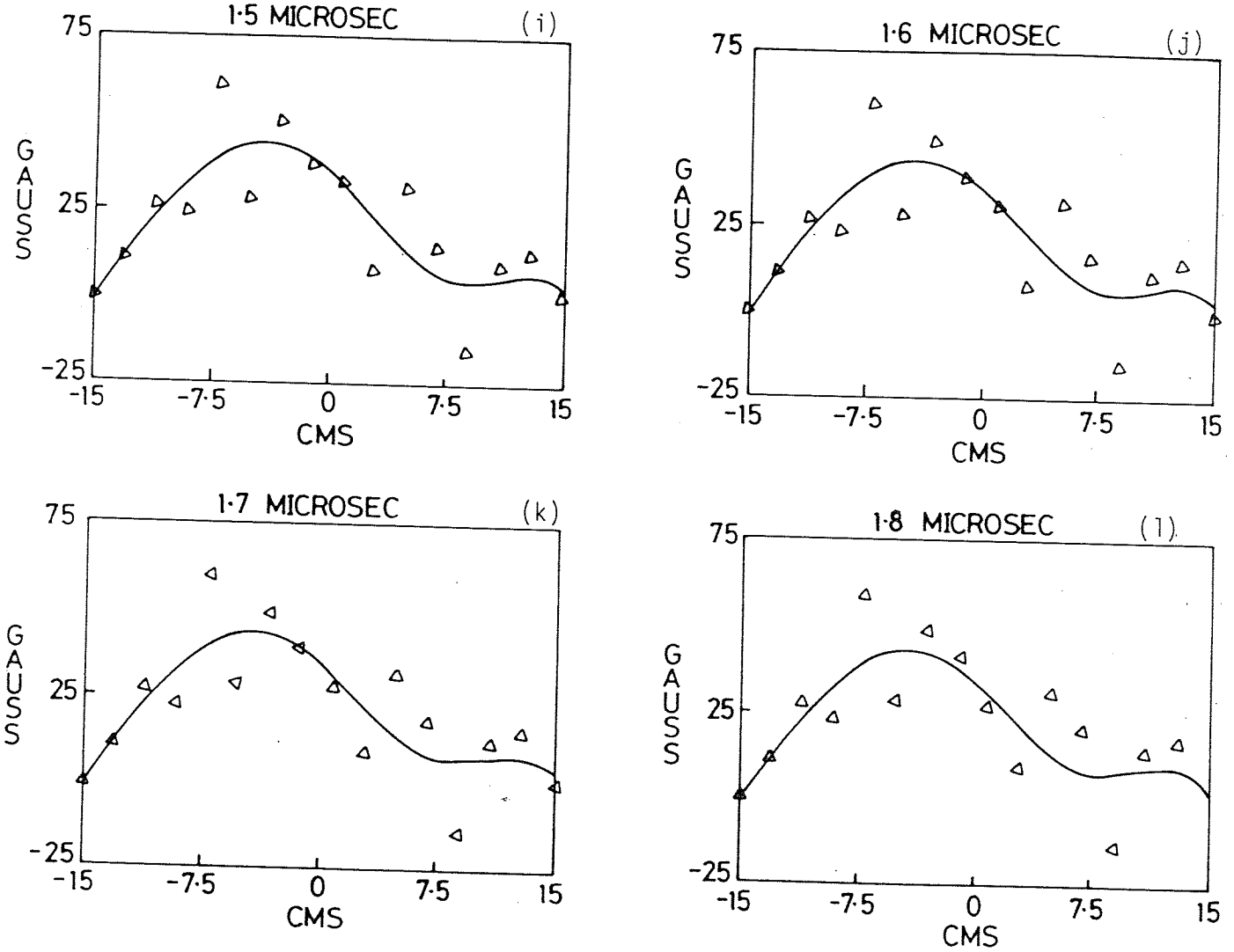

Fig. 3.43: Time evolution of vertical profile of δB_t

column is heated, diamagnetic currents are set up producing a magnetic field which is opposite to the externally applied field inside the heated column. In the presence of a flux conserving wall, the reduction in the magnetic flux inside the heated column due to the diamagnetic currents, results in enhancement of field outside this heated column. Usually a static pressure balance model is used to interpret the diamagnetic loop signals in terms of the plasma perpendicular energy. If the external field is B_o and enhanced field outside the heated column is δB (enhancement of field is known as paramagnetism and decrease in the field is diamagnetism), according to the above model with a sharp boundary separating the heated plasma column and vacuum (or a cool plasma), the pressure balance is given by

$$B_i^2 + 2\mu_o W_\perp = (B_o + \delta B)^2 \qquad (3.23)$$

where $W_\perp$ is the plasma perpendicular energy and B_i is the field inside the hot plasma column.

Using the flux conservation inside the conducting chamber of radius, r_w, we get

$$W_\perp = \frac{B_o \delta B}{\mu_o} \left(\frac{r_{eq}}{r_w}\right)^2 \qquad (3.24)$$

for $\delta B \ll B_o$, where r_{eq} is the equilibrium radius of the heated plasma column.

Limitations of such a model have been discussed by Striffler and Kapetanakos, (1975); Chu and Clark, (1977); Sethian, (1976) and Dove et al., (1976). Some of these limitations are discussed below.

(a). The shielding effect of the plasma (Striffler and Kapetanakos, 1975): When a cool plasma is surrounding the heated column, the paramagnetic field which was assumed to be present in the region between the heated plasma column and

the chamber walls, may not be able to diffuse through the cool plasma under which condition the pressure balance relation (eq. (3.23)) has to be suitably modified.

(b). Beam contributions to the diamagnetism (Striffler and Kapetanakos 1975): In the presence of beam electrons, the diamagnetic flux comes partly from the plasma and partly from the beam. This may become important in the case of rotating beams, where a large portion of the beam energy is in the form of rotational energy. However this may not be a serious limitation in the case of a straight beam and with a small beam to plasma density ratio ($n_b/n_p \ll 1$).

(c). The possibility of plasma expansion and magnetosonic wave generation (Chu and Clark (1977)): In case of a rapid beam energy deposition, plasma does not have enough time to adjust to the new equilibrium position. Hence the total pressure (magnetic + particle) inside the heated channel becomes more than the pressure outside. This leads to what is known as magnetosonic oscillations. This will happen only if the ion collision times and/or the magnetic diffusion times are more than the Alfven time ($\tau_A = r_{eq}/v_A$, v_A is the Alfven velocity). In such a situation, the static pressure balance model is not valid.

(d). The assumption that $\delta B \ll B_o$ in eq. (3.24) may not be valid.

(e). Neglected terms in the pressure balance equation due to axial currents, plasma space charge and field line curvature (Sethian, 1976).

Of these assumptions (d) and (e) are shown to contribute only a few percent (Sethian, 1976) and are valid assumptions.

In addition to the above difficulties, use of a diamagnetic loop for the diamagnetic measurements leads to another problem. The change of hot plasma radius with time

makes it difficult to determine the cross-sectional area. Hence in the diamagnetic loop signal interpretation, the equilibrium radius r_{eq} in eq. (3.24) becomes uncertain. Another difficulty in the diamagnetic loop measurements arises due to hot plasma location. If the location of the hot plasma is a function of time, then also the interpretation in terms of the plasma perpendicular energy becomes uncertain. These two difficulties with the diamagnetic loop can be avoided if the localized measurements of the diamagnetic fields is possible (Dove et al., 1976). In our experiment where there is a change of beam location with time (and hence the anticipated hot plasma column location and its equilibrium radius) necessitated the localized measurements. Additional information regarding the magnetic field configuration will be possible with the local measurements.

The validity of the pressure balance model for our case is justified because of the following reasons. As pointed out by Chu and Clark (1977) one serious limitation of the applicability of the pressure balance model is the magnetosonic wave generation. This becomes particularly important in the high temperature regimes and when ion collision time, τ_i and/or magnetic diffusion time, τ_m are much more than the Alfven time, τ_A. Since in our experiment the magnetic diffusion times are much smaller than τ_A ($\approx$150 ns), it is safe to assume that the static pressure balance model is valid.

If the plasma is heated by REB, inside the heated channel, δB_t (change in toroidal field) will be negative (i.e. diamagnetic) and outside this heated channel δB_t will be paramagnetic as discussed earlier. δB_t observed near outer wall showed an interesting behaviour. Initially the signal is paramagnetic as it should be since it is outside the beam

heated plasma channel, but becomes diamagnetic at about 700 ns and does not reverse polarity afterwards. The rise time of the paramagnetic part of the signal is almost same as the rise time of the net current. The diamagnetic part of the signal may be due to (1) minor radially expanding plasma, (2) heating of the previously cold plasma at this location (incidentally plasma density is high at this location) and (3) major radially outward motion of the hot plasma.

Since the same kind of behaviour of δB_t (i.e. paramagnetic signal changing to diamagnetic) is not seen on the inner side, minor radial plasma expansions is ruled out. From the profile measurements which show a clear shift of the diamagnetic part towards the outer wall it appears that the hot plasma is expanding major radially outward.

The time evolution of the radial profiles of δB_t are shown in figs. 3.39 and 3.40. At 100 ns time we can see a symmetric profile about the minor axis. At this time the beam is near to the outer wall. At later times also a diamagnetic field at centre (more inward compared to the beam location) suggests that major portion of this diamagnetic signal is due to plasma rather than the beam. If it were due to beam the diamagnetic field would have been more near to the outer wall. Abrupt change from diamagnetism to paramagnetism (experimental points in the profile from 200 - 600 ns) is seen near the outer wall. This suggests a sharp boundary between hot plasma and cold plasma outside.

This also suggests no beam loss during this time. Otherwise the beam would have been present at this location and heated the plasma. These profiles become asymmetric at later times (after 700 ns). Vertical profiles of δB_t at R = 45.0 cm are asymmetric from the beginning, even though poloidal fields are symmetric about the mid plane. These

asymmetric profiles must be due to gradients in the plasma density and temperature, since the beam profiles are found to be symmetric.

Any rapid heat loss from the initially hot central plasma due to effects such as radiation or due to the conversion of electron thermal energy into ion streaming energy (Chu et al., 1975) followed by heating of the initially cool outer plasma also can explain the observed evolution of a symmetric radial δB_t profile into an asymmetric one.

The oscillatory signals from diamagnetic loops have been identified as magnetosonic oscillations (Abrashitov et al., 1974, Ekdahl et al., 1974, Kapetanakos et al., 1975). Oscillatory behaviour in the magnetic probe signals also have been reported (Kapetanakos et al., 1975, Prono et al., 1975).

The oscillatory behaviour observed in the δB_t signals (i.e. change of paramagnetic signal into a diamagnetic one) near the outer wall is not due to magnetosonic oscillations, as the magnetic diffusion times (< 100 ns) are much shorter than the period of the oscillations (≈1.0 μs). Furthermore, the oscillatory behaviour in the experiments of Abrashitov et al., (1974) and Kapetanakos et al., (1975) was seen only at high plasma densities (10^{14} cm^{-3}) and were conspicuously absent at lower plasma densities. Also at low energy densities such magnetosonic oscillation are not expected (Chu and Clark, 1977). Since the total injected energy is only about 100 J, even at 100% energy transfer plasma can be heated only to few hundred eV. This corresponds to a plasma perpendicular energy of about $5x10^{15}$ eV cm^{-3}. In the experiments of Abrashitov et al., (1974); Kapetanakos et al., (1975) and Prono et al., (1975), where also oscillatory behaviour is seen, the energy densities are much higher

(5×10^{16} eV cm^{-3} and more). In particular, the oscillatory behaviour in the magnetic probe signals seen in Prono's experiment are at very high energy densities (10^{19} eV cm^{-3}). From these observations along with the fact that the magnetic diffusion times are smaller than the period of oscillation indicate that the observed oscillatory behaviour in the magnetic signals is not due to magnetosonic oscillation.

From the static pressure balance model described earlier, the plasma perpendicular energy is estimated using eq. (3.24). For our experimental values of B_o = 500 gauss, r_w = 15.0 cm, r_{eq} = 7.5 cm and R_o = 45.0 cm, the perpendicular energy is about 50 Joules and the perpendicular energy density, $W_\perp = 6.3 \times 10^{15}$ eV cm^{-3}. For a plasma density of 10^{13} cm^{-3}, this corresponds to about 600 eV.

The total energy thus transferred to plasma is about 50% of the injected energy. Since this occurs at about 300 ns, which is much shorter than the collision time, this energy transfer must be due to some anomalous process involving fast time scales. Since the peak diamagnetic signals appear at about 300 ns, which is nearly same as the net current rise time, the heating must be due to return current processes rather than two stream instability. The appearance of the diamagnetic signals near the minor axis rather than at the beam location during the beam injection also is an indication that the heating is due to return current dissipation. The calculated return current decay time is comparable to the rise time of the diamagnetic signal, further confirming that the heating mechanism is return current dissipation.

Radial plasma expansion velocity was measured with the help of Langmuir probes, using time of flight technique. This was found to be about 7×10^7 cm/s. This low value of the velocity compared to that of the beam indicates that the

measured velocity is indeed due to plasma and not due to beam and further confirms that the trapped beam is not lost to the walls. Since this velocity is more than the Alfven velocity ($\approx 3 \times 10^7$ cm/s) plasma is able to readjust to the new equilibrium state in a time less than the Alfven time (τ_A), justifying the use of static pressure balance model in the beam energy transfer calculation.

3.8 Profiles of the safety factor (q)

The time evolution of the profile of safety factor, q ($= rB_t/RB_\phi$) is calculated and plotted in figs. 3.44(a) to 3.44(f) Here r is the distance from the minimum of the poloidal magnetic field, R is the distance from the major axis and B_ϕ is the measured poloidal magnetic field. In obtaining these profiles the ambient toroidal field, B_t (i.e. the externally applied toroidal field with its 1/R dependence + δB_t measured in the experiment) is used.

The minimum of the q, which is about 0.5 at 200 ns, drops to about 0.2 at 300 ns and remains at this low value. The maximum width of this minimum q region is about 10 cm (from R = 45.0 cm to R = 55.0 cm) up to about 500 ns. At 1.0 μs. this width gets reduced. Another important observation is regarding the q value at the edge. Near the outer wall, where the q value is more than 3.0 at 200 ns drops to less than 3 at 300 ns and to even lower values as the time progresses. This is almost a monotonic decrease of q at the edge with time. The value of q at the edge going to about 1.5 at 1.0 μs.

The above observations regarding the q profiles indicate that the evolution of the beam-plasma system takes it into a low q state. Since we have observed that the beam goes into an equilibrium orbit from the injection point, this

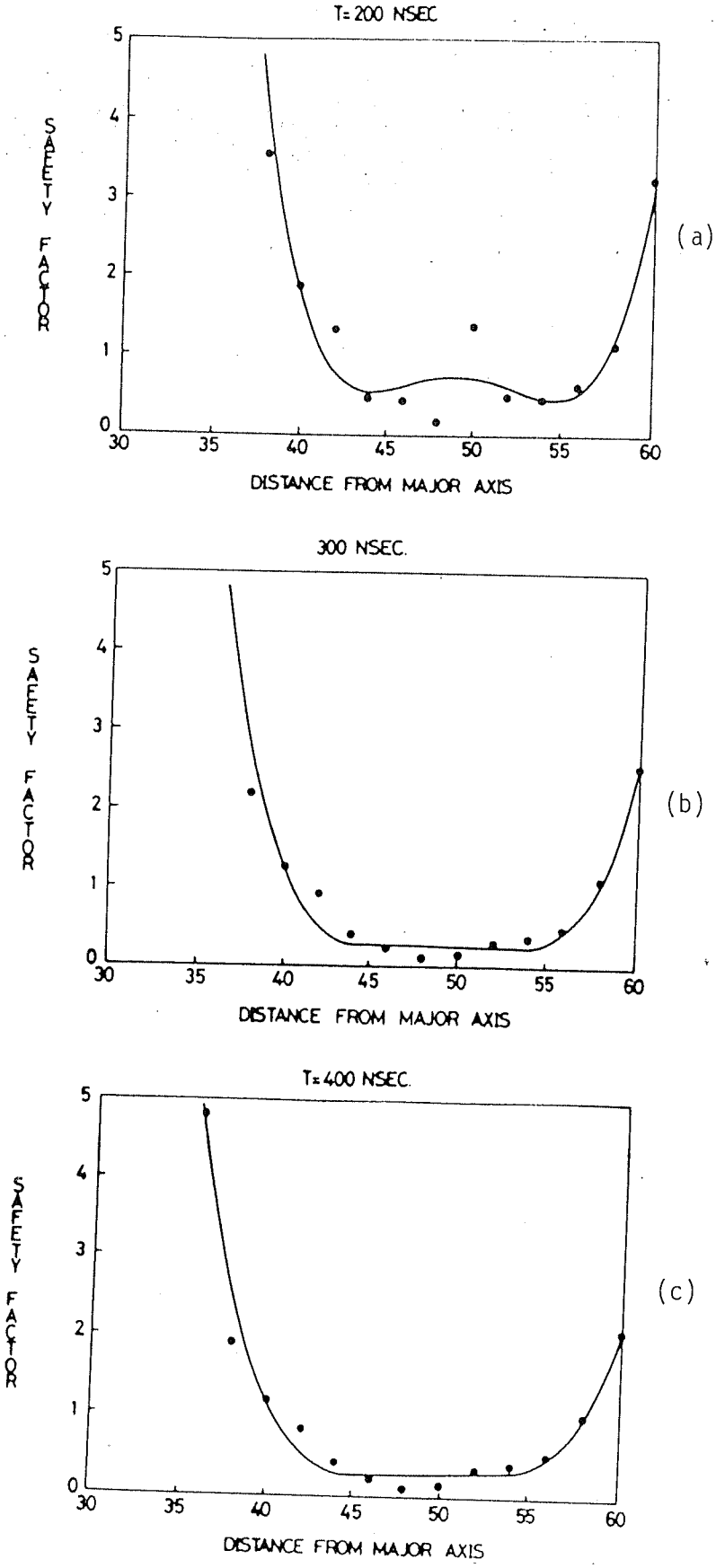

Fig. 3.44: Profiles of safety factor (q)

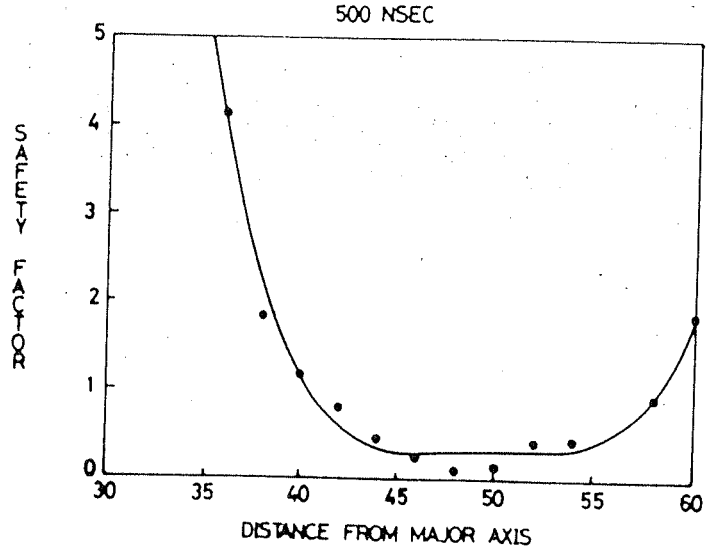

(d)

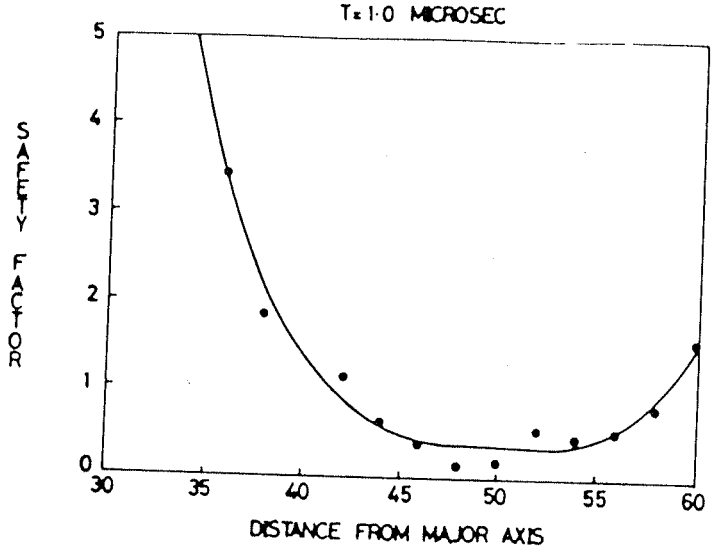

(e)

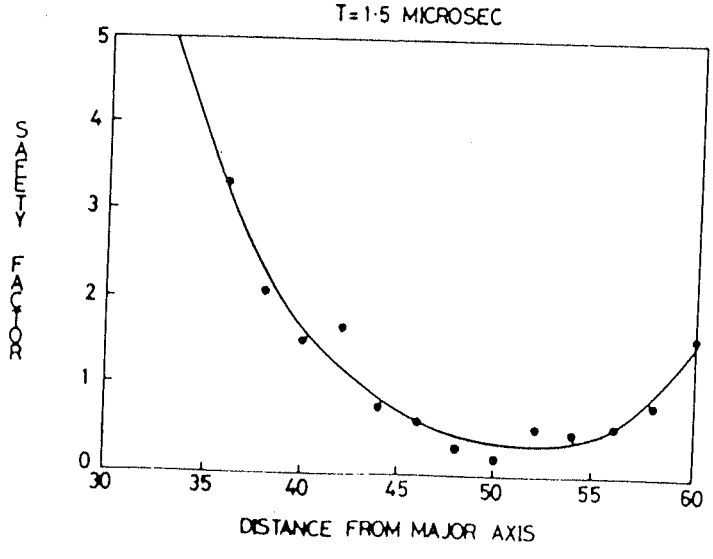

(f)

Fig. 3.44: Profiles of safety factor (q)

equilibrium is also a low q state. Since no external vertical field is used to keep the beam in the equilibrium position and is maintained by the fields due to wall currents only, the beam is most likely in a force free (where the expanding force on the beam is balanced by the force due to wall fields) equilibrium. These observations also support that low q magnetic configurations (q at the centre is much less than 1) which may not be possible in the ordinary ohmic discharge of a tokamak are achievable with REBs in toroidal devices.

3.9 Equilibrium of the current ring

The equilibrium of a current carrying channel inside a perfectly conducting hollow cylinder is a stable one (Mukhovatov and Shafranov, 1971). This is because the fields due to wall currents always force the beam to the equilibrium position and this wall force is proportional to the displacement of the current channel from its equilibrium position. Hence more the displacement, more the restoring force. The equilibrium position is obviously on the axis of the cylinder. In the case of a toroidal geometry, the toroidicity makes poloidal field inside and outside of the ring asymmetric. Due to this asymmetry the equilibrium position of the current channel is shifted outward with respect to the minor axis. For a plasma carrying current confined in a conducting cylinder, this shift (δ_b) is given (in cgs units) by (Mukhovatov and Shafranov, 1971)

$$\delta_b = \frac{r_o^2}{2R_o}\left[\ln\frac{r_o}{r_p} + \left(1 - \frac{r_p^2}{r_o^2}\right)\left(\Lambda + \frac{1}{2}\right)\right] \qquad (3.25)$$

where $\Lambda = \frac{8\pi\bar{p}}{B_\phi^2} + \frac{l_i}{2} - 1$; l_i is the internal inductance per unit length, $\bar{p}$ is the average pressure, r_o and r_p are the minor radii of the vessel and plasma column respectively.

For the case of a relativistic beam carrying current, the shift is given by (Ott and Sudan, 1971)

$$\delta_b = \frac{r_o^2}{2R_o}\left[\ln\left(\frac{r_o}{r_b}\right) + \frac{2I_o}{[(w_b/c)r_b]I_1} + \frac{1}{2}\left(1 - \frac{r_b^2}{r_o^2}\right)\left(\frac{I_o I_2}{I_1^2} - 1\right)\right] \qquad (3.26)$$

where I_o, I_1 and I_2 are the modified Bessel functions with argument $\frac{w_b r_b}{c}$. Here $w_b = \frac{n_b e^2}{\epsilon_o m \Gamma}(1-f_m)$; f_m is the fractional current neutralization and r_b is the beam radius. Comparing eqs. (3.25) and (3.26) we can readily see that they are similar except for the factor $\frac{2I_o}{(w_b r_b)/c}$, which arises because of the centrifugal force on the beam electrons and is equal to I_A/I_b(Ott and Sudan, 1971), where I_A is the Alfven-Lawson limiting current and I_b is the beam current. Eq. (3.26) can be used to calculate the shift of the beam centre if we know the beam energy.

Similar conclusions were obtained for a non-neutral beam current ring in a conducting casing by Kapetanakos et al., (1983). Because of the shift in the current centre, the required external betatron magnetic field will be more than that for a single particle. If B_o is the field required to maintain a single particle at a radius R_o, the magnetic field required for a beam current to be maintained at the same location is found to be given by (Kapetanakos et al., 1983)

$$B_{oz} = B_o\left[1 + \frac{2\nu}{\Gamma}\left(1 + \ln\frac{r_0}{r_b}\right)\right] \qquad (3.27)$$

where ν is Budker's parameter.

In our experiment, where there is no external vertical field, the shift of the current ring is expected. Using eq.

(3.26) and neglecting terms multiplying $I_o I_2 / I_1^2$ (which is a first order quantity), we can estimate the beam energy from the observed shift. Neglecting the first order terms, eq. (3.26) can be written as (Ott and Sudan, 1971)

$$\delta_b = \frac{r_o^2}{2R_o} \left[\ln \frac{r_o}{r_b} + \frac{I_A}{I_b} - \frac{1}{2} \right] \qquad (3.28)$$

Substituting r_o = 15.0 cm, R_o = 45.0 cm, (system parameters) and r_b = 7.5 cm and I_b = 5.0 kAmps and δ_b = 3 cm (observed quantities) in eq. (3.28), we get

$$I_A = 17 \times 10^3 \beta\Gamma = 5034 \text{ Amps}$$

$$\text{giving } \beta\Gamma = 0.2969$$

$$\text{i.e. } \frac{v_b}{c} \left(1 - \frac{v_b^2}{c^2}\right) = 0.2969$$

$$v_b = 8.5 \times 10^7 \text{ m/s}$$

which corresponds to an energy of 22 keV.

Neglecting the toroidal effects, the self magnetic field at the centre of the beam is zero. Hence the particles at the beam centre will experience a centrifugal force and a force due to the field due to wall currents. In equilibrium, these two forces are opposite to each other and get cancelled. This can be expressed as

$$\frac{m\Gamma v_b^2}{R_b} = e v_b B_w \qquad (3.29)$$

where B_w is the magnetic field due to the wall currents at the beam centre and is given by (Mukhovatov and Shafranov, 1971)

$$B_w = \frac{\mu_o I_n \delta_b}{2\pi (r_o^2 - \delta_b^2)} \qquad (3.30)$$

where I_n is the net current. For the parameters of our experiment the above equation gives, B_w = 14 gauss. Substituting this value for B_w and the experimentally observed values for I_n and δ_b in eq. (3.29), we can estimate the beam energy. This gives $\Gamma v_b = 1.18 \times 10^8$ m/s, which corresponds to a beam energy of 40 keV

The above estimates of the beam energy are to be treated as only order of magnitude calculations because of simplifying assumptions and their sensitive dependence on the observed parameters. If we bear this in mind, the above estimates are in good agreement with the earlier estimates of beam energy transfer obtained from the measurements of plasma diamagnetism. The estimates made in this section are complementary to the diamagnetic measurements and are supportive of the claim that about 50% of the beam energy appears as plasma perpendicular energy.

3.10 Comparison with other experiments

For the comparison purpose, we shall restrict ourselves to the experiments where a complete toroidal system was used and the beam was injected into a pre-formed plasma, which are relevant in the context of our experiment. In the experiments on the macrotor tokamak (Bailey et al., 1982) and at Cornell (Proulx, 1981) the beam was injected into a pre-formed plasma carrying current. In the SPAC experiments, gun produced plasma was used with no pre-existing plasma currents.

In the experiments on macrotor tokamak a net current rise of about 5 kAmps was observed. This additional net current was found to last for about 800 μs. But this is not necessarily the beam and beam induced currents. As was analyzed and pointed out in the Cornell experiments (Proulx, 1981), this could have been due to the additional ohmic

current generation following the beam injection. This is most likely true because the microwave signals showed a beam life time of about 1.0 μs. (Bailey et al., 1982). Hence, the amplitude and life time of the beam and beam induced net currents is not clear in these experiments.

In the Cornell experiments, however, after taking the additional ohmic current generation into account, it was shown (Proulx, 1981) that the beam and the beam induced net currents are less than 2 kAmps and the life time is typically about 10 μs.

Comparing these net currents with that observed in our experiment, we find that the net current is higher and lasts for longer times. Considering the low beam energy in our experiments, the results obtained show an efficient beam injection and trapping. However, one important thing to remember is that the system inductance in the macrotor experiment and most likely in the Cornell experiment is higher than that of ours, making it possible to realize higher currents in our experiments. However the longer life times observed in our experiment compared to the other two experiments indicate a beam trapped in a stable equilibrium. A slow net current rise compared to the beam injection duration in the macrotor and Cornell experiment indicates that there may be a slow decay of return currents in these experiments thus accounting for smaller net currents.

Regarding the beam energy transfer to the plasma, higher beam energy transfer (50%) was observed in our experiment compared to those observed in the Cornell experiment (5%). In the macrotor experiment also a high energy transfer (75%) was observed and was indicated to be due to return current processes rather than electron-electron two stream instability. In our experiment also, where a fast return

current decay was observed, the high energy transfer is likely due to return current processes.

In the experiments on the SPAC devices high currents lasting for very long times were observed. The beam life times in the recent experiments was found to be consistent with decay due to Coulomb collisions and the presence of an inductive electric field due to net current decay (Hasegawa et al. 1987). The comparatively fast decay that was observed in our experiment could be due to low beam energies. Since no oscillations were seen in the net current wave forms, the current decay may not be due to any instability. The other loss mechanisms that could be responsible for the observed fast decay are (1) a high neutral gas pressure and (2) field line errors.

The low net currents in our experiment compared to those in the SPAC experiments are also to be understood as the result of low beam energies used.

CHAPTER-IV

CONCLUSIONS

An experimental study of REB injection and trapping in a toroidal device was carried out. A beam generator based on Tesla transformer high voltage generator was fabricated for this purpose. REB was produced with the help of plasma anode method. The torus was filled with plasma prior to the beam injection. The beam was injected into two different plasma densities. Detailed studies were made on the beam and net currents which include space and time resolved measurements of the beam current distribution and self fields. The main conclusion of the study are summarized in the following section and suggestions for further studies are given in the next section.

4.1 conclusions

1) The torus can be filled with high density plasma by operating the gun with low impedance (long pulse length) PFN.
2) The diode currents observed in both the cases of injection (i.e. into low density and high density plasmas) were found to be within the limits expected from calculations of sheath evolution. From the localized measurements, with a miniature Faraday cup, it was established that a spatially well defined beam was injected into the torus.
3) In the case of injection into low density plasma, beam followed the field lines and was lost by hitting the injector from the back. There was no net toroidal current generated in this case indicating a slow return current decay

compared to the beam injection duration. In the case of injection into high density, a net toroidal current was generated. A simultaneous shift of the beam and net currents was observed. In this case, the beam cleared the injector and got trapped. The beam current profile evolution also showed that the beam shifts inward as it goes around the torus and reaches an equilibrium orbit.

4) From the net current measurements at different toroidal locations, it was established that a toroidally continuous current ring was formed when injected into a high density plasma. The rise times of the net current near the cathode and the trapped net current showed that the return current decay time was much smaller than the injection duration. The rise time of the net current was found to be consistent with the calculations of return current decay due to ion-acoustic turbulence. The absence of the ion-acoustic turbulence was indicated to be the reason for the slow return current decay in the case of injection into low density plasma and in the low plasma density regions near the inner wall in the case of injection into high density plasma. Comparison of the observed net currents in the case of injection into high density plasma with that obtained from calculations also indicated a fast return current decay.

5) From the poloidal fields net current profiles were obtained. The effect of wall fields was clearly established on the calculation of net current profiles. From the poloidal field and small Rogowski coil measurements it was established that the current channel shifts inward as the net current rises. This was consistent with the drift injection model, which predicts that a fast return current decay is essential for beam trapping and also explains the non-trapping of the beam when injected into the low density plasma.

6) The changes in toroidal field, (δB_t) were measured. The importance of the localized measurements was clearly brought out in the toroidal beam experiments in estimating the energy transferred to the plasma from diamagnetic measurements. To avoid uncertainties in the interpretation of diamagnetic loop signals, localized measurements were found to be essential. The estimated beam energy from these measurement is about 50% of the injected energy. These measurements also showed that the beam heated plasma expands radially, the conclusions which would have been impossible to reach through measurements with a diamagnetic loop, indicating again the importance of the localized measurements.

7) From the diamagnetic measurements and the net current rise times it was indicated that the plasma heating is mainly due to return current dissipation.

8) From the q profiles obtained from the external and self magnetic fields and the changes in toroidal fields, it was found that initially a high q state goes into a low q state as the beam goes into an equilibrium from its launch position. It was indicated that this is most likely a force free configuration, since no external fields were applied to launch the beam on equilibrium.

9) The final beam energy calculated from the equilibrium position (i.e., shift from the minor axis) and the net currents was consistent with the beam energy obtained from the considerations of beam energy transfer to the plasma and the energy that appears in self magnetic fields.

4.2 Suggestions for further studies

In the experiments reported in this thesis, plasma was injected into the torus across the toroidal magnetic field.

Variation of neither the bulk plasma density nor the toroidal field was possible keeping the other fixed in this injection scheme. Study of the beam injection and trapping was accordingly done at fixed (optimized) plasma densities and toroidal fields. Study of the injection phase (like the one presented in the thesis) as a function of plasma density and toroidal magnetic field should be carried out. This is important since there was already indications that the plasma density is a crucial parameter in the return current dissipation and it was also indicated that at higher toroidal fields the beam trapping is more difficult compared to that at low fields (Proulx, 1981). This implies that a plasma source which can fill the torus irrespective of the toroidal field is necessary.

High current rings will be possible with higher energies. In the experiments reported in the thesis the beam energies are much lower than those in the other experiments. The beam generator can be operated at higher energies (with some modification), and this choice of operation can clearly establish the claim that higher currents are possible with higher energies or can show if any other limitations are there on the attainable ring currents (i.e. other than the energy of the beam).

Another aspect is the current ring life time. The observed life times of about 30 μs are probably due to the low energies of the beam that were used. In this regard the beam generator should be operated at higher energies to establish that the life time of the ring is determined by the beam energy in the absence of any other loss mechanisms. Thorough investigations of these life times should be carried out to understand the loss mechanism. Since we do not see any oscillations in the ring current wave forms, the loss may not

be due to any instability. Calculation of beam loss due to field errors may be aimed at. Another possible reason for the observed beam loss could be due to a high neutral gas pressure built up following the plasma gun firing. This possibility may be checked by filling the torus with another plasma source, where this problem is not there or by replacing the nylon washers with ceramic or glass washers (where the desorption of the gases is substantially reduced).

At present the life time of the current ring is about 30 μs and is much smaller than the magnetic diffusion time of the vessel. Hence no vertical field was necessary to hold the ring in equilibrium; the field required being provided by the wall currents. At high beam energies, if the beam and net currents last for times comparable to or more than the magnetic diffusion time of the vessel, then an external vertical magnetic field will be needed. The existing vertical field coils on BETA can provide only a uniform magnetic field (i.e. the field index is close to zero). For a stable confinement a field with index of about 0.5 is needed. This means additional coils will be necessary for producing the required field.

One important scheme proposed for continuous operation is the repetitive injection of REB. This may need major modifications of the existing beam generator or building another one for the above purpose. So far no experiments have been done in this regard and can be tried out. If successful, this can clearly establish the importance of this choice over the other schemes such as R.F. current drive as an auxiliary current drive scheme.

REFERENCES

1. Conceptual design of BETA, 1982 Internal report of Plasma Physics Programme, Physical Research Laboratory, Ahmedabad, India, No: PPP-DR-82-01
2. BETA- A Modern Basic Plasma Device, 1984 Internal report of Plasma Physics Programme, Physical Research Laboratory, Ahmedabad, India, No: PPP/TR-11/84
3. Abramyan E.A., 1971 IEEE Trans. on Nuclear Science NS-18 447
4. Akopov R.A., Antablyan O.G., Davtyan S.V. and Khanikyants E.K., 1987 Sov. Phys. Tech. Physics 32 289
5. Abrashitov Y.I., Koidan V.S., Konyukhov V.V., Lagunov V.M., Lukyanov V.N., Mekler K.K. and Ryutov D.D., 1974 Sov. Phys. JETP 39 647
6. Alexeff I., Jones W.D., and Lonngren K., and Montgomery D., 1969 Phys. Fluids 12 345
7. Alfven H., 1939 Phys. Review 55 425
8. Altyntsev A.T.,Eskov A.G., Zolotovskii O.A., Koroteev V.I. and Semenov V.N., 1971 JETP Letters 13 139
9. Bailey V., Ecker B., Eichenbeger C., Helava H., Proulx G., Taylor B. and Talmadge S., 1982 in REB Current Drive in Macrotor Tokamak (Physics International company) PIFR-1466-1
10. Bailey V.L., Creedon J.M., Ecker B.M. and Helava H.I., 1983 J. Appl. Physics 54 1656
11. Barak G. and Rostoker N., 1983 Phys. Fluids 26 856
12. Benford J., Putnam S., Stallings C., Guillory J. and Shope S., 1973 Phys. Rev. Letters 31 346
13. Benford J., Guillory J. and Stallings C., 1974a J. Appl. Physics 45 1657
14. Benford J., Ecker B. and Bailey V., 1974b Phys. Rev.

Letters 33 574

15. Bogdankevich L.S. and Rukhadze A.A., 1971 Sov. Phys. Uspekhi 14 163
16. Boscolo I., Brautti G., Coisson R., Leo M. and Luches A., 1975 Rev. Sci. Instruments 46 1535
17. Breizman B. and Ryutov D.D., 1974 Nucl. Fusion 14 873
18. Brower L.F., Kusse B.R. and Meixel G.D., 1974 IEEE Trans. on Plasma Science PS-2 193
19. Budker G.I., 1973 in Controlled Fusion and Plasma Physics (Proc. 6th European Conf., Moscow) vol.2 136
20. Chernin D., Mondelli A. and Roberson C. 1984 Phys. Fluids 27 2378
21. Christofilos N.C., 1951 in Proc. Second U.N. Int. Conf. on the Peaceful Uses of Atomic Energy (U.N., Geneva) 32 279
22. Chu K.R., Clark R.W., Lampe M., Liever P.C. and Manheimer W.M., 1975 Phys. Rev. Letters 35 94
23. Chu K.R. and Clark R.W., 1977 Phys. Rev. Letters 38 704
24. Cox J.L. and Bennett W.H., 1970 Phys. Fluids 13 182
25. Craggs J.W., and Meek J.M., 1954 in High Voltage Laboratory Technique (Butterworths, London) 104
26. Davidson R.C. and Uhm H.A., 1982 Phys. Fluids 25 2089
27. Dove W.F., Gerber K.A. and Hammer D.A., 1976 Appl. Phys. Letters 28 173
28. Ehst D.A., 1982 in A Demonstration Tokamak Power Plant Study (DEMO) (Argonne National Laboratoy) ANL/FPP/82-1 Chapter - 4
29. Ekdahl C., Greenspan M., Kribel R.E., Sethian J. and Wharton C.B., 1974 Phys. Rev. Letters 33 346
30. Fainberg Y.A., Shapiro V.D. and Shevchenko V.L., 1970 Sov. Phys. JETP 30 528
31. Ferch R.L. and Sudan R.N., 1975 Plasma Physics 17 905

32. Finkelstein D., Goldberg P. and Schuchatowitz J., 1966 Rev. Sci. Instruments 37 159
33. Finn J.M. and Manheimer W.M., 1983 Phys. Fluids 26 3400
34. Fiorentino E., Letardi. T. and Marino A., 1982 II Nuova Cimento 71B 205
35. Gilad P., Kusse B.R. and Lockner T.R., 1974 Phys. Rev. Letters 33 1275
36. Gilad P., Kusse B.R. and Lockner T.R., 1975 Phys. Fluids 18 607
37. Golden J., Pasour J., Perhing D.E., Smith K., Mako F., Slinker S., Mora F., Orrick N., Altes R., Fliflet F., Champney P. and Kapatanakos C.A., 1983 IEEE Trans.on Nuclear Science NS-30 2114
38. Goldenbaum G.C., Dove W.F., Gerber K.A. and Logan B.G., 1974 Phys. Rev. Letters 32 830
39. Graybill S.E. and Uglum J.R., 1970 J. Appl. Physics 41 230
40. Greenspan M.A., Ekdahl C., Sethian J.D. and Wharton C.B., 1980 Phys. Fluids 23 205
41. Hammer D.A. and Papadopoulos K., 1975 Nuclear Fusion 15 977
42. Hasegawa M., Narihara K., Tomita Y., Kubo S., Matsui M., Tsuzuki T. and Mohri A., 1987 J. Phys. Soc. Japan 56 1370
43. Hoffmann C.R.J., 1975 Rev. Sci. Instruments 46 1
44. Hui B. and Lau Y.Y., 1984 Phys. Rev. Letters 53 2024
45. Ikuta K., Jpn. J. Appl. Physics 11 1684
46. Ikuta K., 1972 J. Phys. Soc. Jappan 32 497
47. Jain K.K.and John P.I., 1984 Pramana, 23 1
48. Jain K.K. and John P.I., 1986 Phys. Fluids 29 3445
49. Jain K.K., John P.I., Punithavelu A.M. and Rao P.P., 1980 J. Physics E 13 928
50. Jain K.K., Chenna Reddy D. and John P.I., 1985 Rearch

Report of Plama Phyics Programme, Phyical Reearch Laboratory, Ahmedabad, India, No: PPP/RR-6/85

51. Jain K.K., Chenna Reddy D., John P.I. and Saxena Y.C. 1986 Sadhana 9 19

52. Jansen G.C.A.M., Bonnie J.H.M., Granneman E.H.A., Krementsov V.I. and Hopman H.J., 1984 Phys. Fluids 27 726

53. John P.I., 1982 in Proc. Technology of Electrical Insulation and High Voltage Pulse Techniques (Bombay: Bhabha Atomic Research Centre) 335

54. Kapetanakos C.A. and Hammer D.A., 1973 Appl. Phys. Letters 23 17

55. Kapetanakos C.A. and Sprangle P., 1985 Physics Today Feb. 1985 1

56. Kapetanakos C.A., Black W.M. and Chu K.R., 1975 Phys. Rev. Letters 34 1156

57. Kapetanakos C.A., Sprangle P. and Marsh S.J., 1982 Phys. Rev. Letters 49 741

58. Kapetanakos C.A., Sprangle P., Chernin D.P., Marsh S.J. and Haber I., 1983 Phys. Fluids 26 1634

59. Korn P., Sandel F. and Wharton C.B., 1973 Phys. Rev. Letters 31 579

60. Kusse B.R. and Lockner T.R., 1974 Plasma Physics 16 19

61. Langmuir I., 1929 Phys. Rev. 33 954

62. Lee R. and Sudan R.N., 1971 Phys. Fluids 14 1213

63. Linhart J.G., 1960 in Plasma Physics (North-Holland, Amsterdam) 24

64. Lockner T.R. and Kusse B.R., 1978 J. Appl. Phys. 49 2357

65. Lovelace R.V. and Sudan R.N., 1971 Phys. Rev. Letters 27 1256

66. Mako F., Manheimer W., Kapetanakos C.A., Chernin D. and Sandel F., 1984 Phys. Fluids 27 2211

67. Masuzaki M., Mohri A., Tsuzuki T. and Ikuta K., 1975

Jpn. J. Appl. Physics 14 1413

68. Matsuzawa H. and Suganomata S., 1982 Rev. Sci. Instruments 53 694

69. Miller P.A. and Kuswa G.W., 1973 Phys. Rev. Letters 30 958

70. Miller P.A., Poukey J.W. and Wright T.P., 1975 Phys. Rev. Letters 35 940

71. Miller R.B., 1982 in Introduction to the Physics of Intense Charged particle Beams (Plenum Press, New York)

72. Mohri A., Masuzaki M., Tsuzuki T. and Ikuta K., 1975 Phys. Rev. Letters 34 574

73. Mohri A., Ikuta K. and Masuzaki M., 1977a J. Phys. Soc. Japan 42 1025

74. Mohri A., Masuzaki M., Narihara K., Tsuzuki T., Yamanaka K. and Ikuta K., 1977b in Plasma Physics and Controlled Nuclear Fuasion Research (Proc. 6th Int. Conf., Berchtesgaden, 1976) IAEA Vienna, Vol.III 395

75. Mohri A., Narihara K., Tsuzuki T., Kubota Y., Tomita Y., Ikuta K. and Masuzaki M., 1979 in Plasma Physics and Controlled Nuclear Fuasion Research (Proc. 7th Int. Conf., Innsbruck, 1978) IAEA Vienna , Vol.III 311

76. Mohri A., Narihara K., Tomita Y., Tsuzuki T., Hasegawa M. and Ikuta K., 1981 in Plasma Physics and Contolled Nuclear Fusion Research (Proc. 8th Int. Conf., Brussels,1980) IAEA Vienna, Vol.III 511

77. Mohri A., Narihara K., Tomita T., Hasegawa M., Tsuzuki T. and Kobata T., 1982 Physica Scripta T2:2 399

78. Mohri A., Narihara K., Tomita Y., Hasegawa M., Kubo S., Tsuzuki T., Kobata T. and Fleischmann H.H., 1985 in Plasma Physics and Controlled Nuclear Fusion Research (Proc. 9th Int. Conf., London, 1984) IAEA Vienna, Vol.3 395

79. Mukhovatov V.S. and Shafranov V.D., 1971 Nuclear Fusion 11 605

80. Nagesh K.V., 1982 in Proc. Technology of Electrical Insulation and High Voltage Pulse Techniques (Bombay: Bhabha Atomic Research Centre) 237

81. Narihara K., 1981 Jap. J. Appl. Physics 20 L683

82. Narihara K., 1982 Research Report of Institute of Plasma Physics, Nagoya Univ. IPPJ-576

83. Narihara K., Hasegawa M., Tomita Y., Tsuzuki T., Sato K. and Mohri A., 1983 Research Report of Institute of Plasma Physics, Nagoya Univ. IPPJ-621

84. Narihara K., Tomita Y., Kubo S., Hasegawa M., Matsui M., Tsuzuki T. and Mohri A., 1987 in Plasma Physics and Controlled Nuclear Fusion Research (Proc. 11th Int. Conf., Kyoto, 1986) IAEA Vienna, Vol.2 687

85. Nation J.A., 1970 Appl. Phys. Letters 27 107

86. Nation J.A., 1979 Particle Accelerators 10 1

87. Ott E., 1971 Plasma Physics 13 529

88. Ott E. and Sudan R.N., 1971 Phys. Fluids 14 1226

89. Papadopoulos K., 1975 Phys. Fluids 18 1769

90. Prono D., Ecker B., Bergstrom N. and Benford J., 1975 Phys. Rev. Letters 35 438

91. Proulx G.A., 1981 Ph.D. Thesis, Cornell University

92. Roberson C.W., Mondelli A., and Chernin D., 1983 Phys. Rev. Letters 50 507

93. Rostoker N., 1973 Part. Accelerators 5 93

94. Rostoker N., 1980 Comments on Plasma Physics 6 91

95. Rudakov L.I. and Samarsky A.A., 1973 in Controlled Fusion and Plasma Physics (Proc. 6th European Conference, Moscow) vol.1 487

96. Sagdeev R.Z., 1967 in Magneto-Fluid and Plasma Dynamics (Proc. of Symposia in Applied Mathematics, edited by Grad

H.) American Mathematics Society, Providence, Rhode Island vol.18 281

97. Sander K.F., 1969 Plasma Physics 3 353
98. Sethian J.D., 1976 Ph.D. Thesis , Cornell University
99. Sethian J.D., Gerber K.A., Spector D.N., and Robson A.E. 1978 Phys. Rev. Letters 41 798
100. Sprangle P. and Kapetanakos C.A., 1978 J. Appl. Physics 49 1
101. Striffler C.D. and Kapetanakos C.A., 1975 J. Appl. Physics 46 2509
102. Suzuki T., Murakami H., Saito Y., Yamagishi A. and Inaba H., 1980 Rev. Sci. Instruments 51 1485
103. Suzuki Y. and Kato S.K., 1984 in Proc. of Collaborative Research on Particle Beam Applications to Fusion Research (IPP, Nagoya Univ.) IPPJ-678, 200
104. Tanaka M., Hayashi T.,Harafuji K., Nakayama Y. and Sato T., 1987 in Plasma Physics and Controlled Nuclear Fusion Research (Proc. 11th Int. Conf., Kyoto, 1986) IAEA Vienna, Vol.2 65
105. Thode L.E., 1976 Phys. Fluids 19 305
106. Thode L.E. and Sudan R.N., 1975 Phys. Fluids 18 1552
107. Toepfer A.J. and Poukey J.W., 1973 Phys. Fluids 16 1546
108. Uhm H.S., Davidson R.C. and Petillo J.J., 1985 Phys. Fluids 28 2537
109. Widner M., Alexeff I., Jones W.D. and Lonngren K.E., 1970 Phys.Fluids 13 2532
110. Widner M.M. and Poukey J.W., 1976 Phys. Fluids 19 1838
111. Yonas G., Poukey J.W., Prestwich K.R., Freeman J.R., Toepfer A.J. and Clauser M.J., 1974 Nuclear Fusion 14 731
112. Yoshikawa S. and Christofilos N.C., 1971 in Plasma Physics and Controlled Nuclear Fusion Research (Proc. 4th Int. Conf., Madison, 1971) IAEA Vienna, Vol.II 357